

Medizinische Fakultät der Martin-Luther-Universität Halle-Wittenberg

Deciphering OTUD3 functions and its potential role in human neurodevelopmental disease

Dissertation

zur Erlangung des akademischen Grades des

Doktor rerum medicarum (Dr. rer. medic.)

für das Fachgebiet Medizinische Physiologie und Pathophysiologie

vorgelegt

der Medizinischen Fakultät

der Martin-Luther-Universität Halle-Wittenberg

von Diplom Biochemiker Florian Job

geboren am 03.05.1988 in Nordhausen

Betreuer: Prof. Dr. Thorsten Pfirrmann

1. Gutachter: PD Dr. Dagmar Quandt

2. Gutachter: M.D. Ph.D. Grazia Maria Simonetta Mancini, Rotterdam

01.12.2020

08.06.2021

Abstract

Posttranslational modification of proteins with ubiquitin is involved in 26S proteasomal degradation, DNA repair, endocytosis and signaling processes. While E1, E2 and E3 enzymes enable the covalent ubiquitin attachment to substrates, deubiquitinases as cysteine- or metalloproteases can reverse this reaction.

So far, deubiquitinase OTUD3 was identified as tumor suppressor in breast cancer, whereas in non-small lung cancer a pro-oncogenic role was shown. In this thesis, an autosomal recessive inherited *OTUD3* mutation c.1061_1063delAGA (p.Lys356del) is firstly described in association with Angelman Syndrome (AS)-like phenotypes. Defect was detected in a Kurdish family with four affected children of two consanguineous healthy couples. To strengthen the putative link of *OTUD3* dysfunction to neurodevelopmental disease high degree of conservation of *OTUD3* gene, protein and in patients deleted Lys356 residue during evolution was confirmed. qPCR revealed high levels of *OTUD3* mRNA in skin, testes and brain areas important for locomotion, speech and visualization. Notably, pSMAD1/5 signaling was desensitized while proliferation was enhanced in patient derived LCLs.

Patients clinically presented with overlaps to AS as *UBE3A* defect. In a cohort of AS-like patients lacking genetic *UBE3A* diagnostic findings *OTUD3* was Sanger sequenced and a MLPA assay was established to account for copy number variations (CNVs) of exons. Sequencing revealed no variants likely to be disease causing. Multiple CNVs were found in four unrelated patients absent in healthy blood donor cohort. In one patient CNVs were identified as *de novo* by parental DNA analyses. Most strikingly, via GeneMatcher platform we got aware of one diseased twin boy with autosomal recessive inherited homozygous *OTUD3* c.G739A (p.D247N) mutation associated with intellectual and motoric disabilities, seizures, speech disorder, scoliosis and blindness. Immunfluorescence microscopy proved colocalization of endogenous OTUD3 with polymerized microtubules, mitotic spindles, the midbody and primary cilia. Strikingly, *N*-terminal GFP-tagged *OTUD3* constructs were transfected in HeLa cells and enabled the identification of a *C*-terminal located microtubule-binding site, NES and a putative *N*-terminal NLS within OTUD3. Phenotypic characterization of here generated *OTUD3* k.o. cells revealed cell line specific alterations like elongated and more frequent filopodia formation in HEK293T and enlarged HeLa cells in comparison to wildtype cells.

To sum up, this thesis highlights the potential novel role of *OTUD3* in the pathogenesis of neurodevelopmental syndromes by inherited or *de novo* genetic variations. Secondly, novel functions of the uncharacterized *N*- and *C*-terminal domain of OTUD3 like nuclear-cytosol shutteling mediated by NES and NLS and microtubule association were assigned.

Referat

Die posttranslationale Modifizierung von Proteinen mit Ubiquitin markiert diese für den Abbau durch das 26S Proteasom und reguliert Prozesse wie DNA-Reparatur, Endozytose oder Signaltransduktionwege. Deubiquitinasen fungieren als Cystein- oder Metalloproteasen und können die Ubiquitinierung umkehren. Die Deubiquitinase OTUD3 wurde kürzlich als Tumor-Suppressor bei Brust-Krebs und als Onkogen beim nicht-kleinzelligen Lungenkarzinom funktional beschrieben.

In dieser Dissertation wird erstmalig eine autosomal rezessiv vererbte *OTUD3* Mutation c.1061_1063delAGA (p.Lys356del) in Assoziation mit einer schwerwiegenden Entwicklungsstörung untersucht. Die Mutation wurde in einer kurdischen Familie mit insgesamt vier betroffenen Kindern von zwei konsanguinen und gesunden Elternpaaren detektiert. Das *OTUD3* Gen, Protein und die in den Patienten deletierte Aminosäure Lys356 zeigten eine hohe evolutionäre Konservierung. Weiterführende qPCR Analysen zeigten hohe *OTUD3* mRNA Spiegel in Geweben wie der Haut, Testis und dem Gehirn. In Patienten LCLs konnte eine reduzierte pSMAD1/5 Signaltransduktion und eine erhöhte Proliferation der Zellen nachgewiesen werden.

Die Index-Patienten weisen Analogien zum *UBE3A* Defekt, bekannt als Angelman Syndrom (AS), auf. In einer AS Kohorte, aber ohne genetischen *UBE3A* Befund, wurden die *OTUD3* Exons sequenziert und mittels MLPA auf Kopiezahlveränderungen (CNV) untersucht. Die Sequenzierungsergebnisse lieferten keine weiteren Hinweise auf potentiell pathogene *OTUD3* Mutationen. In vier unabhängigen Patienten wurden multiple Exon-CNVs detektiert. Bei einem Patienten handelte es sich um *de novo* CNVs. Via GeneMatcher Plattform wurde ein weiterer Patient mit einer autosomal rezessiv vererbten homozygoten *OTUD3* c.G739A (p.D247N) Mutation identifiziert. Der Patient präsentiert sich klinisch mit einer geistigen und motorischen Entwicklungsstörung, Krämpfen, Sprachstörung, Skoliose und Blindheit.

Endogenes OTUD3 kolokalisiert mit polymerisierten Mikrotubuli, Mitosespindeln, dem Midbody und primären Zilien. Die Transfektion von N-terminal GFP-getaggten *OTUD3* Konstrukten in HeLa Zellen führte zur Identifizierung einer C-terminalen Mikrotubulin-Bindungsdomäne, einer NES, sowie einer putativen N-terminalen NLS. In HEK293T *OTUD3* k.o. Zellen wurden elongierte Filopodien beobachtet und beim HeLa *OTUD3* k.o. leicht vergrößerte und abgerundete Zellen.

Die hier gesammelten Ergebnisse ermöglichen erste Hinweise auf eine Genotyp-Phänotyp Korrelation von vererbaren und/oder *de novo* *OTUD3* Defekten zu Patienten mit neurologischen Entwicklungsstörungen. Darüber hinaus konnten den N- und C-terminalen Domänen des OTUD3's erste Funktionen wie dem Zellkern-Zytosol Transport mittels NLS und NES und der Mikrotubuli-Bindung zugeordnet werden.

I Contents

1. Introduction	1
1.1 Ubiquitination as post-translational modification	1
1.1.1 Ubiquitin and ubiquitin-like proteins	1
1.1.2 The 'ubiquitin code'	3
1.2 Deubiquitinating enzymes	5
1.2.1 Catalytic mechanisms and structural features	5
1.2.2 Functions and specificity of deubiquitinases	7
1.3 The ubiquitin pathway and hereditary human diseases	8
1.3.1 E3 ligase associated diseases	8
1.3.2 Impact of deubiquitinases in neurological diseases	10
1.3.3 Clinical relevance of ovarian-tumor domain-containing protein 3 (OTUD3).....	11
2. Aims of thesis	13
3. Materials and methods	14
3.1 Chemicals	14
3.2 Instruments and consumables	14
3.3 Enzymes/ Antibodies/ Inhibitors/ Additives	15
3.4 Kits and standards	16
3.5 Oligonucleotides and vectors	17
3.6 Bacterial strains/ mammalian cell lines	19
3.7 Patient material	19
3.8 Media/buffers/antibiotics/supplements	19
3.9 Micro- and molecular biology	20
3.9.1 Transformation of <i>E. coli</i> via electroporation.....	20
3.9.2 Plasmide isolation	21
3.9.3 Single Oligonucleotide Mutagenesis and cloning Approach	21
3.9.4 Cloning	21
3.9.5 Sanger sequencing	22
3.9.6 DNA precipitation	23
3.9.7 DNA extraction	23
3.9.8 RNA extraction	23
3.9.9 cDNA synthesis and qPCR	23
3.9.10 Nucleic acid concentration determination	24
3.9.11 Agarose gel electrophoresis.....	24
3.9.12 Multiplex ligation-dependent probe amplification (MLPA).....	24
3.9.13 Long-range PCR	25
3.9.14 Alignment and evolutionary conservation analyses	25

3.10 Biochemical analyses.....	26
3.10.1 SDS PAGE.....	26
3.10.2 Western blot.....	26
3.10.3 NaDoc/ TCA precipitation.....	27
3.10.4 pSMAD1/5 read out.....	27
3.10.5 Cell fractionation by ultracentrifugation.....	27
3.10.6 Ubiquitin conjugation assay.....	28
3.11 Cell biological analyses.....	28
3.11.1 Cultivation, passaging and cryopreservation of cells.....	28
3.11.2 Cell counting assay.....	28
3.11.3 Protein concentration measurement using BCA assay.....	29
3.11.4 Transfection of plasmids and siRNAs.....	29
3.11.5 Synchronization of HeLa cells.....	29
3.11.6 Induction of primary cilia in NIH3T3 cells.....	29
3.11.7 MTT assay.....	29
3.11.8 Immunofluorescence microscopy.....	30
3.11.9 Generation of <i>OTUD3</i> knock-out cell lines using CRISPR/ Cas9.....	30
4. Results.....	31
4.1 <i>OTUD3</i> is highly evolutionary conserved.....	31
4.2 Linking <i>OTUD3</i> variations to neurodevelopmental disease phenotypes.....	33
4.2.1 <i>OTUD3</i> c.1061_1063delAGA co-segregates with AS-like defect.....	33
4.2.2 Finding of a patient with homozygous c.G739A <i>OTUD3</i> variant.....	34
4.2.3 <i>OTUD3</i> sequencing in a cohort with negative test results for AS.....	35
4.2.4 CNVs of <i>OTUD3</i> exons might be associated to human developmental disease.....	36
4.3 Molecular insights into <i>OTUD3</i> p.Lys356del patient cells.....	39
4.3.1 <i>OTUD3</i> mutation does not influence expression, activity and localization.....	39
4.3.2 Patient LCLs show altered pSMAD1/5 levels.....	42
4.3.3 Patient LCLs possess higher proliferation activity.....	43
4.4 <i>OTUD3</i> is differentially expressed in human tissues.....	44
4.5 Localization studies of <i>OTUD3</i>	46
4.5.1 Endogenous <i>OTUD3</i> localization is conserved across species and tissues.....	46
4.5.2 <i>OTUD3</i> decorates mitotic spindles, primary cilia and midbody.....	48
4.5.3 Terminal domains of <i>OTUD3</i> mediate microtubule binding and localization.....	48
4.5.4 <i>OTUD3</i> co-sediments with polymerized microtubules.....	52
4.6 <i>OTUD3</i> knock-out using CRISPR/ Cas9 technology.....	53
4.6.1 Generation and screening of positive <i>OTUD3</i> knock-out clones.....	53
4.6.2 <i>OTUD3</i> knock-out has cell line specific effects on cell morphology.....	55

5. Discussion	56
5.1 Correlation of <i>OTUD3</i> genotypes to AS-like phenotypes	56
5.1.1 <i>OTUD3</i> as candidate gene for neurodevelopmental disease	56
5.1.2 Evaluation of <i>OTUD3</i> SNV and CNV results.....	57
5.1.3 p.Lys356del <i>OTUD3</i> mutation and cellular consequences	61
5.2 Functional relevance of <i>OTUD3</i> 's terminal domains	63
5.2.1 Identification of a microtubule-binding site	63
5.2.2 Description of NES und NLS sequences	65
5.3 Consequences of <i>OTUD3</i> dysfunction.....	67
6. Summary	68
7. References	69
8. Theses	80

II Abbreviations

Aa	Amino acid
AMP	Adenosine monophosphate
AS	Angelman Syndrome
ATP	Adenosine triphosphate
BCA	Bicinchoninic acid
BMP4	Bone morphogenetic protein 4
BMPRIA	Bone morphogenetic protein receptor type IA
CNV	Copy number variation
CRISPR/ Cas	Clustered Regularly Interspaced Short Palindromic Repeats and CRISPR- associated genes
DAPI	4',6-diamidino-2-phenylindole
(c; g) DNA	(complementary, genomic) Deoxyribonucleic acid
DUB	Deubiquitinase
<i>E. coli</i>	Escherichia coli
e.g.	Exempli gratia/ for example
EGF (R)	Epithelial growth factor (receptor)
FACS	Fluorescence-activated cell sorting
GFP	Green fluorescent protein
HD	Healthy donor
HECT	Homologous to E6AP Carboxy Terminus
JAMM/MPN+	JAB1/MPN/MOV34 metalloenzymes
JMD	Machado-Joseph disease protein domain proteases
kDa	Kilodalton
k.d.; k.o.	Knock-down; Knock-out
LB	Luria-Bertani
LCL	Lymphoblastoid cell lines
MAF	Minor allele frequency
MAP	Microtubule-associated protein
MCPIP	Monocyte chemotactic protein-induced proteins
MLPA	Multiplex ligation-dependent probe amplification
MRI	Magnetic resonance images
mTOR	Mechanistic target of rapamycin
MTT	3-(4,5-dimethylthiazol-2-yl)-2,5-diphenyltetrazolium bromide
NEM	N-Ethylmaleimide
NES	Nuclear export signal

nF-kB	Nuclear factor 'kappa-light-chain-enhancer' of activated B-cells
NLS	Nuclear leading sequence
NMR	Nuclear magnetic resonance
NOC	Nocodazole
OD	Optical density
OFC	Occipitofrontal circumference
ORF	Open reading frame
OTU	Ovarian tumor
OTUD3	ovarian-tumor domain-containing protein 3
(q) PCR	(quantitative) Polymerase chain reaction
PD	Parkinson's disease
PDGF	Platelet derived growth factor
pI	Isoelectric point
PI3K-AKT	Phosphatidylinositol 3-kinase-protein Kinase B
pSMAD	Phosphorylated SMAD (fusion of <i>Caenorhabditis elegans</i> Sma genes and the <i>Drosophila Mad</i> , mother against decapentaplegic)
PTEN	Phosphatase and tensin homolog
PTM	Post-translational modification
Ras-MAPK	Ras-mitogen-activated protein kinase
RING	Really Interesting New Gene
(si; m) RNA	(small interfering; messenger) Ribonucleic acid
Rpm	Revolutions per minute
SNV	Single nucleotide variation
SOMA	Single Oligonucleotide Mutagenesis and cloning Approach
TGF	Transforming growth factor
TSG	Twisted gastrulation
TUBES	Tandem ubiquitin binding entities
UBD	Ubiquitin binding domain
UBL	Ubiquitin-like proteins
Ub-PA	Ubiquitin-propargylamid
Ub-VME	Ubiquitin-vinylmethylester
UCH	Ubiquitin C-terminal hydrolase
USP	Ubiquitin specific proteases
UV	Ultraviolet

1. Introduction

1.1 Ubiquitination as post-translational modification

1.1.1 Ubiquitin and ubiquitin-like proteins

In 2001, the Human Genome Project led to the surprising finding that our genome encompasses only about 30.000-40.000 open reading frames for proteins [1]. Already three years later, the Human Genome Sequencing Consortium published a lower number of 20.000-25.000 protein coding genes and more recent studies narrowed down this number of genes to 19.000 [2,3]. In contrast, the human proteome has an estimated number of over one million proteins [4]. The increasing complexity from the genomic to the proteomic level is facilitated by post-transcriptional mechanisms like e.g. alternative splicing or RNA editing and post-translational modifications (PTMs).

PTMs are defined as covalent and often enzyme catalyzed chemical modifications within proteins that can modulate their activity, folding, stability, turnover, cellular localization and interactions with other proteins or molecules. The complexity of PTMs and their regulatory network properties seems to be unlimited, because:

1) PTMs can occur on different amino acid side chains or the *N*- or *C*-terminus of a protein. 2) Proteins can possess single or multiple PTMs. 3) An existing PTM can be targeted by other PTMs. 4) Many PTMs can be reversed and 5) occur space and time dependent (e.g. according to the cell cycle or different stimuli like oxidative stress or signaling and differentiation processes). In eukaryotes, more than 300 different types of PTMs have been identified including the most common ones like phosphorylation, methylation, acetylation, glycosylation, various types of lipidation, carbonylation, nitrosylation, sumoylation and linkage of ubiquitin moieties, namely ubiquitination [5].

Ubiquitin consists of 76 amino acids and is one of the most highly conserved, abundant and stable proteins in eukaryotic organisms. The 8.5 kDa polypeptide was first purified from bovine thymus in the early 1970's by Goldstein and co-workers [6]. Within the next decades it was discovered that ubiquitin acts as a post-translational protein modifier and gets covalently bound to target proteins in an energy-dependent manner [7]. Thereby, the *C*-terminal glycine residue of ubiquitin gets linked to lysine residues of target proteins and regulates biological processes like DNA repair, endocytosis, receptor trafficking and degradation of proteins by the 26S proteasome [8–12].

The ubiquitination process is stringently regulated and requires the sequential action of three key enzymes: an ubiquitin-activating enzyme (E1), an ubiquitin-conjugating enzyme (E2) and an ubiquitin ligase (E3) (Figure 1A).

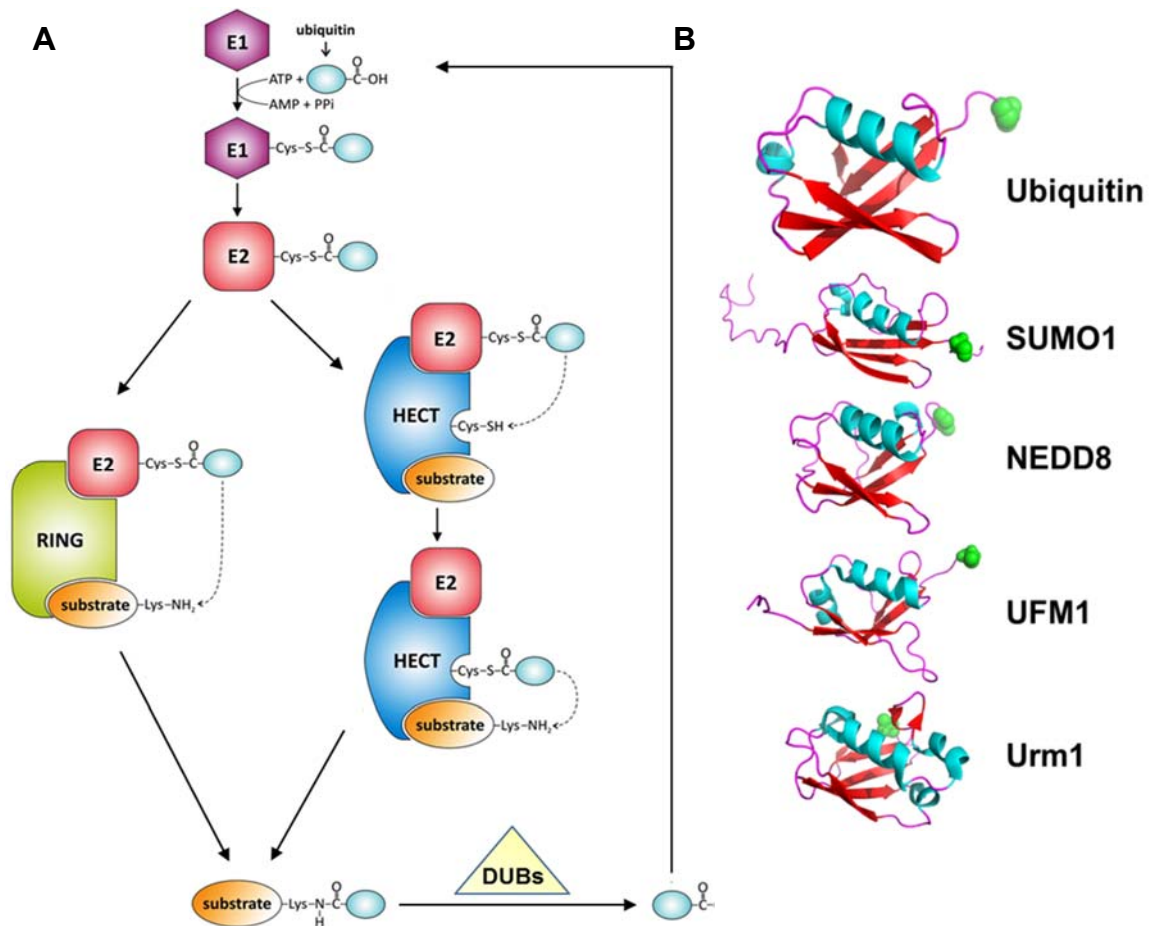


Figure 1) Ubiquitination plays an essential role in regulation of many cellular processes. A) Schematic representation of enzymatic three step mechanism of ubiquitination. An ubiquitin-activating enzyme (E1) activates and binds ubiquitin on its C-terminal glycine in an ATP dependent manner. Next, activated ubiquitin gets transferred to an ubiquitin-conjugating enzyme (E2). Finally, an ubiquitin ligase (E3) featuring so called RING or HECT domains mediates isopeptide formation between ubiquitin's C-terminus and lysine ϵ -amino groups within substrates. The reaction can be reversed by deubiquitinases (DUBs). Figure was modified from [13]. B) Ubiquitin (1UBQ) and ubiquitin-like proteins NEDD8 (1NDD), SUMO1 (1A5R), UFM1 (1WXS) and Urm1 (2QJL) show high similarity of secondary and tertiary structure. The common fold is called β -grasp fold. Images were created using the indicated pdb-files and Pymol software. Secondary structures are shown as cartoon. Green spheres indicate glycine residues that get linked to lysine side chains of target proteins.

In the first step of the reaction, ubiquitin gets activated via E1 that binds ATP and ubiquitin and catalyzes the acyl-adenylation of ubiquitin's C-terminus. A thioester bond is formed between the E1 active site cysteine residue and ubiquitin's activated C-terminal carboxyl group while AMP gets released. Afterwards, ubiquitin gets transferred to an active cysteine site of an E2 enzyme in a transthioesterification reaction. The last step, catalyzed by E3 ligases forms an isopeptide bond between the C-terminus of ubiquitin and the ϵ -amino group of a lysine residue within the target protein [14–16]. Some cases are known where ubiquitin gets conjugated to cysteine, threonine, serine or N-terminal methionine residues of proteins [15–17].

In general, E3 ligases can be divided into two classes: HECT (Homologous to E6AP Carboxy Terminus) and RING (Really Interesting New Gene) domain possessing ligases. HECT domain E3 ligases interact with the E2 enzyme and bind ubiquitin to an internal active cysteine residue via transthiolation reaction before ubiquitin gets transferred to the target protein. More widespread RING domain ligases mediate the direct transfer of ubiquitin from E2 to the substrate [18,19]. In mammals there are only two E1 enzymes, about 30 E2 proteins and nearly 800 E3-ligases known, suggesting that E3 ligases mainly mediate target specificity [20].

Several proteins related to ubiquitin in part to its sequence, but predominantly to its 3D structure and function have been described and were termed as ubiquitin-like proteins (UBLs) [21,22] (Figure 1B). Prominent UBL examples are SUMO1, NEDD8, Ufm1 and URM1 that are involved in various cellular processes like nuclear transport, apoptosis, cell cycle progression, splicing, antiviral host defense and degradation. [23–27].

The vast majority of proteins will undergo ubiquitination within their cellular lifetime considering that besides many other functions ubiquitination targets up to 80% of proteins for degradation by the 26S proteasome [28]. Thus, the fate of a protein is precisely determined by the attachment of ubiquitin or ubiquitin-like modifiers and their complex architectures that can be build up and are referred to as ‘ubiquitin code’ [29].

1.1.2 The ‘ubiquitin code’

Fast developing proteomic approaches that are often mass spectrometry based enable new insights into the complexity of ubiquitin linkage types existing *in vivo* and their encoded outcomes. The simplest and well-studied type of ubiquitin modification is the attachment of one ubiquitin moiety to a substrate protein via its C-terminal glycine so called monoubiquitination (Figure 2D). In cells monoubiquitination events are abundant and contribute to DNA repair, signal transduction and vesicle sorting [30–32].

Next complexity increase of ubiquitination signals is achieved by multi-monoubiquitin modifications, which trigger e.g. EGF and PDGF receptor internalization and lysosomal degradation [11] (Figure 2D).

Once ubiquitin is attached to a substrate protein, its seven internal lysine residues (K6, K11, K27, K29, K33, K48, K63) or its N-terminal methionine (M1) can serve as acceptor for further ubiquitination steps (Figure 2A/B). Generated ubiquitin chains that can differ in the number of linked ubiquitin molecules are summarized as polyubiquitinations and can be divided into homotypic (one linkage type) and heterotypic (different linkage types) modifications (Figure 2D).

Proteins tagged by K48 polyubiquitin target substrates for 26S proteasomal degradation, whereas K63 linked chains has nondegradative roles such as NF- κ B pathway activation and endocytosis [33,34].

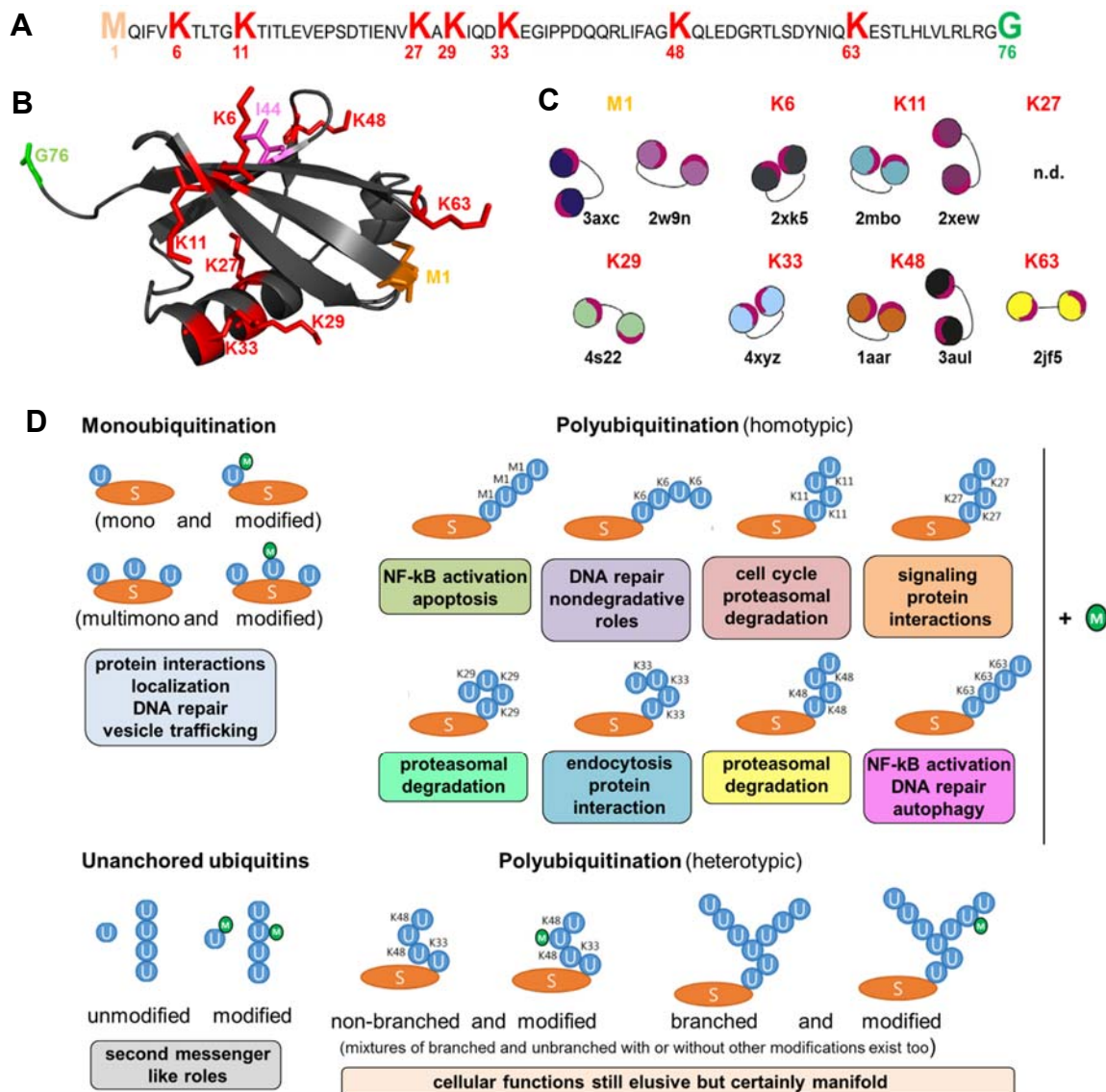


Figure 2) Distinct ubiquitin linkage types encode manifold *in vivo* functions. A) Amino acid sequence of human ubiquitin. C-terminal glycine residue (G76; green), internal lysines (red), N-terminal methionine (M1; orange). B) 3D structure of ubiquitin (cartoon optic; pdb 1ubq) reveals different orientations of all lysine residues (red sticks) and M1 (orange). G76 residue is flexible and exposed in contrast to the globular ubiquitin structure enabling attachment to targets. Isoleucine 44 (magenta stick) builds the center of an important hydrophobic interaction surface between ubiquitin molecules in chains and ubiquitin binding partners. C) Schematic overview of ubiquitin chain topologies based on available crystal or NMR structures (pdb codes see above). I44 patch is shown in magenta. Depending on the linkage type ubiquitin chains adopt more open or closed conformations. n.d.- no pdbs available. Edited from [35]. D) The type of ubiquitination pattern on substrates dictates the fate of cellular proteins. Linked or unanchored ubiquitin (-chains) itself can be further modified by UBLs, phosphorylation and acetylation (shown as green sphere) expanding the complexity and dynamics of mediated signals. Edited and updated from [36].

Biological relevance of M1, K6, K11, K27, K29 and K33 chains are more elusive but gain emerging attention. M1 chains serve as positive regulator of NF- κ B signal transduction and can be associated with apoptosis [37,38].

Less is known about K6 linkages and their cellular importance. It was shown that upon proteasome inhibition K6 chains were not enriched, suggesting non-degradative roles [39]. K11 chains operate as alternative degradation signals for cell cycle regulation components [40,41]. Most elusive remain K27 linkages, which are supposed to serve as scaffolds for the recruitment of DNA damage response factors as p53 binding protein 1 [42]. Finally, homotypic K29 polyubiquitin chains mark substrates for proteasomal degradation and K33 chains regulate post-golgi membrane protein trafficking [43,44].

Interestingly, depending on the linkage type ubiquitin chains adopt varying topologies (Figure 2C). Based on crystal and NMR structures, it was shown that ubiquitin chains exist in more open or closed conformations [45,46].

The next level of diversity is achieved by heterotypic ubiquitin modifications that can build up non-branched and branched conformations (Figure 2D). It is hypothesized that *in vivo* all possible heterotypic ubiquitin linkage types co-exist. Evidence is provided by the finding that K63 chains are modified with M1 chains in non-branched and branched architectures [47].

Continuously, the complexity of the 'ubiquitin code' is increasing. UBLs such as SUMO and NEDD8 can modify existing ubiquitin chains on target proteins [48–50].

Next, six of seven lysine residues of ubiquitin can become acetylated and further eight of potential eleven sites phosphorylated in mammals [51–53]. Finally, free ubiquitin or free ubiquitin chains present in cell lysates as unmodified, acetylated or phosphorylated entities fulfill independent second messenger like functions [54,55].

1.2 Deubiquitinating enzymes

1.2.1 Catalytic mechanisms and structural features

Since the discovery of ubiquitin in the 1970's, research was mainly focused on mechanisms how ubiquitin gets linked to substrates for their degradation via the 26S proteasome and subsequently on various nondegradative roles of distinct ubiquitin linkages *in vivo* (see 1.1.1 and 1.1.2).

Notably, the genome of eukaryotes lacks genes coding for free monomeric ubiquitin protein that is abundant in cell lysates. In humans two different classes of ubiquitin genes exist: monomeric ubiquitin-ribosomal fusion genes (*UBA52* and *UBA80*) and stress-inducible polyubiquitin genes (*UBB* and *UBC*). The latter are composed of 3-4 and 9-10 tandem ubiquitin coding entities [56–58]. Thus, there is no *de novo* synthesis of monomeric ubiquitin and therefore the existence of ubiquitin-specific enzymes that release free ubiquitin from substrates or polyubiquitin chains to restore the cellular ubiquitin pool was hypothesized early. In the 1980's, it was first shown in reticulocyte

extracts that ubiquitination can be reversed by ubiquitin-specific processing proteases releasing free available ubiquitin [59]. Today, these proteases that hydrolyze isopeptide bonds (or peptide bonds) in an ubiquitin-specific manner are better known as deubiquitinases (DUBs).

The human genome encodes for approximately 100 DUBs, whereas about 80 of them are supposed to be active enzymes in cells [60]. According to catalytic domain sequence homologies the DUB family can be classified in at least six groups: ubiquitin specific proteases (USPs), ubiquitin C-terminal hydrolases (UCHs), ovarian tumor proteases (OTUs), Machado-Joseph disease protein domain proteases (JMD), JAB1/MPN/MOV34 metalloenzymes (JAMM/MPN+) and monocyte chemotactic protein-induced proteins (MCPIP) [61,62].

Members of the USP, UCH, OTU, JMD and MCPIP family own cysteine protease activity, whereas JAMM/MPN+ enzymes are typical zinc-dependent metalloproteases.

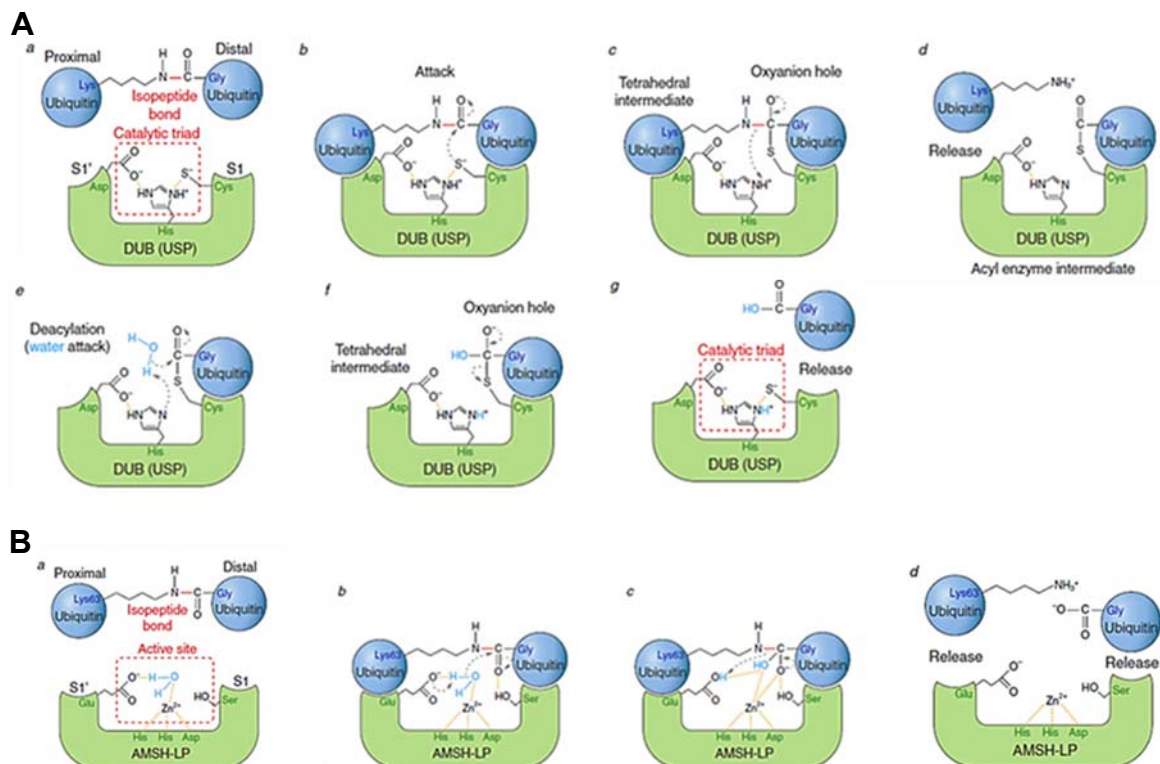


Figure 3) Catalytic mechanisms of DUBs. DUBs can hydrolyze isopeptide bonds or peptide bonds by two common mechanisms. A) Cysteine-dependent mechanism is employed by five of six DUB subfamilies (USP, UCH, OTU, Josephins, MCPIP). B) DUB JAMM family members are metalloproteases and their catalytic activity resembles the mechanism of thermolysin. Modified from [62].

Cysteine-dependent DUBs contain a conserved catalytic diad or triad and their reaction mechanism is similar to that of plant protease papain (Figure 3A) [63].

The catalytic core of zinc-dependent metalloprotease DUBs consists of two invariant histidines, an aspartate and serine side chain and two coordinated zinc ions. Hydrolysis mechanism of isopeptide bonds is predicted to be similar to other metalloproteases such as thermolysin (Figure 3B) [64]. Recently, crystal structures of AMSH-LP and in complex with bound di-ubiquitin were solved and supported the so far predicted reaction mechanism of metalloprotease DUBs [65]. Each DUB subfamily is characterized by a distinct catalytic core fold, but share two common principles:

- 1) The DUB activity is cryptic. Unwanted isopeptide hydrolysis by DUBs must be avoided and tightly controlled [66]. NMR and crystal structures of many DUBs reveal that ubiquitin binding induces conformational changes within the catalytic core of the DUB and thereby activates the enzyme [65,67,68]. In addition, other regulatory mechanisms that control DUB activity are known like phosphorylation, ubiquitination, sumoylation or protein-protein interactions with e.g. E3 ligases [69–71]. Transcriptional regulation of DUB expression and specific localization of DUBs are other important extra layers of activity control [72].
- 2) The DUB domain composition is modular. Besides the highly conserved catalytic domain of each DUB subfamily many other protein-protein interaction domains or short structural conserved regions are present. These additional domains are typical ubiquitin binding domains (e.g. UBA, UIM), zinc finger motifs, PH domains, but also intrinsically disordered regions as potential sites for post-translational modifications [62].

The number of active DUBs (~ 80) in comparison to known E3 ligases (~600) as their counterpart is about eight times lower. This numeric contradiction implies that functional control of DUBs and the interplay with ubiquitin substrates and other interaction partners consists of several additional layers to guarantee cellular protein homeostasis.

1.2.2 Functions and specificity of deubiquitinases

Physiological roles of DUBs are an emerging field of research interest, but functions and exact mechanisms of their action remain elusive. A first function of DUBs is the generation of free ubiquitin from translated ubiquitin genes encoding ubiquitin chains or ubiquitin fusions to ribosomal proteins (see 1.2.1).

Secondly, DUBs can reverse the action of E3 ligases by removing single ubiquitin moieties or trim or cleave entire ubiquitin chains from proteins and thus edit E3 ligase dictated fate of proteins. DUBs can rescue or promote proteasomal degradation of ubiquitin tagged proteins. Three DUBs (USP14, UCHL5, POH1) associate directly with the 19S proteasomal regulatory particle of the 26S proteasome in higher eukaryotes

and deubiquitinate substrates prior to their proteasomal degradation to recycle ubiquitin molecules [73].

DUBs display important roles within the lysosomal pathway and receptor trafficking. USP8 and AMSH associate with the core endosomal sorting complexes required for transport (ESCRT) degradation machinery. Loss of AMSH activity leads to the accumulation of the EGFR as a consequence of its impaired lysosomal degradation [74,75]. Contrary, loss of USP8 causes hyperubiquitination of EGFR and other receptors like MET and ERBB3 and their enhanced degradation [76,77].

USP19 bears a predicted transmembrane domain. The C-terminus of USP19 is anchored in the ER membrane, while its catalytic domain remains in the cytoplasm [78]. USP19 modulates transcription of major myofibrillar proteins [79]. It was shown that USP19 rescues model substrates from ER-associated degradation when overexpressed [78].

Several DUBs can be linked to DNA dependent processes like DNA repair, replication and transcription. Histones H2A and H2B get deubiquitinated by JAMM family members MYSM1 and BRCC36 suppressing DNA repair pathways [80,81].

In vitro studies suggest that members of the largest DUB family the USPs are mainly promiscuous for different ubiquitin linkage topologies [82]. Known exceptions are USP14 that possesses K48 ubiquitin chain specificity and CYLD which recognizes and cleaves K63 and linear ubiquitin chains [83,84]. In contrast, members of the OTU family exhibit some degree of specificity for different linkage types within ubiquitin chains. As example, OTUB1 processes K48-linkages [85], OTUD7B/Cezanne prefers K11-ubiquitin chains [86] and OTUD3 preferentially hydrolyses K6-, K11 and K27 ubiquitin linkages [87]. The metalloproteases AMSH, AMSH-LP, CSN5, BRCC36, POH1 and MYSM1 display K63 linkage specificity as well as the Josephin family member ATXN3 [88–90].

1.3 The ubiquitin pathway and hereditary human diseases

1.3.1 E3 ligase associated diseases

Improper clearance of proteins or imbalance within the ubiquitin-proteasome system is causative for human diseases. Thus, it is not surprising that mutation of E3 ligase coding genes (~ 600 genes) can be linked to several human hereditary diseases.

Angelman Syndrome (AS) was first described in 1965 and named after the British pediatrician Harry Angelman. AS patients are characterized by developmental delay, intellectual disability, seizures, ataxia, speech impairment, some degree of autistic behavior and commonly a happy demeanor (Figure 4A) [91].

AS establishes as consequence of E3 ligase E6AP deficiency, which is encoded by the *UBE3A* gene located on chromosome region 15q11-13. In the brain, paternally

inherited *UBE3A* allele is silenced and only the maternally copy is expressed [92–94]. Several mechanisms can cause AS due to the lack of maternally derived *UBE3A* expression in the brain: 1) Deletions of the *UBE3A* containing region 15q11.2-q13, 2) paternal uniparental disomy of chromosome 15, 3) *UBE3A* loss of function mutations in the maternal copy of chromosome 15, and 4) rare imprinting defects.

Interestingly, as *UBE3A* the human *HERC2* gene, encoding E3 ligase HERC2, is located on chromosome region 15q11-13 too. Homozygous missense mutations in *HERC2* can be found in patients that show a phenotypically mild form of AS [95,96]. Protein based analyses revealed that HERC2 interacts with E6AP and activates E6AP ligase [97].

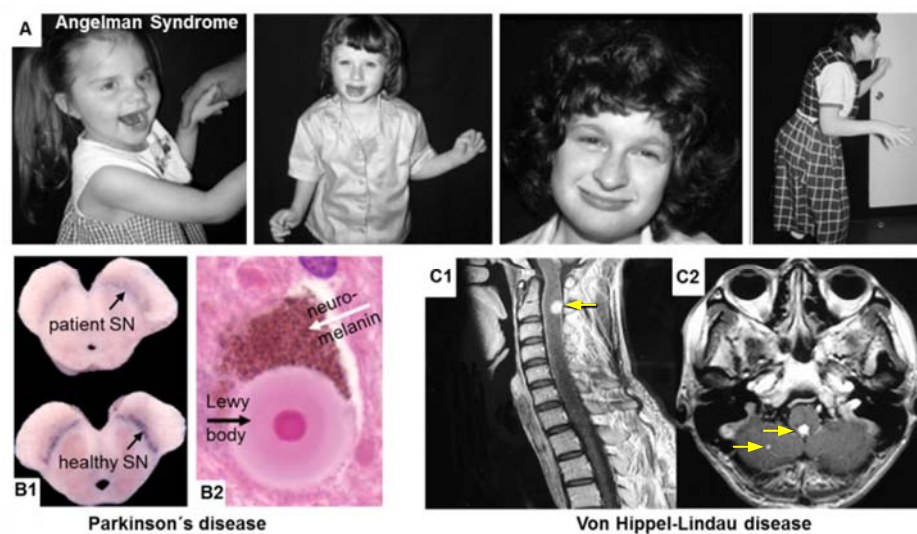


Figure 4) Clinical examples for inherited E3 ligase defects. A) Phenotypes of AS patients. AS is also known as happy puppet syndrome. Adapted from [98]. B1/B2) Parkinson's disease pathology. B1) PD patients show depigmented substantia nigra (SN) in comparison to a healthy brain in cross sections of the midbrain. Depigmentation occurs due to the loss of dopaminergic neurons containing neuromelanin as a cellular oxidation product of dopamine or norepinephrine. B2) The SN of PD patients contain Lewy bodies within the cytoplasm of the neurons. Taken from [99]. C1/ C2) MRI of Von Hippel-Lindau patients. Yellow arrows indicate nodular lesions. Taken from [100].

Parkinson's disease (PD) is characterized by progressive gait and posture abnormalities due to the loss of dopaminergic neurons from the substantia nigra of the midbrain and the presence of cytoplasmic inclusions (named Lewy bodies, Figure 4 B1/B2) [101,102]. Patients suffer from muscle tremors, stiffness and bradykinesia. The E3 Ligase Parkin (gene: *PARK2*) links PD to the ubiquitin pathway and is well described in literature. Over 120 different pathogenic mutations in *PARK2* are known and over 600 families have been studied worldwide [103,104]. About 50% of *PARK2* mutations account for autosomal recessive juvenile parkinsonism [105,106]. Failure of Parkin E3 ligase activity to ubiquitylate target proteins leads to their accumulation and aggregation which is toxic for neuronal cells of the substantia nigra [107].

Besides developmental and neurodegenerative diseases E3 ligase mutations can be connected to other human genetic malignancies like *BRCA1* gene to breast or ovarian cancer [108]. Another example is the autosomal dominant inherited von Hippel-Lindau disease which is a consequence of germline mutations within the *VHL* gene. Patients differ in penetrance of the disease and develop highly vascularized benign or malignant tumors and cysts, hemangioblastomas in the nervous system, retinal angiomas, clear-cell renal cell carcinomas and pheochromocytomas (Figure 4 C1/C2) [109]. On the other hand, certain homozygous or compound heterozygous germline *VHL* mutations lead to congenital polycythemia, thrombosis and other vascular abnormalities, but without tumors [110].

1.3.2 Impact of deubiquitinases in neurological diseases

As counterpart to E3 ligases, mutated DUBs have been implicated in human genetic diseases as well. Typical for neurodegenerative diseases is the accumulation of aggregated proteins in insoluble deposits. These inclusions contain high levels of ubiquitinated proteins and key players of the ubiquitin-proteasome-pathway implying a fundamental role of this axis in neurodegeneration in general [101,111].

The DUB Ataxin-3 is encoded by the *ATXN3* gene on chromosome 14 and is known for disassembling K48- and K63- polyubiquitin chains from substrates [90,112]. The clinical significance of Ataxin-3 is underlined by the neurologic disorder Machado-Joseph disease (MJD), also known as spinocerebellar ataxia-3 (SCA3) [113].

MJD is an autosomal dominant inherited disease and causes progressive cerebellar ataxia combined with signs of pyramidal dysfunction (e.g. spasticity, rigidity) and dementia in some cases. The MJD phenotype is similar to that of PD. MJD is one of nine existing polyQ disorders. CAG trinucleotide expansion within exon 10 of the *ATXN3* gene is considered to be disease causing, if the number of repeats ranges between 68-79 [113,114].

One of the most abundant proteins in neurons is the DUB UCHL-1, accounting for up to 2% of total soluble protein within brain tissue [115,116]. Interestingly, UCHL-1 is enriched in protein aggregates or inclusion bodies, suggesting a participation of this DUB in PD and Alzheimer [117,118]. More strikingly, a rare familial *UCHL-1* mutation causes early-onset PD due to the reduction of DUB activity [119,120]. In 2013, a novel autosomal recessive inherited *UCHL-1* mutation was identified in three siblings of a family. This mutation is accompanied by early-childhood manifestation of a neurodegenerative syndrome that is characterized by blindness, cerebellar ataxia, nystagmus, dorsal column dysfunction and spasticity including upper motor neuron dysfunction. The identified *UCHL-1* mutation abolishes hydrolase activity of the enzyme and lowers the affinity to ubiquitin at least seven-fold in comparison to wildtype [121].

A syndrome called Microcephaly-capillary malformation (MIC-CAP) is featured by microcephaly along with progressive cortical atrophy, epilepsy, severe developmental delay and capillary malformations on the skin [122–124]. Whole-genome-sequencing uncovered recessive mutations in unrelated families in the gene encoding for the DUB STAMBP. Patient material based analyses proved reduced STAMBP expression, elevated levels of ubiquitin-protein-aggregates, increased apoptosis and impaired activation of signaling-pathways like RAS-MAPK and PI3K-AKT-mTOR [125].

Recently, siblings of a consanguineous Palestinian family with cerebellar ataxia, hypogonadotropic hypogonadism and dementia showed homozygosity for two missense mutations in two genes, *RNF216* (p.R751C) as E3 ligase and *OTUD4* (p.G333V) as DUB. Both variants segregated with disease in the family. The phenotype of the affected siblings is assumed to be caused by the interplay of hypomorphic mutations in both identified genes. Knock-down (k.d.) of either *RNF216* or *OTUD4* in zebrafish model organism resulted in similar malformed embryos, whereas simultaneous k.d. led to much severe affected phenotypes [126].

Comprehensive datasets using large cohorts and reports of several unrelated families confirming more securely genotype-phenotype correlation of a DUB gene to a neurodegenerative disorder are missing.

1.3.3 Clinical relevance of ovarian-tumor domain-containing protein 3 (OTUD3)

The ovarian-tumor domain containing protein 3 (OTUD3) is one of 16 active DUB members of the OTU subfamily. In human, the *OTUD3* gene is located on chromosome region 1p36.13 and is composed of eight exons which encode the 45.1 kDa OTUD3 protein. In general, OTUD3 can be divided into five domains: a *N*-terminal region (1-64 aa), a catalytic OTU domain (65-189 aa), a short interdomain region (190-229 aa), an UBA-like interaction site (230-270 aa) and a *C*-terminal region (271-398 aa) (Figure 5). No structures of full-length OTUD3 are available. In 2013, a crystal structure of the catalytic OTU domain of OTUD3 was published [127]. The crystal structure showed that the highly conserved catalytic OTU domain contains a catalytic triad of D73, C76 and H182 (Figure 5 B/C). In addition, *in vitro* deubiquitination assays using synthetic ubiquitin substrates demonstrated that OTUD3 hydrolyzes predominantly K6, K11 and K27 ubiquitin chains [87,127]. Natural substrates of OTUD3 were unknown till 2015. In HCT116 cells, OTUD3 overexpression was concomitant with an increase of endogenous PTEN level and its prolonged half-life in cycloheximide chase experiments. Vice versa, OTUD3 depletion using siRNA approach led to a reduction of PTEN protein and a shortened half-life of the tumor suppressor. Thus, OTUD3 stabilizes PTEN. Furthermore, *in vitro* it was shown that OTUD3 directly interacts with

and de-polyubiquitylates PTEN [128]. PTEN is one of the most frequently mutated genes in cancer [129–132]. In addition, an *OTUD3* transgenic mouse model reflects the phenotype of *PTEN* transgenic mice including reduced whole body size and smaller organs in comparison to wildtype mice (Figure 5 D/E).

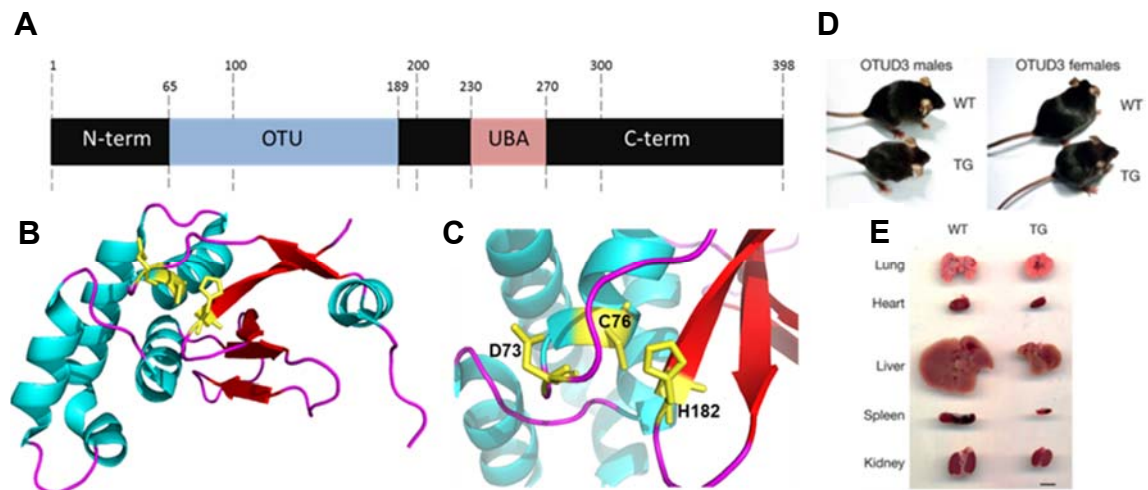


Figure 5) OTUD3 resembles a catalytic triad and is involved in tumorigenesis.

A) Schematic representation of OTUD3 and its domains. B) Crystal structure of catalytic OTU domain of OTUD3. Chain is shown as cartoon and coloured by secondary structure elements. Catalytic triad residues are shown as sticks and stained in yellow. C) Zoomed view of the catalytic core of OTUD3. Figures B and C were generated using Pymol and pdb file 4BOU. D) Transgenic (TG) OTUD3 mice compared to wildtype (WT) mice. E) Size comparison of organs of OTUD3 TG and wildtype mice. D/E taken from [128].

Sequencing of human breast cancer tissues identified heterozygous E86K and compound heterozygous OTUD3 R79T/E86K mutations within cancer material but not within the adjacent tissue. Strikingly, cancer tissues containing the identified heterozygous *OTUD3* mutations featured remarkably reduced PTEN protein levels. Thus, loss-of-function mutations of *OTUD3* can be linked to human cancer and *OTUD3* is downregulated and promotes tumorigenesis in breast cancer [128]. Moreover, as tumor suppressor OTUD3 was reported to deubiquitinate and stabilize p53 in invasive breast carcinoma cells inducing growth inhibition and apoptosis [133]. Vice versa, in non-small lung cancer a pro-oncogenic role of *OTUD3* was shown [134].

Novel studies illustrate that OTUD3 associates with and deubiquitinates DNA topoisomerase 2A (TOP2A) that in turn interacts with PTEN [135]. TOP2A functions in chromosome untangling, segregation of sister chromatids before anaphase and is needed for decatenation checkpoint activation [136]. These findings reveal that OTUD3 plays a critical role in maintaining genomic stability by regulating decatenation processes. Descriptions of *OTUD3* linked to hereditary genetic diseases are so far missing.

2. Aims of thesis

This thesis is based on the recent finding of a novel inherited genetic neurodevelopmental syndrome in a consanguineous family of Kurdish origin [137]. Three affected children suffered from alalia, central hypotonia, mental retardation, secondary microcephaly, visual defects and seizures in their early childhood. The mother was pregnant and wished to terminate pregnancy to avoid giving birth to another affected child. A second consanguineous couple within this family revealed another severely affected child.

Using genome-wide linkage scan with subsequent fine mapping and haplotype analyses the disease locus was mapped to chromosome region 1p36.12 and affection for the unborn fetus was excluded. The mother continued pregnancy and gave birth to a healthy boy. After indirect prenatal diagnostics the determined disease-linked locus containing 58 genes was Sanger-sequenced and the potential causative genetic defect c.1061_1063delAGA located in the *OTUD3* gene was identified. In all affected children the identified mutation was homozygous, whereas parents and healthy siblings were heterozygous reflecting autosomal recessive inheritance of disease. In the context of this thesis two major aims arise:

A) Clinical relevance of *OTUD3* in human genetic developmental disease

To strengthen the putative link of *OTUD3* mutation c.1061_1063delAGA to neurological disorder further patients with similar clinical phenotypes, but without identified molecular genetic basis should be sequenced and checked for novel putative disease causing *OTUD3* mutations. In addition, a multiplex ligation-dependent probe amplification (MLPA) read out should be established to analyze copy number variations (CNV) of *OTUD3* exons. *OTUD3* sequencing and CNV analyses should contribute to a genotype-phenotype correlation of *OTUD3* to developmental human disease. First insights into the molecular consequences of the *OTUD3* mutation c.1061_1063delAGA should be provided in this thesis using patient derived cells like primary fibroblasts and lymphoblastoid cell lines (LCLs). Does the identified mutation influence the transcriptional or translational level of *OTUD3* or signaling pathways?

A) Basic characterization of *OTUD3*

It is planned to characterize *OTUD3* concerning its evolutionary conservation, expression in human tissues and localization of full-length *OTUD3* or truncated variants. Localization studies should provide novel insights into so far uncharacterized *OTUD3* domains and their functions. Applying CRISPR/Cas9 technology an *OTUD3* knock-out in different cell lines should be generated and characterized in comparison to wildtype cells. Gained knowledge about *OTUD3* and its properties is mandatory to understand how *OTUD3* defects might result in disease states and phenotypes.

3. Materials and methods

3.1 Chemicals

All chemicals were obtained by Sigma-Aldrich, Carl Roth, Merck, AppliChem or Invitrogene, unless stated otherwise.

3.2 Instruments and consumables

Table 1: List of used instruments, consumables and respective suppliers.

Instrument/ consumable	Supplier
PCR Thermocycler	
TGRADIENT Thermocycler	Biometra
Tpersonal Thermocycler	Biometra
Centrifuges	
Biofuge Pico	Heraeus
Centrifuge micro 200, Universal 210 and 320	Hettich Zentrifugen
Centrifuge 5415 R	Eppendorf
Heraeus Biofuge Stratus	Thermo Scientific
Optima TL 100 ultracentrifuge	Beckmann Coulter
Sigma 2K15	Sigma-Aldrich
Sorvall RC-5B	Thermo Scientific
Spectrophotometer	
Nanodrop® Spectrophotometer ND-100	peQLab Biotechnology
Sterile hood	
Aura 2000 M.A.C. Cell culture fume hood	BioAir Instruments
Herasafe fume hood	Thermo Scientific
KS12	Thermo Scientific
Incubator/ Thermoblock	
Biosafe Plus incubator	IBS Integra Bioscience
Heat block MS100	Universal Labortechnik
Hera cell culture incubator	Heraeus Holding GmbH
Incubator: Function line	Heraeus Instruments
Incubator shaker: innova TM430 and TM423	New Brunswick Scientific
Thermomixer 5437	Eppendorf
Shaker	
RM5V-30 CAT	M. Zipperer
Rocky 100	Labortechnik Fröbel
Electrophoresis	
Bio-Rad Gel Doc 2000	Biorad Laboratories
Electrophoresis power supply E844	Consort
Gel stick UV documentation	Intas Scientific
Power Pack P25	Biometra
Microscope	
Microscope, AxioCam, Power Supply 232	Zeiss
Zeiss Axio Imager 2 Fluorescence	Zeiss
Western Blot analyses	
BioRad Imager system	Biorad
CL-Xposure™ Film (5x7 inches)	Thermo Scientific
Western Blot Chamber	VWR
Whatman filter paper	Sigma-Aldrich
Cell culture	
Cell culture flasks (T25, T75); well plates (6-96 wells)	Sigma-Aldrich
Neubauer chamber	H. H. Medizinalbedarf
x-well Tissue Culture Chambers	Sarstedt

Table 1 continued

Instrument/ consumable	Supplier
Real-Time PCR	
MicroAmp Fast Optical 96-Well Reaction Plate (0.1 ml)	Applied Biosystems
MicroAmp™ Optical Adhesive Film	Applied Biosystems
StepOnePlus™ Real-Time PCR-System	Applied Biosystems
Fluorescence-activated cell scanning (FACS)	
Accuri™ C6	BD Biosciences
FACS-Diva™	BD Biosciences
LSR Fortessa™	BD Biosciences
Polystyrene filter cap falcons (5 ml)	Corning
Sequencing	
3500 genetic analyzer	Applied Biosystems
Others	
gentleMACS Dissociator	MACS Milteny
gentleMACS Tubes	MACS Milteny
Magnetic Stirrer	NeoLab
MicroPulser™ electroporator	VWR
Multiskan Ex platereader	Thermo Scientific
pH-Meter Delta 340	Mettler
UP200S Ultrasonic processor	Dr. Hielscher GmbH
Vortex-2 Genie	Scientific Industries
Weighing Machine KERN 440-35N	Sartorius

3.3 Enzymes/ Antibodies/ Inhibitors/ Additives

Table 2: Summary of applied enzymes, antibodies, inhibitors and additives.

Enzymes	Supplier
DpnI (20000 U/ml)	NEB
ExoSAP-IT PCR Product Cleanup	ThermoScientific
FastAP Thermosensitive Alkaline Phosphatase (1 U/μL)	ThermoScientific
5x HOT FIREPol® EvaGreen® qPCR Mix Plus (ROX)	SolisBidyne
5x FIREPol® Master Mix with 7.5 mM MgCl ₂	SolisBidyne
HindIII	NEB
Phusion Polymerase (2000 U/ml)	NEB
Q5 DNA Polymerase (2000 U/ml)	NEB
RNAse A	Sigma-Aldrich
Shrimp alkaline phosphatase (SAP) (1 U/ml)	Fermentas
Tag DNA ligase (40000 U/ml)	NEB
Taq DNA Polymerase (5000 U/ml)	NEB
T4 DNA Ligase	NEB
T4 Polynucleotide Kinase (10000 U/ml)	NEB
XhoI	NEB
Antibodies	Supplier
Donkey anti-mouse Cy3 (AP192C)	Sigma-Aldrich
Donkey anti-mouse FITC 488 (NBP1-75122)	Novus Biologicals
Goat anti-rabbit Dylight488 (ab96899)	Abcam
Monoclonal anti-acetylated-tubulin (mouse; T6793)	Sigma-Aldrich
Monoclonal anti-actin-Ab-5 (mouse; 612656)	BD Biosciences
Monoclonal anti-alpha-tubulin (mouse; T9026)	Sigma-Aldrich
Monoclonal Anti-GFP-HRP (mouse; 130-091-833)	Miltenyi Biotec GmbH
Phospho-Smad1/5 (Ser463/465) (41D10) (rabbit; 9516S)	Cell Signaling Technology
Polyclonal anti-BMP1A (ab38560)	Abcam
Polyclonal anti-OTUD3 (rabbit; NBP1-90485)	Novus Biologicals
Polyclonal anti-OTUD3(rabbit; PA5-24508)	Thermo Scientific
Secondary anti-rabbit IgG-Alexa488 (A-11034)	Invitrogen

Table 2 continued

Inhibitors	Supplier
Aprotinin	Sigma-Aldrich
FcR Blocking Reagent (mouse)	Miltenyi Biotec
LDN-193189	Cellagen Technology
Leptomycin B	Sigma-Aldrich
MG132	Sigma-Aldrich
N-Ethylmaleimide (NEM)	Sigma-Aldrich
Nocodazole	Sigma-Aldrich
Proteinase K	Sigma-Aldrich
Ubiquitin propargylamide (Ub-PA)	BostonBiochem
Ubiquitin vinylmethylester (Ub-VME)	BostonBiochem
RiboLock RNase Inhibitor (40 U/ μ L)	ThermoScientific
Additives	Supplier
ATP (10 mM)	ThermoScientific
Betaine solution (5 M)	Sigma-Aldrich
dNTP mix(10 mM each)	NEB
5x GC enhancer	NEB
NAD ⁺	Sigma-Aldrich

3.4 Kits and standards

Table 3: Applied Kits and electropheris marker.

Kits	Supplier
Annexin V-FITC apoptosis detection Kit	Abcam
AquaGenomic™ Solution (gDNA Purification)	MoBiTec GmbH
BigDye® Terminator v1.1 Cycle Sequencing Kit	Applied Biosystems
DyeEx® 2.0 Spin Kit	Qiagen
Gene Jet Gel Extraction Kit	Thermo Scientific
Gene Jet PCR Purification Kit	Thermo Scientific
GeneSolution siRNA (1 nmol)	Qiagen
HiPerFect Transfection Reagent	Qiagen
<i>In vitro</i> Toxicology Assay Kit, MTT based	Sigma-Aldrich
Lipofectamine® 2000 reagent	Invitrogene
Long PCR Enzyme Mix	Thermo Scientific
Pierce BCA Protein Assay Kit	Thermo Fisher Scientific
Pierce® ECL-Plus Western Blot Substrate	Thermo fisher
Plasmid Midi Kit	QIAGEN
POP-7™ Performance Optimized Polymer 3500 Series	Applied Biosystems
ProtoScript cDNA synthesis Kit	NEB
Quick Ligase Kit	NEB
Rneasy Mini Kit	QIAGEN
SALSA® MLPA® Reagent kit EK1-FAM P-300-100R (LOT A2-0111 and LOT B1-1014)	MRC Holland
μ MACS™ GFP Tagged Protein Isolation Kit	MACS Milteny
Standards	Supplier
1 kb DNA Marker „O“ GeneRuler, 100bp	Fermentas
Marker GeneRuler	
GeneScan™ 500 ROX™ Size Standard	Applied Biosystems
Prestained protein ladder broad range	NEB

3.5 Oligonucleotides and vectors

Sequencing, cloning and qPCR primers were derived from metabion GmbH, whereas random primers were supplied by Invitrogen. MLPA oligonucleotides were ordered as recommended by MRC Holland at Integrated DNA Technologies.

Table 4: Primers for *OTUD3* exon sequencing (gDNA template).

name	forward primer [5'-3']	reverse primer [5'-3']	size [bp]
SE1	CACGTTGAGTACCATCCACCACTAG	GCTTGTCCGCCTCACTCGCAG	666
SE2	GCATGAAGCATCATTGTTTTAGACG	CCAATGCATTACTCCTGAAGGAC	269
SE3	GCAGTCTTGTATTGTTCAACTAGC	GTTAGGCTCGTAGACCAAGTTAC	412
SE4	CCAATTAGTGTCTCATAGACCTG	CACAGATTCTCAATGCCAACTTTC	362
SE5	GTGACTCAAAGTACAATGAGTGG	CATTAAGCCACATACACTAATC	469
SE6	GGTCCTGAAACCTTGTGTTAATTC	CTGAAGCAGAGACAGGACCTAG	398
SE7	GTAGGGACCCAGGTAATTTTGG	CACACTACTTTTATAAATCAG	394
SE8	GCCACCATCTCCCTTCTAGCAGG	GGCTTCGTTGGTTGTGTTGCG	362

Table 5: Primers for qPCR analysis of *OTUD3* (cDNA template).

Name	forward primer [5'-3']	reverse primer [5'-3']	size [bp]
qOTUD3	GAGAAATAATGCAGAAGAGAATC	CTGGCACCCTGCCACCCTC	90
qGAPDH	TGCACCACCAACTGCTTAGCA	GGCATGGACTGTGGTCATGAG	87

Table 6: Primer sequences for qPCR analysis of *OTUD3* exons (gDNA template).

name	forward primer [5'-3']	reverse primer [5'-3']	size [bp]
qE1	GGAATCGGCCGGAGTCTGGC	GCACCTCCCGCAGCTTCAGC	99
qE2	GCTTGTTCAGAGCTCTTGGTGATC	CTTCCCGCTGCTTTATCATGTAGT	99
qE3	CCAGTTTGGCAAAGCCTGGTAC	CTGCCACAAAGGGGCATTAAGTTG	110
qE4	GCAGCGTGAGGGAGTTACACAT	GGAGATGTGCAGGTGCCTCTGA	96
qE5	GATCAAGACAAAGGGAATGGACTC	CATTACAACTTTCTGGACAGCATCC	77
qE6	GTCCAGAACCTGGAAGCTGAAAATT	CTTGGTTCATCCGAAGCACGGCA	77
qE7	GCAGAAGAGAATCTTGAGCCAG	GTCCTGCCTTCATTTAAGCCCTGA	116
qE8	GTCACAAACAAACAGAGGCGAGAA	GTTATTGTCCCTGTGGCTACCTCT	111

MLPA analysis of *OTUD3* exons (gDNA template):

A MLPA probe consists of two adjacent oligonucleotides: the Left Probe Oligonucleotide (LPO) and the Right Probe Oligonucleotide (RPO). All LPOs contain an identical forward primer binding site (FPBS) at their 5' end, whereas RPOs possess identical reverse primer binding sites (RPBS) at their 3' end. Fluorescently labeled primers used for probe amplification are supplied with SALSA® MLPA® Reagent kit EK1-FAM P-300-100R. To generate probes with a unique length for each *OTUD3* exon the left hybridizing sequences (LHS) and right hybridizing sequences (RHS) complementary to genomic *OTUD3* sequences and optional included stuffer regions have to differ in their length. RPOs were ordered 5' phosphorylated to ensure ligation of LPO and RPO. All oligonucleotides were designed in accordance to MRC Holland's guideline "Designing synthetic MLPA probes" version 15 [138].

Table 7: Sequences of designed MLPA probes for *OTUD3* exons.

Name	probe [5'-3'] (LPO: FPBS/ stuffer/ LHS + RPO: RHS/ stuffer/ RPBS)	size [bp]
Exon 1 (A)	LPO: GGGTTCCTAAGGGTTGGA CCTCTTA CCGGGCAGCGGCAGCCGAAAA GC RPO: CGAGGCCGAGCGCAAGCGGGACGAG TAC TCTAGATTGGATCTTGCTG GCAC	100
Exon 1 (B)	LPO: GGGTTCCTAAGGGTTGGA CAAGGAGCGGC GGAATCGGCCGAGTCT GCGGGCGGC GCGGCTGCGAGGAGGAGTTC RPO: GTCAGCTTCGCCAACCAGCTGCAGGCCCTGGGGCTGAAGCTGCGGGAG GTGCCGGGGGA C TCTAGATTGGATCTTGCTGGCAC	160
Exon 2	LPO: GGGTTCCTAAGGGTTGGA GAGCTCTTGGTGATCAATTGGAGGGACA CTCACGAAATCATC RPO: TCAAGCACAGACAGGAGACAGTGGACTACATGATAA AGC TCTAGATT GGATCTTGCTGGCAC	123
Exon 3	LPO: GGGTTCCTAAGGGTTGGA GTACTTTTGCTGGCAATGATGCAATTGTAG RPO: CCTTTGCAAGAAATCATCAGTTGAATGTAGTG TCTAGATTGGATCTTGCT GGCAC	104
Exon 4	LPO: GGGTTCCTAAGGGTTGGA CAGAGAAAAGCAGCGTGAGGGAGTTACAC ATCGCATATC RPO: GGTATGGAGAGCACTACGACAGTGTTCGGAGGATC TCTAGATTGGATCT TGCTGGCAC	116
Exon 5	LPO: GGGTTCCTAAGGGTTGGA GATCAAGACAAAGGGAATGGACTCTGAAG ACGACCTGAGAGATGA RPO: AGTAGAGGATGCTGTCCAGAAAAGTTTGT AATGCAACTGGATGTTCA G TCTAGATTGGATCTTGCTGGCAC	134
Exon 6	LPO: GGGTTCCTAAGGGTTGGA GATTTTAATTTAATAGTCCAGAACCTGGAA GCTGAAAATTATAAATTG RPO: AATCTGCAATAATTGCCGTGCTTCGGATGAA CCAAGGGAAGAGAAATA TCTAGATTGGATCTTGCTGGCAC	139
Exon 7	LPO: GGGTTCCTAAGGGTTGGA GTGGCCCTTTGTGGGAGGAGGGTGGCAG TGGTGCCAGAATCTTTGGAAATCAG RPO: GGCTTAAATGAAGGCAGGACCGAAAACAATAAGGCACAGGCCAGCCCTA TCTAGATTGGATCTTGCTGGCAC	144
Exon 8	LPO: GGGTTCCTAAGGGTTGGA GAAGAAGAAGCGGCAGGAGGAGAGGCACC GCCACAAAGCCCTGGAGAGCAGAGGTA RPO: GCCACAGGGACAATAACAGAAGCGAAGCAGAGGCCAACACGCAGGTCAC CTTGGT CTAGATTGGATCTTGCTGGCAC	153

Table 8: *OTUD3* variants, cloning primers and vectors.

name (amino acids)	Vector	source/ cloning primer [5'-3']
<i>OTUD3</i> knock-out		
<i>OTUD3</i> CRISPR/Cas9 KO Plasmid (human) (sc-407077)	---	Santa Cruz Biotechnology
<i>untagged OTUD3</i> variants		
<i>OTUD3</i> wildtype (1-398)	pCS2+	C. Mai, group of Prof. Hollemann, Martin-Luther-University Halle- Wittenberg
<i>OTUD3</i> ΔK356 (1-397)	pCS2+	C. Mai, group of Prof. Hollemann, Martin-Luther-University Halle- Wittenberg
<i>N-terminal GFP tagged OTUD3</i> variants		
WT (1-398)	pEGFP C1	Prof. T. Pfirrmann, group of Prof. Hollemann, Martin-Luther-University Halle- Wittenberg
ΔK356 (1-379)	pEGFP C1	Prof. T. Pfirrmann, group of Prof. Hollemann, Martin-Luther-University Halle- Wittenberg
C76S (1-398)	pEGFP C1	Prof. T. Pfirrmann, group of Prof. Hollemann, Martin-Luther-University Halle- Wittenberg
ΔNterm (65-398)	pEGFP C1	this work/ SOMA primer: GTACAAGTCCGGACTCAG ATCTCGACTGAAGCTGCGGGAGGTGCCGGGGGACGGC A
ΔCterm (1-271)	pEGFP C1	this work/ fwd: CAGATCTCGAGAATCCCGAAAG rev: GTACCAAGCTTTCACCGAAGCACGGCAATTATTGC

Table 8 continued

Δ Nterm Δ OTU (190-398) and Δ Nterm Δ OTU Δ K356 (190-397)	pEGFP C1	this work/ fwd: GTCAACTCGAGGAAATGACAACCTCAGAGGCAC rev: GAATTCGAAGCTTGAGTCAGATG
Δ Nterm Δ OTU Δ UBA (271-398)	pEGFP C1	Prof. T. Pfirmann, group of Prof. Hollemann, Martin-Luther-University Halle- Wittenberg
Δ UBA Δ CTerm (1-229)	pEGFP C1	this work/ fwd: CAGATCTCGAGAATCCCGAAAG rev: GTACCAAGCTTTCATCTCAGGTCGTCTTCAGAG

3.6 Bacterial strains/ mammalian cell lines

Table 9: List of bacterial strains and suppliers.

Bacterial strains	Supplier
<i>E. coli</i> XL1-Blue	Stratagene
HaCaT	Martin-Luther-University Halle-Wittenberg, Prof. Seliger
HEK293T	ATCC
HeLa	ATCC
HT22	Martin-Luther-University Halle-Wittenberg, Prof. Dehghani
LCLs	Charité Berlin, Prof. K. Sperling
NiH3T3	ATCC
Primary fibroblasts	Charité Berlin, Prof. K. Sperling

3.7 Patient material

DNA samples of patients with similarity to AS but without identified molecular basis were derived from the Institute of Human Genetics Halle (Prof. K. Hoffmann) and the Institute of Human Genetics, Charité Berlin (Prof. K. Sperling). DNA samples from healthy blood donors were available at the Institute of Human Genetics Halle (Prof. K. Hoffmann). Frozen post-mortem tissues of human brain areas of schizophrenia patients were obtained from the Institute of Forensic Medicine of the Johann Wolfgang Goethe University in Frankfurt, Main, Germany (group of Prof. Rujescu). The research was approved by the University's Internal Review Board. LCL and primary fibroblast cultures of patients and sex and age matched controls were provided by the Institute of Human Genetics, Charité Berlin (Prof. K. Sperling). All used patient derived samples were collected after obtaining written informed consent from the participants in accordance with the ethics committee.

3.8 Media/buffers/antibiotics/supplements

10x PBS: 1.37 M NaCl, 27 mM KCl, 80 mM Na₂HPO₄, 18 mM KH₂PO₄ in dH₂O, pH 7.4

TE buffer: (Tris/EDTA buffer): 10 mM Tris-HCl (pH 7.5) with 1 mM EDTA

MT buffer (microtubule buffer): 0.1 M PIPES, 2 mM EDTA, 1 mM EGTA, 0.5 % (v/v), Triton-X-100; 4 M Glycerin, pH 6.9

UC buffer (ultracentrifugation): 50 mM HEPES, 0.15 M NaCl, 1% (v/v) NPI-40, 0.5 % (w/v) Sodium deoxycholate, 0.1 % (w/v) SDS pH 7.4

10x TBE buffer: 0.89 M Tris, 0.89 M boric acid and 20 mM EDTA in dH₂O.

10x Agarose gel loading buffer: 50 mM EDTA, 50% glycerol (v/v), 0.05% Bromphenol blue and 0.05% Xylencyanol in 20 mM Tris-HCl, pH 7.5.

Luria-Bertani (LB) medium: 20 g LB Base dissolved in 1 l dH₂O and autoclaved

Luria-Bertani (LB)- agar plate: 32 g LB Agar dissolved in 1 l dH₂O and autoclaved. If necessary, ampicillin (100 µg/ml), kanamycin (30 µg/ml) or tetra cycline (12.5 µg/ml) was added (agar temperature below 50°C).

Cell culture media and supplements:

DMEM, RPMI-1640 and DMEM/ HamsF12 (1:1) media were obtained from Sigma. Media were supplemented with 10% heat inactivated fetal calf serum (FCS), 2 mM L-glutamine, 100 U/ml penicillin and 100 µg/ml streptomycin all supplied by PAA and further referred to as cultivation medium.

10x SDS running buffer: 0.25 M Tris pH 8.8, 1.92 M glycine, 1 % SDS (w/v)

5x SDS sample buffer: 300 mM Tris/ HCl pH 6.8, 10% (w/v) SDS, 50% (v/v) glycerine, 0.5% (w/v) bromphenol blue, (5 mM DTT was freshly added before use)

resolving gel (10%)

5.0 ml Rotiphorese® Gel 30
3.8 ml 1.5 M Tris/HCl pH 8.8,
0.2% (w/v) SDS
6.2 ml H₂O
120 µl 10% (w/v) APS
12 µl TEMED

stacking gel (4%)

0.4 ml Rotiphorese® Gel 30
0.75 ml 0.5 M Tris/HCl pH 6.8,
0.2% (w/v) SDS
1.85 ml H₂O
12 µl 10% (w/v) APS
3 µl TEMED

Western blot transfer buffer: 150 mM glycine, 20 mM Tris/HCl (pH 8.3), 10% (v/v) Ethanol 96%

10x Ponceau staining solution: 2% (w/v) Ponceau S, 30% (w/v) TCA, 30% sulfosalicylic acid

10x TBS buffer : 730 mM NaCl, 27 mM KCl, 4 M Tris, pH 7.5

TBST buffer: 1x TBS buffer + 0.1% Tween 20 (v/v)

3.9 Micro- and molecular biology

3.9.1 Transformation of *E. coli* via electroporation

1-10 ng plasmid or up to 2 µl of ligation reaction was added to 50 µl electrocompetent *E. coli* XL1 blue cells on ice and gently mixed. After 5 min the set up was transferred to a precooled 1 mm electroporation cuvette. The cuvette was placed to an electroporator and pulsed once with 500 V for 8 msec. 600 µl prewarmed LB medium was used for resuspension. After 30 min at 37°C the cells were plated on a LB agar plate containing a respective antibiotic for selection. Plates were incubated at 37°C overnight.

3.9.2 Plasmide isolation

Plasmid preparation was performed using Plasmid Midi Kit (Qiagen) in accordance to the manufacturer's protocol.

3.9.3 Single Oligonucleotide Mutagenesis and cloning Approach

Single Oligonucleotide Mutagenesis and cloning Approach (SOMA) was applied to generate *N*-terminal GFP-tagged OTUD3 variant lacking the *N*-terminal domain (Δ NTerm (65-398 aa)) of OTUD3 in pEGFP C1 vector (see 3.5) [139]. First, the SOMA oligonucleotide designed for Δ NTerm OTUD3 variant in pEGFP C1 vector was 5' phosphorylated in a 50 μ l set up. The reaction contained 1x reaction buffer, 4 mM Δ Nterm (65-398) oligonucleotide (see 3.5), 1 mM ATP, 10 U T4 polynucleotide Kinase and dH₂O and was incubated for 30 min at 37°C followed by an enzyme inactivation step at 65°C for 20 min. Secondly, the following 50 μ l SOMA reaction was prepared: 1x High-Fidelity buffer, 0.2 mM 5' phosphorylated oligonucleotide Δ NTerm (65-398), 100 ng pEGFP C1 plasmid template (containing WT OTUD3 (1-398 aa)) (see 3.5), 1 mM NAD⁺, 2 U High-Fidelity DNA Polymerase, 1 μ l *Taq*-Ligase, 0.2 mM dNTPs and dH₂O. In a thermo cycler the set up was initially denatured for 1 min at 95°C. Afterwards, DNA was amplified in a 30 cycle reaction (denaturation: 95°C- 1 min; annealing: 55°C- 1 min; extension and ligation: 65°C- 4 min). *DpnI* digestion according to the manufacturer's protocol was performed to specifically degrade methylated template DNA [140]. Mutagenized plasmid was purified using Qiagen PCR purification kit and transformed as described in 3.9.1 into *E. coli* and plated for selection on agar plates containing kanamycin. On the next day, single clones were picked and plasmid preparations (see 3.9.2) were conducted. Positive clones were first screened by diagnostic restriction digestion with *XhoI* and *HindIII*. Therefore, up to 1 μ g plasmid DNA was double digested at 37°C for 2 h with 2 U of each restriction enzyme in 1x cut smart buffer. Fragments were separated on 1.5% agarose gels by electrophoresis (see 3.9.11). Positive clones were further confirmed by sanger-sequencing (see 3.9.5).

3.9.4 Cloning

Cloning of *N*-terminal GFP-tagged OTUD3 variants Δ NTerm, Δ CTerm, Δ NTerm Δ OTU, Δ NTerm Δ OTU Δ K356 and Δ UBA Δ CTerm was performed using primers containing 5' restrictions sites (see 3.5). The forward primers contained a 5' *XhoI* restriction site, whereas the reverse primers contained a 5' *HindIII* site. Respective PCR products for cloning were generated in a 25 μ l reaction volume containing: 0.5 U Q5 Polymerase, 0.4 mM dNTPS, 0.5 μ M forward primer, 0.5 μ M reverse primer, 100 ng template (pEGFP C1 containing WT or Δ K356 OTUD3), 1x Q5 buffer, 1x QC enhancer, 2% (v/v) DMSO and dH₂O. Reactions were 5 min denatured at 95°C, followed by a cycling

program (32 cycles: 98°C 30 s, 60°C 30 sec, 72°C 30 s). PCR products were visualized with UV light on a 1.2 % agarose gel and sliced for further purification applying Gene Jet Gel Extraction Kit protocol. 2 µg of purified PCR product was double digested with 50 U *Xho*I and *Hind*III each in 1x cut smart buffer for at least 6 h. Double digested PCR products were purified with Gene Jet PCR Purification Kit.

In addition, 5 µg of pEGFP C1 vector containing WT *OTUD3* was double digested with 20 U *Xho*I and 20 U *Hind*III and simultaneously dephosphorylated with 4 U FastAP in 1x cut SMART buffer at 37°C overnight. Digested vector was separated via agarose gel electrophoresis on a 0.8% agarose gel and afterwards sliced from the gel. The linearized vector was purified from the gel slice using Gene Jet Gel Extraction Kit.

Ligation of vector and PCR product was performed according to the Quick Ligase Kit protocol of NEB. Positive clones were screened by diagnostic restriction with *Xho*I and *Hind*III and further confirmed by sanger-sequencing (see 3.9.5).

3.9.5 Sanger sequencing

For sequencing Sanger method was applied [141]. Exons and flanking intron regions of genes were PCR amplified from purified g;cDNA samples. Standard PCR was performed in a 25 µl reaction including 1x FIREPol® Master Mix with 7.5 mM MgCl₂, 1-100 ng template gDNA and 0.4 µM of forward and reverse primer. Cycling included a 10 min initial denaturation step, followed by 30- 34 cycles of 30 s denaturation, 45 s annealing and 40 s of elongation.

Depending on the quantity of visualized PCR product on 1.5% agarose gel 1-4 µl of reaction were mixed with 0.5 µl ExoSAP-IT and H₂O (ad 5 µl) and incubated for 15 min at 37°C. Reaction was terminated by an incubation step at 80°C for 15 min. Afterwards, 2.3 µl H₂O, 2 µl BigDye™ Terminator v1.1 5X Sequencing Buffer, 0.4 µl BigDye™ Terminator 3.1 Ready Reaction Mix and 0.3 µl of sequencing primer (10 µM) was added to the tube. Reactions were placed in a thermo cycler with the following cycling conditions: 96°C 1 min, 25 cycles: 96°C for 10 s, 50°C for 5 s and 60°C for 4 min. After cool down to 4°C reactions were loaded on DyeEx® 2.0 Spin Kit columns for purification. All steps were performed as described by the manufacturer. Purified product was transferred in a 96 well plate and 12 µl of Hi-Di™ formamide was supplemented. For analyses, samples were loaded at the Institute for Human Genetics or the „Zentrum für Medizinische Grundlagenforschung“ (ZMG) in Halle on ABI-Prism 3100 Genetic Analyzer instrument. For high throughput DNA sequencing GATC LIGHTRUN 96 service was utilized. Evaluation of sequences was supported by sequence scanner and sequence pilot software at the Institute of Human Genetics in Halle.

3.9.6 DNA precipitation

To purify or concentrate solutions containing DNA ethanol precipitation was performed. 10% (v/v) 3 M sodium acetate (pH 5.2) was added to the DNA solution and vortexed. 1.5 fold volumes of cold absolute ethanol were supplemented and the tube was inverted a few times. The set up was incubated at -20°C at least 2 h or overnight. Next, the tube was centrifuged 15 min at full speed in a benchtop centrifuge to pellet DNA. The supernatant was discarded and the pellet was washed twice with 75% ethanol. The pellet was air dried for 10 min and resuspended in water or for MLPA assay in TE buffer (10 mM Tris-HCl pH 8.2, 0.1 mM EDTA).

3.9.7 DNA extraction

gDNA was extracted from cell culture material with AquaGenomic™ Solution Kit from MobiTec GmbH in accordance to the manufacturer's instructions.

3.9.8 RNA extraction

RNA was isolated from 25 cm² confluent primary fibroblast cultures or LCL suspensions using Rneasy Mini Kit according to the manufacturer's protocol.

Frozen post-mortem tissues of human brain areals of shizophrenia patients were investigated for *OTUD3* mRNA levels. 1 ml Trizol reagent was added to ~100 mg of brain tissue and the sample was homogenized using gentleMACS™ Dissociator. Afterwards, the set up was centrifuged for 3 min at 3000 rpm at 4°C. The supernatant was collected and transferred into a new tube and incubated for 5 min at room temperature. 200 µl of chloroform was added and the sample was mixed rigorously. After 3 min of incubation the sample was centrifuged (15 min, 10000 rpm, 4°C). The upper phase was mixed with 500 µl isopropanole and after 10 min of incubation the samples were centrifuged for 10 min at 10000 rpm and 4°C. The RNA pellet was washed twice with 500 µl 75% ethanole. The pellet was air dried and resuspended in 30-50 µl DEPC-water.

RNA extraction from HEK293T and HeLa cells was mainly conducted as described above using Trizol reagent. In contrast, pelleted cells were lysed using a 20G needle and syringe. RNA was subsequently used for cDNA synthesis or stored at -80°C for further processing.

3.9.9 cDNA synthesis and qPCR

OTUD3 mRNA levels were investigated in primary fibroblasts (patients:787, 788; matched controls: ctrl1, ctrl2), LCLs (patients:179 (784), 180(788); matched controls: 126, 1095), HEK293T and HeLa cells, human post-mortem brain material and a RNA panel of 18 human tissues (Stratagene) by quantitative PCR (qPCR).

1 µg of total RNA was reverse transcribed into cDNA in a 20 µl reaction set up using ProtoScript cDNA synthesis Kit and random hexamer primers. A 20 µl qPCR set up contained 10 ng cDNA, 1x HOT FIREPol® EvaGreen® qPCR Mix Plus (passive reference ROX), and 1.25 µM primers. Used intron-spanning PCR primer pairs for *OTUD3* and *GAPDH* as endogenous control see 3.5. Primer pair efficiency was controlled in a standard template dilution experiment and calculated to be similar (*OTUD3*: 96.7%; *GAPDH*: 98.2%; data not shown). A qPCR run on StepOnePlus (ABI) started with an initial hot start for 15 min at 95°C, followed by 36 cycles with a denaturation step for 20 s at 95°C, 30 s annealing step at 55 °C and an extension step of 20 s at 72°C. Afterwards, a melt curve was recorded. First, the samples were heated for 30 s at 95°C and then cooled for 30 s at 65 °C. The samples were heated again to 95°C and in increments of 0.3°C fluorescence signals were measured to confirm homogeneity of the generated PCR product. $2^{-\Delta\Delta C_t}$ method established by Livak and Schmittgen and the SteponePlus software package (ABI) was used to determine relative expression levels [142]. Data were collected in triplicates and in three independent experiments. Results are presented as mean \pm SEM. *OTUD3* expression in human brain post-mortem material from three unrelated subjects was analysed and data were collected for each brain area in triplicates. Data are shown as mean \pm SD.

3.9.10 Nucleic acid concentration determination

Nucleic acid concentrations were determined by NanoDrop instrument measuring UV absorption at 260 nm in 2 µl of a loaded sample. An absorption of 1 at 260 nm equals a concentration of 50 ng/ µl for dsDNA and 40 ng/ µl for ssRNA. A ratio of A260/ A280 above 1.8 was indicative for pure DNA and ~2.0 for pure RNA preparation.

3.9.11 Agarose gel electrophoresis

PCR fragments were separated depending on their size on 0.8% – 2% (w/v) agarose gels in 1x TBE buffer for up to 90 min and 80- 150 V. For visualization 1 µl ethidium bromide (10 mg/ ml) per 50 ml of heated agarose gel solution was added. 5 µl of standard markers were loaded on the gel for size control of produced fragments (see 3.4). Samples were 1:10 diluted in 10x loading buffer. After sample loading and separation, products were visualized using the UV light Gel Doc system from Biorad.

3.9.12 Multiplex ligation-dependent probe amplification (MLPA)

MLPA experiments were performed according to MRC Holland's one-tube protocol for DNA detection and quantification [143]. All DNA samples used for MLPA were ethanol precipitated and the pellet was resuspended in TE buffer (10 mM Tris-HCl pH 8.2, 0.1

mM EDTA) to exclude buffer effects during MLPA evaluation. A reaction contained 75 ng of gDNA that was denatured for 20 min at 95°C in a total volume of 5 µl TE buffer. Afterwards, 1.5 µl MLPA buffer, 0.5 µl *OTUD3* specific probemix (containing 0.8 µl of 1 µM oligonucleotide and 200 µl TE buffer) and 1 µl P300 reference probemix (kit supplied containing control oligonucleotides; Lot: P300-B1 or P300-A2) was added and hybridized for 16-18 h at 60°C.

On the next day, oligos were ligated to target gDNA. Therefore, the cycler temperature was set to 54°C. Premixed ligase reaction (25 µl dH₂O, 3 µl Ligase-A buffer, 3 µl Ligase-B buffer and 1 µl Ligase65- enzyme) was added to the tubes. Ligation was performed for 15 min at 54°C and terminated at 95°C for 10 min. A volume of 10 µl PCR master mix (7.5 µl dH₂O, 2 µl SALSA PCR primer mix, 0.5 µl SALSA polymerase) was added. PCR included 35 cycles of: 95°C for 30 s, 60°C for 30 s, 72°C for 1 min and a final incubation at 72°C for 20 min. Finally, 1 µl reaction was supplemented with 0.4 µl ROX-500 size standard and 8.9 µl in Hi-Di formamide. Before fragments were separated using ABI 3130xl Genetic Analyzer C at the „Zentrum für Medizinische Grundlagenforschung“ the set up was denatured 5 min at 95°C. Evaluation of MLPA experiments was supported by sequence pilot software and MLPA tool.

3.9.13 Long-range PCR

Long-range PCR was performed in compliance with the Long PCR Enzyme Mix Kit protocol. In brief, a 50 µl set up was prepared and cycled in a thermo cycler as described below:

50 µl reaction:

100 ng gDNA
1x Long-range PCR reaction buffer + MgCl₂
0.2 mM dNTPs
1 µM of each primer (forward and reverse)
4% (v/v) DMSO
1 U Enzyme Mix
ad 50 µl H₂O

PCR program:

5 min at 95°C
36 cycles: 20 s at 95°C
30 s at 60°C
3-10 min at 68°C
(depending on fragment size)
5-15 min at 68°C
(depending on fragment size)
hold at 12°C

3.9.14 Alignment and evolutionary conservation analyses

Fasta sequences of *OTUD3* from different species were obtained by Blast tool [144] and aligned using T-Coffee and Boxshade tool [145]. A phylogenetic tree was established using maximum-likelihood and one-click mode procedure [146]. Data collected from the genomic web tool [147], ncbi gene [148] or Xenbase [149] was utilized for synteny analyses.

GenBank accession numbers: *Branchiostoma belcheri* XM_019782191; *Crassostrea gigas* XM_011447637; *Coturnix japonica* XM_015882304; *Danio rerio* NM_212922; *Gallus gallus* XM_424363; *Homo sapiens* NM_015207; *Mesocricetus auratus*

XM_005081047; *Monodelphis domestica* XM_001377743; *Mus musculus* NM_028453; *Oryctolagus cuniculus* XM_002716005; *Pan troglodytes* XM_513073; *Rattus norvegicus* NM_001191983; *Strongylocentrotus purpuratus* XM_001191596; *Takifugo rubripes* XM_003962965; *Xenopus laevis* NM_001095317; *Xenopus tropicalis* NM_001005056; *Ictalurus punctatus* XM_017487660; *Python bivittatus* XM_007423107; *Pogona Vitticeps* XM_020781148; *Corvus cornix cornix* XM_010412490; *Bos taurus* XM_002685731; *Physeter catadon* XM_007121577; *Calithrix jacchus* XM_009000544; *Macaca mulatta* XM_015129797; *Cavia porcellus* XM_003471361.

3.10 Biochemical analyses

3.10.1 SDS PAGE

Electrophoretic separation of protein samples was performed discontinuously and under denaturing conditions as described earlier [150]. Polyacrylamide (PA) gels (dimensions: 8x 11 cm and 0.8 cm thickness) were composed of a 10 % resolving gel covered by a 4% stacking gel (see 3.8). Samples were diluted 1:5 in 5x SDS sample buffer, heated for 5 min at 95°C and afterwards indicated amounts of samples were loaded on the gel. As size standard 5 µl of PageRuler™ prestained protein ladder was loaded. Electrophoresis was run at 120 V for up to 60 min in 1x SDS running buffer and in VWR SDS PAGE chambers.

3.10.2 Western blot

The transfer of proteins from SDS PA gels to nitrocellulose membranes was carried out by tank blot procedure according to the instructions of the blot chamber manufacturer VWR [151]. Blotting was conducted in pre-cooled western blot transfer buffer, at a voltage of 300 mA for 90 min and stirring. Afterwards, the nitrocellulose membrane was reversibly stained in 1x Ponceau staining solution to control protein transfer to the membrane. Membranes were blocked in 1x TBST containing 5% (w/v) milk powder for 2-3 h at room temperature. Then, membranes were incubated with respective primary antibodies and indicated dilutions overnight at 4 °C (see 3.3). On the next day, membranes were washed 3x in 1x TBST for 10 min, before an HRP- coupled secondary antibody was applied (see 3.3) for 1 h at room temperature. Membrane was washed again 3x for 10 min in 1x TBST. Detection was performed using Pierce® ECL- Plus Western Blot Substrate Kit and CL- Xposure™ films or a BioRad Imager system. For loading control experiments, membranes were stripped in 0.2 M glycine, 3.5 mM SDS, 1% (v/v) Tween-20 (pH 2.2) for 20 min. Afterwards, membranes were washed 5 times for 5 min in 1x TBST prior blocking for 1 h in 1x TBST containing 5% (w/v) milk powder. All experiments were performed three times.

3.10.3 NaDoc/ TCA precipitation

Sodium deoxycholate binds to proteins in a similar manner like SDS and the addition of TCA leads to the formation of deoxycholic acid whereupon proteins quantitatively precipitate. Thus, this method can be used to concentrate protein solutions or to desalt protein solutions [152]. 10 % (v/v) of a 1% sodium deoxycholate and 20% (v/v) of a 50% TCA solution was added to the sample. The tube was inverted several times and centrifuged for 15 min at 13 000 rpm at 4°C. The pellet was washed with 1 ml of cold acetone and centrifuged again before it was resuspended in 1x SDS sample buffer.

3.10.4 pSMAD1/5 read out

5x 10⁵ LCLs from patients and sex- and age-matched controls were seeded and cultivated with or without 100 ng/ml recombinant human BMP4 (R&D Systems) in 24-well plates for 20 h. Intracellular pSMAD1/5 levels were determined on fixed cells as recently described [153]. In brief, prior to specific antibody staining in FACS buffer (PBS, 1% FCS, 0.3 mM EDTA) cells were incubated with FcR Blocking Reagent (1:1000 dilution) for 15 min on ice. Cells were fixed for 10 min at 37°C with 4% paraformaldehyde. After two washing steps cells were permeabilized in 90% methanol buffer for 30 min on ice. Antibody staining was performed using anti-phospho-SMAD1/5 and anti-rabbit IgG-Alexa488 antibody in FACS buffer for 30min on ice (see 3.3). Flow cytometry data were collected using LSR Fortessa™ flow cytometer and FACS-Diva™ instrument and FlowJo™ (Tree Star) software. Comparison of protein levels between individuals *delta mean fluorescence intensities* Δ MFI, meaning the subtraction of background MFI from specific MFI, was calculated. Experiments were 3-5 times replicated and t-test was performed to check significance of results.

3.10.5 Cell fractionation by ultracentrifugation

Cells were seeded in 10 cm² plates. At 80% of confluency cells were transfected with pCS2+ plasmid coding for wildtype OTUD3 according to the Lipofectamine® 2000 reagent transfection protocol (see 3.11.4). 16-20 h later, medium was refreshed and if needed nocodazole was supplemented for 2 h at 37°C. Afterwards, cells were lysed in 1 ml UC buffer for 20 min on ice. 50 µl of lysate were diluted 1:2 in 5x SDS sample buffer for analysis. The residual lysate was centrifuged at 4°C for 10 min. 750 µl of the supernatant were further centrifuged for 1 h at 80 000 rpm in a cooled ultracentrifuge. Supernatant containing the soluble tubulin fraction was mixed 1:1 with 5x SDS sample buffer. The insoluble pellet fraction including polymerized tubulin was washed twice with cold acetone before 250 µl of heated 5x SDS sample buffer were added. The pellet fraction was sonicated for 30 s with amplitude of 6. Indicated amounts of

collected samples were loaded on SDS PA gels, separated by electrophoresis and analyzed by western blot (see 3.10.1 and 3.10.2).

3.10.6 Ubiquitin conjugation assay

Cells were seeded in 6 well plates and allowed to grow to 90% confluency. After trypsinization and two washing steps with PBS cell pellets were lysed in 20 mM Tris/HCl (pH 8.0), 100 mM NaCl, 1 mM EDTA, 0.5 % (v/v) Triton-X100 and freshly added 1 mM PMSF, 1 mM Aprotinin, 50 μ M MG132, 1 mM DTT and 2 mM ATP.

Cell lysates were incubated 1 h at 37°C with or without 1 μ g Ubiquitin-propargylamid (Ub-PA) or Ubiquitin-vinylmethylester (Ub-VME). Ub-PA/ Ub-VME is an irreversible cysteine protease specific inhibitor. Linked ubiquitin molecule leads to a size shift of ~ 8 kDa of the analyzed protease in western blot analyses. In addition, if indicated 10 mM N-ethylmaleimide (NEM) as irreversible cysteine protease inhibitor was added 15 min prior to ubiquitin-substrates. Reactions were terminated by the addition of 1x SDS loading buffer supplemented with 5% (v/v) β - mercaptoethanole and heated for 10 min at 95°C. Samples were analyzed by SDS gel electrophoresis and western blot analyses (see 3.10.1 and 3.10.2).

3.11 Cell biological analyses

3.11.1 Cultivation, passaging and cryopreservation of cells

All cells were cultured at 37°C and humidified 5% CO₂ atmosphere using specified medium and supplements in the cell culture incubator Hera cell. Cells were passaged every 3-4 days at high confluency and split in a ratio of 1:4. For detachment, cells were incubated 5 min with trypsin/EDTA at 37°C and centrifuged 5 min at 110 g. Pellets were washed twice with PBS before seeding into a new flask.

For storage, cryo cultures were prepared. 0.5- 1x 10⁶ cells were resuspended in FCS containing 10 % (v/v) DMSO and stored at -150°C in a N₂ freezer.

3.11.2 Cell counting assay

Cell numbers were determined using a Neubauer chamber and microscope. Only living cells were counted. Discrimination between living and dead cells was carried out by trypan blue staining. Therefore, LCL cells were pelleted by centrifugation (110 g, 3 min) and washed once with PBS. Pellets were mixed in a 1:1 ratio with PBS and trypan blue solution (0.4%) before counting of at least four 1 mm² squares (divided in 16 squares with 0.25 mm x 0.25mm areas).

1 ml cultivation medium containing 5x 10⁴ LCL cells of OTUD3 defect patients and matched controls were seeded into a 12-well plate. Freshly seeded wells were subsequently counted (t=0). The plate was incubated for 72 h at 37°C. After 24 h and

48 h 500 µl fresh cultivation medium was added. After 72 h cell number was determined as described above. All samples were seeded and evaluated as duplicates. Three independent experiments were performed and data are given as SEM. Statistical significance was calculated applying t-test method.

3.11.3 Protein concentration measurement using BCA assay

Determination of protein concentration within cell lysates was performed according to the Pierce BCA Protein Assay Kit. Reaction were set up in 96-well plates as triplicates and read out occurred in a microplate reader at 560 nm wavelength.

3.11.4 Transfection of plasmids and siRNAs

Transfection of plasmids was performed using Lipofectamine® 2000 reagent protocol. Afterwards, transfection complexes were added in a drop wise manner to the cultivation medium of ~ 80% confluent cells. Cells were incubated 16-20 h at 37°C and were further analyzed. siRNA transfections were performed using HiPerFect Transfection Reagent kit and manufacturer's instructions. Four siRNAs targeting OTUD3 (GeneSolution siRNAs Kit) were co-transfected in cells with a final concentration of 20 nm each. As control a Mock siRNA was transfected. After 24 h cells were analyzed via fluorescence microscopy or cell lysates were analyzed by western blot approach (see 3.11. 8 and 3.10.2).

3.11.5 Synchronization of HeLa cells

To investigate, if endogenous OTUD3 co-localizes with tubulin structures during mitosis HeLa cells were G2-M phase synchronized. Cells were seeded in 12-well plates on coverslips. At 50-60% confluency, 5 mM thymidine was supplemented for 18 h. Medium was replaced and after 8 h of incubation 100 ng/ ml nocodazole was added for further 16 h. Medium was changed and after 1 h of incubation cells were fixed on the coverslip according to 3.11.8.

3.11.6 Induction of primary cilia in NiH3T3 cells

At 50-60% confluency cultivation medium was replaced by medium without FCS and cells were starved for 36-48 h at 37°C to induce primary cilia in NiH3T3 cells.

3.11.7 MTT assay

The 3-(4,5-dimethylthiazol-2-yl)-2,5-diphenyltetrazolium bromide (MTT) dye was used to investigate the metabolic activity of LCL cells of patients and matched controls. MTT is a yellow and water soluble tetrazolium dye, which gets reduced by cellular NAD(P)H-dependent oxidoreductases forming an insoluble and violet formazan product. The MTT assay was performed in two different modes:

A) Applying a constant cell number: 5×10^5 cells were pelleted in tubes by centrifugation at 110 g for 5 min followed by one PBS washing step. Pellets were gently resuspended in 110 μ l MTT solution (100 μ l PBS, 10 μ l MTT dye) and subsequently incubated at 37°C for 2 h. Insoluble formazan crystals were dissolved by adding 100 μ l MTT solubilization solution and mixing. Read out was carried out in a 96-well plate reader of 100 μ l of solution at 560 nm wavelength and 690 nm.

B) Time dependency experiment: 1×10^5 cells were seeded in 1 ml cultivation medium per well in 12-well plates. After 0, 24, 48 and 72 h MTT read out was performed as described for A. 500 μ l fresh cultivation medium was added after 24 and 48 h to the wells. For evaluation, MTT signal at $t = 0$ h was normalized to 1 and results are given as x-fold viability, thus reflecting the number of viable cells.

Recorded values at 560 nm were subtracted by the values measured at 690 nm. Measurements were performed in triplicates and in five independent experiments. Significance of results was tested using t-test.

3.11.8 Immunofluorescence microscopy

For immunofluorescence analysis, cells were seeded on coverslips in 12-well plates under standard conditions. In case of primary fibroblasts, HT22 and HEK293T cells were grown on poly-lysine coated cover slips. NiH3T3 cells were grown on 0.1% (w/v) gelatin coverslips. Depending on the compatibility of the primary antibodies cells were fixed and permeabilized by two methods:

(a) Cells were washed twice with PBS prior fixation in 4% paraformaldehyde (PFA) for 30 min at 4°C. Afterwards a permeabilization step in PBS containing 0.2% (v/v) Triton X-100 for 5 min at 4°C was performed. (b) Cells were fixed in -20°C cold methanole for 10 min. Dried coverslips were incubated for 10 min at room temperature in MT buffer.

In accordance, cells were washed (3x 10 min PBS) and 30 min incubated in PBS and 2% BSA. Coverslips were incubated with indicated primary at 4°C overnight. Next, coverslips were washed with PBS (3x 5 min) and blocked with 2% (w/v) BSA in PBS for 30 min. Finally, fluorescently labeled secondary antibodies were applied for 1 h at 37°C. After 2x 5 min washing steps in PBS coverslips were dipped 5x into water to remove remaining salts and once into ethanol for dehydration. DNA was stained with DAPI diluted in Mowiol which was used to fix the coverslip onto a microscope glass slide. Pictures were taken with Zeiss Fluorescence Microscope.

3.11.9 Generation of *OTUD3* knock-out cell lines using CRISPR/ Cas9

To generate *OTUD3* knock-out (k.o.) cell lines commercially available *OTUD3* CRISPR/Cas9 KO Plasmid was used [154]. The protocol to obtain and identify *OTUD3* k.o. clones is established in chapter 4.6.

4. Results

4.1 OTUD3 is highly evolutionary conserved

Sequence alignments of DUBs and an available crystal structure of truncated OTUD3 (aa 52-209 of 398) proved that OTUD3 contains a highly conserved OTU domain and a UBA domain. The OTU domain (aa 65-189) comprises a catalytic triad of a conserved cysteine, aspartate and histidine residue mediating cysteine protease activity, whereas the UBA domain (aa 230-270) is a well described interaction site for ubiquitin, UBLs or other proteins in literature [127,155]. No data is available characterizing genomic *OTUD3* conservation, full-length OTUD3 protein conservation or focusing the *N*- and *C*-terminal regions and their potential structures or functions.

First, vertebrate synteny analysis was performed (see 3.9.14). BLAST analysis revealed a high degree of similarity of gene arrangements surrounding the *OTUD3* locus in different eukaryotic classes like Mammalia, Aves, Actinopterygii and Amphibia. Notably, upstream of *OTUD3* numerous linear ordered *PLA2* genes were found, whereas downstream of *OTUD3* an arrangement of genes encoding *NBL1*, *HTR6*, *TMCO4* and *RNF186* was present. Only in zebrafish less genomic conservation was observed (Figure 6A).

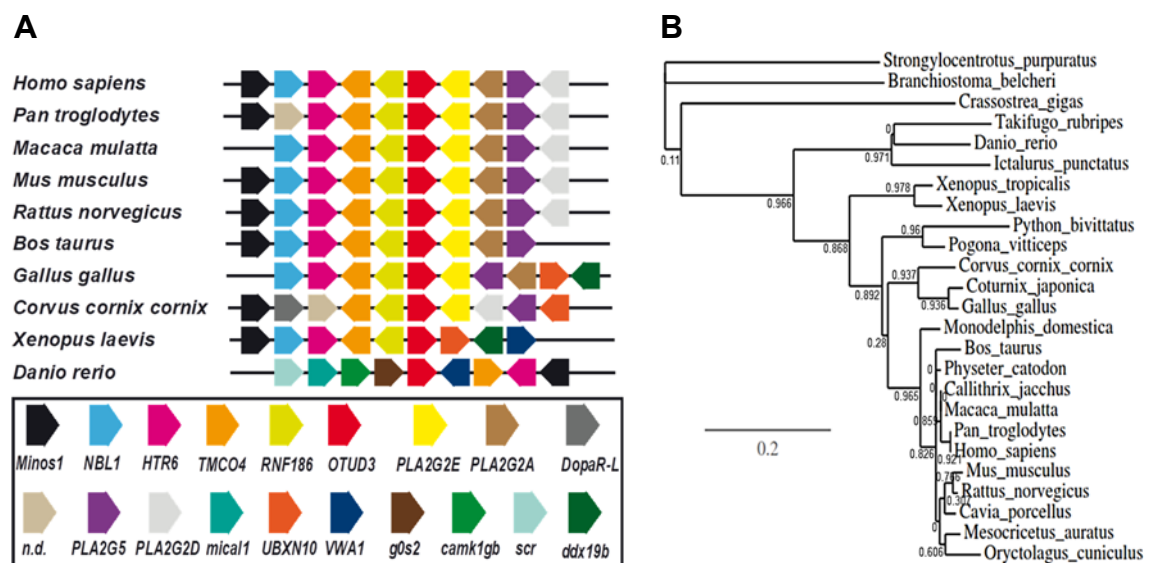


Figure 6) *OTUD3* gene locus and *OTUD3* protein sequence is highly conserved across eukaryotes. A) Schematic synteny analyses proved that *OTUD3* (red arrow) is present in all analyzed species. Identity, order and ORF orientation of genes located up- or downstream of *OTUD3* (shown as coloured arrows) is evolutionary conserved. The ORF direction is indicated by the arrowhead. B) Phylogramm of (putative) full-length *OTUD3* protein sequences. The branch length is proportional to the number of substitutions per site and values next to the nodes indicate bootstrap support values. Evolutionary distance is shown as bar next to the phylogramm. A relative divergence of 20% over time was found. Gen bank accession numbers of used sequences for A and B see 3.9.14.

Next, amino acid sequence alignments of OTUD3 were conducted encompassing 25 eukaryotic organisms representing eight classes: *Echinoidea* (*Strongylocentrotus purpuratus*; purple sea urchin), *Bivalvia* (*Crassostrea gigas*; pacific oyster), *Leptocardii* (*Branchiostoma belcheri*; lancelets), *Actinopterygii* (*Danio rerio*, *Takifugu rubripes*, *Ictalurus punctatus*; ray-finned fishes), *Amphibia* (*Xenopus tropicalis*, *Xenopus laevis*; claw frogs), *Reptilia* (*Pogona vitticeps*, *Python bivittatus*), *Aves* (*Corvus japonica*, *Gallus gallus*, *Corvus cornix cornix*; birds), *Mammalia* (*Physeter catadon*, *Monodelphis domestica*, *Ornithorhynchus cuniculus*, *Rattus norvegicus*, *Mus musculus*, *Bos taurus*, *Mesocricetus auratus*, *Cavio porcellus*, *Macaca mulatta*, *Callithrix jacchus*, *Pan troglodytes*, *Homo sapiens*) (see 3.9.14). The phylogenetic tree uncovered a high evolutionary conservation of OTUD3. Especially, mammals, birds, fishes, amphibians and reptiles demonstrated a close phylogenetic lineage (Figure 6B). Interestingly, aligned amino acid sequences uncovered a highly conserved region located within the OTUD3 C-terminal region spanning amino acids 340-363. Notably, this region is characterized by a high content of charged amino acids (Figure 7).

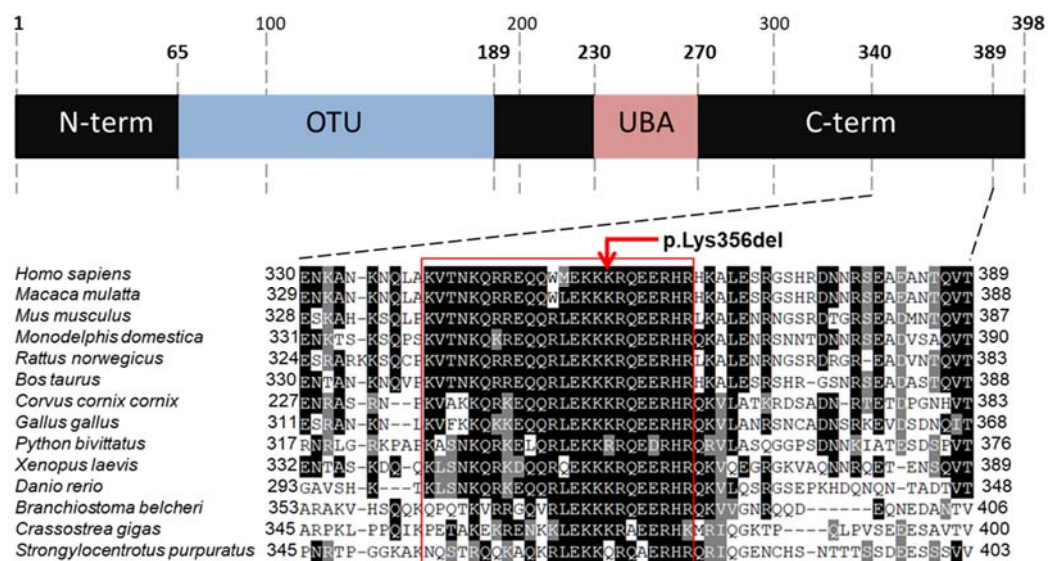


Figure 7) Alignment of OTUD3 across different species revealed a novel, conserved and highly charged C-terminal domain. Schematic representation of full-length OTUD3. OTU domain is shown in blue and UBA-like domain is shown in rose. Black boxed amino acids are highly conserved. The red box marks the novel identified domain within OTUD3's C-terminus (aa 340-363).

Taken together, synteny analyses and amino acid alignments proved that OTUD3/OTUD3 is highly evolutionary conserved across the eukaryotic kingdom. In addition, besides the known conserved OTU and UBA domain the C-terminal region of OTUD3 shows high conservation suggesting potential structural and functional importance of this region. Within the next chapters of this thesis OTUD3 p.Lys356del mutation located within the C-terminus of OTUD3 potentially associated with AS-like phenotypes will be described and molecular consequences will be investigated.

4.2 Linking *OTUD3* variations to neurodevelopmental disease phenotypes

4.2.1 *OTUD3* c.1061_1063delAGA co-segregates with AS-like defect

To date, there is no data available connecting *OTUD3* to genetic hereditary human disease. This thesis describes a novel neurodevelopmental syndrome with overlapping phenotypes to AS putatively caused by an *OTUD3* defect.

Initially, a consanguineous couple with five children, of whom three showed a severe previously unknown genetic syndrome, was studied. A second consanguineous couple within the family branch revealed another affected cousin with overlapping clinical characteristics (Figure 8A). Patients showed distinctive facial appearance like long facies, deep-set eyes and long nasal bridges with downward slanted tips. Additionally, short philtrums, full and everted lips, a prominent jaw and deep-set and posteriorly rotated ears with helical dysplasia were described (Figure 8C). The syndrome was accompanied by secondary microcephaly, alalia, severe intellectual disability, central hypotonia associated with ataxia, autistic behavior and seizures in their early childhood. The mother was pregnant and wanted to terminate pregnancy. By indirect prenatal diagnostics and genome wide linkage-scan with adjacent fine mapping and haplotype analyses the disease locus was mapped to chromosome 1p36.12 and an affection of the unborn fetus was excluded. Strikingly, the mother gave birth to a healthy child [137].

To identify the potential disease causing mutation high-throughput sequencing of 58 genes within the identified linkage interval was performed following NimbleGen enrichment (NimbleGen, Roche). Several alterations were found and evaluated by pathogenicity prediction tools and allele and genotype frequencies published in databases dbSNP, 1000Genomes and ExAC. None of the detected variations absent in population matched controls co-segregated with disease phenotype (data not shown). Next, exons and flanking intron regions not sufficiently covered by initial NimbleGen assay for technical reasons were PCR amplified and Sanger sequenced in index patient 784 (see 3.9.5).

Mutation c.1061_1063delAGA located within exon eight of *OTUD3* was found homozygous in patient 784. All other affected children (787, 788, 9408) were homozygous for the mutation too. Healthy siblings (785, 786, C052), cousin (13389) and parents (782, 783) were heterozygous for c.1061_1063delAGA demonstrating autosomal recessive inheritance (Figure 9A/B). Furthermore, AGA deletion was not detected on 150 population-matched control chromosomes or annotated homozygous in ExAc or gnomAD database (Table 10). On protein level, the identified triplet deletion leads to a deletion of a single lysine residue (p.Lys356del), located within the highly

conserved C-terminal region of OTUD3 (Figure 7). Mutation is predicted to be “disease causing” by MutationTaster tool (Table 10).

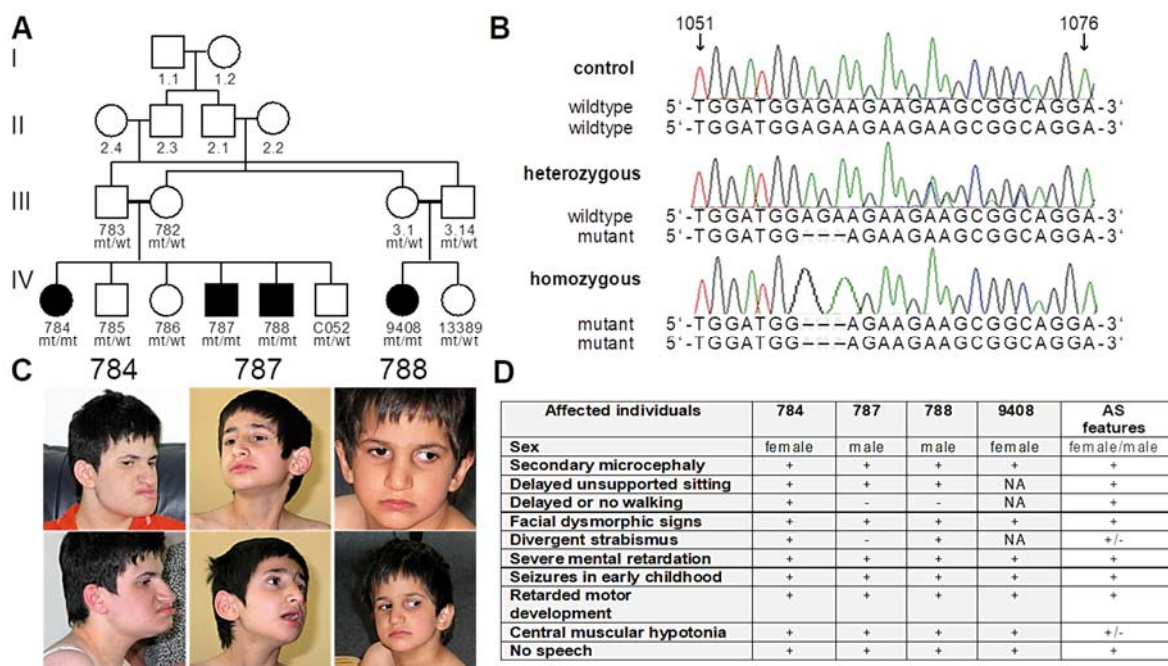


Figure 8) Novel autosomal recessive inherited OTUD3 mutation likely results in neurodevelopmental defects similar to AS. A) Pedigree of the consanguineous index family of Kurdish origin. All affected family members are homozygous for the mutation c.1061_1063delAGA (black filled symbols) located within exon eight of OTUD3. The identified mutation results in a deletion of a single lysine residue (p.Lys356del). mt- mutant allele; wt- wildtype allele. B) Representative Sanger sequencing results of a healthy blood donor control (two wildtype alleles), heterozygous father (wildtype and mutant allele) and affected child 784 (two mutant alleles). C) Facial appearance of the patients 784,787 and 788. D) Clinical features of the affected children are similar with typical AS characteristics. Summary based on [137,156].

4.2.2 Finding of a patient with homozygous c.G739A OTUD3 variant

To identify further patients with OTUD3 variants likely associated with a neurodevelopmental disease phenotype GeneMatcher platform was used [157]. Six years after registration a first potential genotype-phenotype match was provided by the tool. We contacted Prof. Grazia Mancini at the Department of Clinical Genetics, Erasmus Medical Center in Rotterdam and were informed about consanguineous parents and their 15-years old twins. Parents and one twin was healthy, whereas the other twin presented with intellectual disability, small head circumference, seizures, hypotonia, osteopenia and fractures, scoliosis and is congenital blind. In addition, his communication/ language is limited to a few words. Neurological examination showed walking with support, but a wheel chair is mandatory. Facial appearance of the affected twin partially overlaps with male patients described in 4.2.1 Figure 8C in respect to a bulbous nose tip, prominent lips and philtrum.

Genetic investigation by trio whole exome sequencing revealed a homozygous c.G739A (rs1311291528) mutation resulting in D247N exchange on protein level in the affected boy, whereas parents were heterozygous. DNA of the healthy twin was analysed by Sanger sequencing and proved heterozygous *OTUD3* c.G739 exchange. Thus, an autosomal recessive inheritance within the family was demonstrated. Amino acid exchange D247N is located amidst the highly conserved UBA domain of *OTUD3*. In ExAc, 1000Genomes and gnomAD database mutated allele was not listed homozygous. MutationTaster predicted c.G739A as a disease causing mutation. PolyPhen-2 rated the mutation as possibly damaging (HumDiv score: 0.941; HumVar score: 0.622) and SIFT tool as deleterious [158-161].

4.2.3 *OTUD3* sequencing in a cohort with negative test results for AS

Notably, phenotypes of in 4.2.1 investigated patients overlap with characteristics of AS patients (Figure 8D). Thus, *OTUD3* sequencing of further 121 patients, with similar phenotypes and negative AS diagnostic findings (unaltered *UBE3A* copy numbers and methylation patterns) was performed (see 3.5 and 3.9.5).

Within the AS-like cohort we identified in 24% (29 of 121) of patients a set of *OTUD3* variants (Table 10). In 12% of patients sequencing data for exon 1 is missing, although several primers were designed and tested. The potential disease-causing impact of all discovered variants was evaluated using different databases like MutationTaster2, PolyPhen-2, 1000Genomes and gnomAD (Table 10) [158–161].

MutationTaster2 and Polyphen-2 predicted a heterozygous/ homozygous missense variant (rs10916668, c.997G>A, p.A333T) alone or in combination with a second SNV (rs2298110, c.962A>G, p.N321S) as compound heterozygous, to be a benign variant. A silent heterozygous variant (rs61769077, c.603G>A, p.T201T) in eight patients was predicted to lead to a splice site defect using MutationTaster2. However, in 1000Genomes and gnomAD the variant was frequently annotated heterozygous as well as homozygous. Furthermore, one patient revealed a heterozygous p.R347Q missense SNV (rs61752512, c.1040G>A) that is rare (MAF< 0.01), but prediction tools revealed conflicting interpretations regarding its clinical relevance. Within the provided AS-like cohort one DNA sample of index patient 784 (see 4.2.1) was present with homozygous *OTUD3* c.1061_1063delAGA (p.Lys356del) mutation.

To conclude, most of the identified *OTUD3* variants were classified as benign polymorphisms. In those patients with possibly pathogenic variants (besides the index family patient) the genotype was not matching an autosomal recessive inheritance. Performed analyses are limited to the discovery of deep intronic mutations or large genomic rearrangements including *OTUD3* gene locus.

Table 10) Evaluation of potential pathogenicity of identified *OTUD3* variations in AS-like cohort using databases. No.-number of patients; MAF- minor allele frequency; het- heterozygous; hom- homozygous; n.d.-no data; FQ- allele frequency based on gnomAD v.2.1.1..Based on [158-161].

No.	Exon	DNA variation	Protein variation	1000 Genomes	Mutation-taster	PolyPhen-2	gnomAD FQ
8	4	c.603G>A (het)	p.T201T	A/G 0.107 G/G 0.891 A/A 0.002 MAF 0.04	splice defect	n.d.	Het 0.045 Hom 0.0015
7	7	c.962A>G (het)	p.N321S	A/A 0.960 A/G 0.040 MAF0.03	poly-morphism	benign in HumDiv (score 0.000) and HumVar (score 0.000)	Het 0.041 Hom 0.0028
		c.997G>A (het)	p.A333T	A/G 0.113 G/G 0.887 MAF 0.05	poly-morphism	benign in HumDiv (score 0.004) and HumVar (score 0.005)	Het 0.073 Hom 0.0046
11	7	c.997G>A (het)	p.A333T	A/G 0.113 G/G 0.887 MAF 0.05	poly-morphism	benign in HumDiv (score 0.004) and HumVar (score 0.005)	Het 0.073 Hom 0.0046
1	7	c.997G>A (hom)	p.A333T	A/G 0.113 G/G 0.887 MAF0.05	poly-morphism	benign in HumDiv (score 0.004) and HumVar (score 0.005)	Het 0.073 Hom 0.0046
1	8	c.1040G>A (het)	p.R347Q	A/G 0.006 G/G 0.994 MAF<0.01	poly-morphism	possibly damaging in HumDiv (0.878) and benign in HumVar (0.084)	Het 0.0015 Hom 0.0000036
1	8	c.1061-1063delAG A (hom)	p.Lys356del	AGA/AGA 0.998 AGA/- 0.001 MAF<0.001	disease causing	n.d.	Het 0.00016 Hom not found

4.2.4 CNVs of *OTUD3* exons might be associated to human developmental disease

Detection of putative *OTUD3* CNVs by Sanger sequencing of exons and flanking intron regions as conducted in 4.2.1 is not likely considering large intron regions as putative hot spots for CNVs.

A MLPA assay was established to investigate CNVs of *OTUD3* exons (see 3.9.12). DNA samples previously used for sequencing and available DNA samples of healthy blood donors as control cohort were ethanol precipitated and resuspended in TE buffer to exclude buffer effects (see 3.9.6).

After precipitation 105 DNA samples of AS-like phenotypes and 96 samples derived from healthy blood donors were eligible for MLPA screening. Probes designed specific for each *OTUD3* exon see 3.5. Note, that every probe has a unique length enabling size separation of amplified fragments by capillary electrophoresis and peak quantification. MLPA experiments were performed according to MRC Holland's one-tube protocol for DNA detection and quantification (see 3.9.12). Electropherograms with commercially available control DNA proved, that for exon 2 to exon 8 of *OTUD3* peaks were explicit separated and peak height was slightly higher than the probemix included control fragment peaks (P300 fragments) (data not shown). Datasets for CNVs of *OTUD3* exon 1 are missing, probably due to the high GC content within exon 1 and bad accessibility by PCR based methods.

101 of 105 analysed patient DNA samples (96.2%) showed no *OTUD3* CNVs. In addition, all 96 healthy blood donor samples were without CNV findings too. Strikingly, four novel patients (04999, 05251, 06116, 06273) showed noticeable CNV aberrations (Figure 9A). To ensure the findings of first MLPA screening the experiment was repeated for all four patients with similar findings.

Follow up qPCRs and long-range PCRs covering *OTUD3* gene locus were performed to validate MLPA results (see 3.5., 3.9.9, 3.9.11 and 3.9.13). Below, results for each patient with putative *OTUD3* CNVs are separately summarized. Results are presented in Figure 9 A/B for MLPA, 9 C/D for qPCR and Figure 10 for long-range PCR.

Patient 04999: Via MLPA assessment patient 04999 revealed a duplication of exon 6 and a deletion of exon 8 of *OTUD3*. Via qPCR approach duplication of exon 6 and deletion of exon 8 were confirmed. Notably, up to fivefold copies of exon 6 were measured by qPCR. In addition, exon 5 revealed duplications (~twofold copies) and exon 7 a heterozygous deletion in qPCR. However, parental DNAs of patient 04999 were followed up by MLPA and qPCR and proved no indication for *OTUD3* CNVs. Respective long-range PCR products with control and parental DNAs of patient 04999 could be generated, but not for patient 04999 providing evidence for *de novo* insertions and deletions within *OTUD3*.

Patient 05251: Patient 05251 showed indication for duplication of *OTUD3* exon 6 and deletion of exon 8 in MLPA experiments. qPCR detected a threefold excess of exon 6 too, but contrary levels of exon 5 were found twofold elevated and copy number of exon 8 was without alteration to control. In long-range PCR set up only a PCR product spanning exon 7 to exon 8 was detected, but signal intensity was lower in comparison to control products.

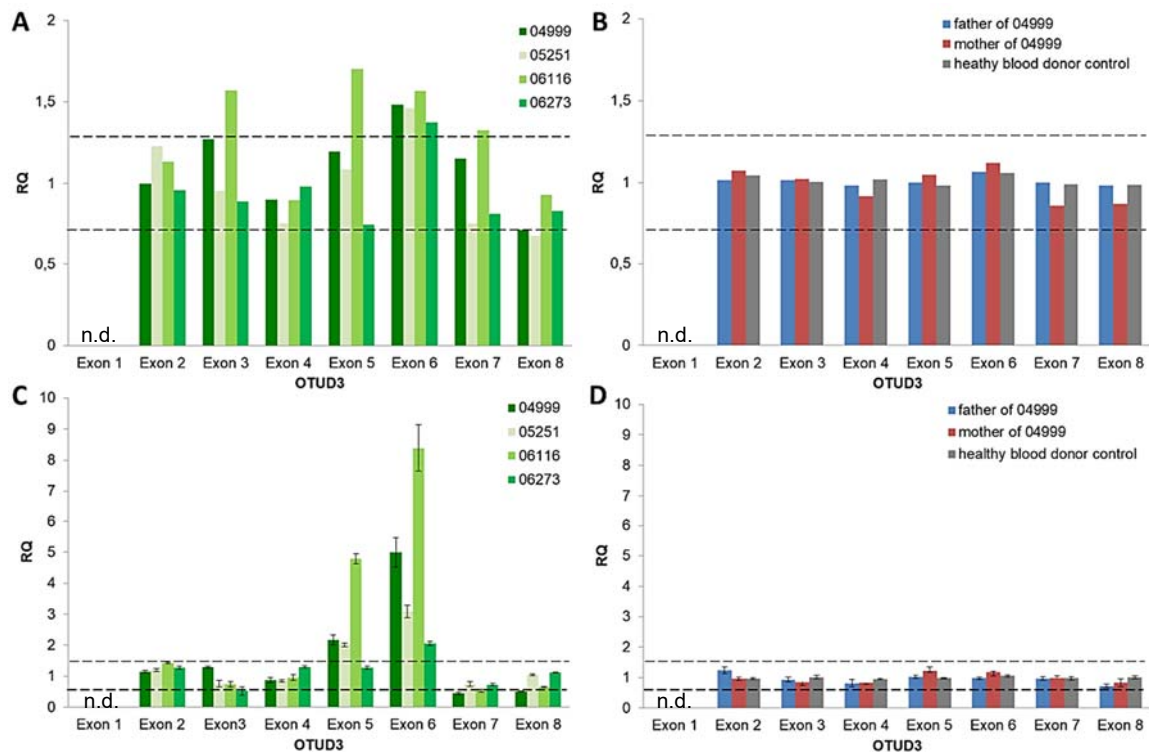


Figure 9) MLPA and qPCR enabled the identification of *OTUD3* CNVs in four unrelated patients with neurodevelopmental disease. A) MLPA analyses of exons 2-8 of *OTUD3* uncovered novel potential disease causing *OTUD3* CNVs. Four patients (04999, 05251, 06116 and 06273) of 105 screened patients with AS-like symptoms showed CNVs. Interestingly, all patients possess duplications of exon 6. Presented MLPA graphs are representative for one MLPA run. B) MLPA assay of parents of 04999 proved that CNVs detected in 04999 are *de novo*, because parents showed no CNVs. A representative healthy blood donor control is presented. C/D) qPCR analysis of patients 04999, 05251, 06116, 06273 and parents of 04999 strengthened the finding of presence of *OTUD3* CNVs. Again, all analyzed patients showed duplications of exon 6. qPCR data were collected in triplicates and in three to five independent experiments. RQ values were calculated by $2^{-\Delta\Delta C_t}$ method. For normalization GAPDH was used. Results are presented as mean \pm SEM. Black dotted lines mark the cut off for potential CNVs: RQ>1.3 indicates duplications and RQ< 0.7 deletions in MLPA assay; RQ> 1.4 indicates duplications and RQ< 0.6 deletions using qPCR. n.d.- no data.

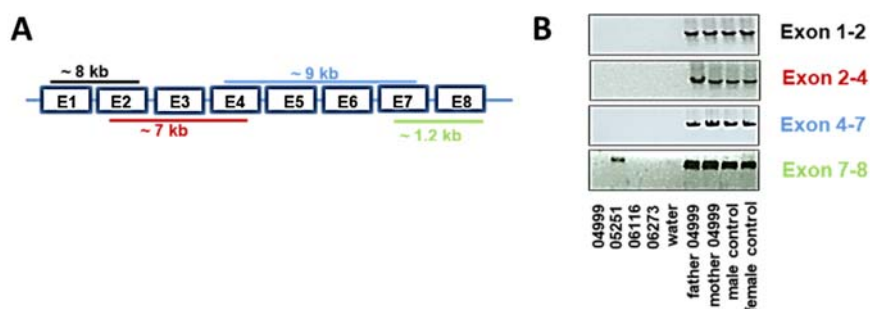


Figure 10) Long-range PCR covering *OTUD3* suggests rearrangements of exons in recently identified AS-like patients. A) Schematic overview of *OTUD3* exons, generated long-range PCR products and expected fragment sizes. B) PCR products control and parental DNAs of patient 04999 could be generated. All recently identified patients (04999, 05251, 06116 and 06273) showed no PCR products. Only patient 05251 possessed at least one allele for region covering exon 7-8. Additionally, long-range PCR for products of exon 4-7 were obtained from DNA of 96 healthy blood donors as control (data not shown).

Patient 06116: MLPA detected duplications of exon 3, 5, 6 and 7. In both MLPA runs, peak separation pattern of *OTUD3* probes and of control and normalization fragments was altered (small additional peaks, some asymmetric peaks) in comparison to all other performed MLPA runs (data not shown). Before the MLPA run was repeated, DNA was ethanol precipitated a second time to exclude impure DNA preparation, but without qualitative effect on the second MLPA result. Supported evaluation by sequence pilot software and MLPA tool was considered as inaccurate by the software. However, in line with MLPA findings duplication of exon 5 (~ fivefold excess) and of exon 6 (~eightfold elevated) was verified by qPCR. Via Long-Range PCR no PCR product was detected, strengthen the collected data for the presence of putative CNVs of *OTUD3* in patient 06116.

Patient 06273: Combination of MLPA and subsequent qPCR analysis of *OTUD3* exons enabled the identification of exon 6 duplications in patient 06273. No PCR products were obtained via long-range PCR.

To sum up, screening of *OTUD3* CNVs via MLPA and follow up by qPCR analysis and long-range PCR identified four novel unrelated patients with overlapping phenotypes to index family patients. Notably, in all patients duplications of exon 6 were detected. *De novo* CNVs of *OTUD3* were confirmed in patient 04999 by demonstrating parents without CNVs. Three of four patients (04999, 05251 and 06116) showed multiple CNV sites within *OTUD3*. From long-range PCR experiments it was hypothesized that in all four patients both *OTUD3* alleles were affected, because no PCR products were detectable, except for patient 05251 and region representing exon 7-8 of *OTUD3*.

4.3 Molecular insights into *OTUD3* p.Lys356del patient cells

4.3.1 *OTUD3* mutation does not influence expression, activity and localization

To gain first insights into molecular consequences of the recently identified *OTUD3* mutation (c.1061_1063delAGA) patient derived cell lines like primary fibroblasts and lymphoblastoid cell lines (LCLs) were analyzed focusing *OTUD3* expression, activity and localization. All following experiments were performed in comparison to *OTUD3* wildtype controls (sex and age-matched).

First, RNA was isolated from fibroblasts and LCL cultures (see 3.9.8) and subsequently reverse transcribed into cDNA (see 3.9.9). Using qPCR approach and intron-spanning primers for *OTUD3* and *GAPDH* as housekeeping gene control an effect of the homozygous c.1061_1063delAGA *OTUD3* mutation at the transcriptional level in fibroblasts and LCLs was excluded in comparison to control cells (Figure 11A).

For Western blot protein analyses of OTUD3 patient derived fibroblasts and matched controls were trypsinized at high confluency and lysed (see 3.11.1 and 3.10.2). BCA assay was performed to determine the total lysate protein concentration (see 3.11.3). 20 μg of each cell lysate was applied for ubiquitin-conjugation assays and was incubated in presence or absence of 1 μg Ubiquitin-propargylamid (Ub-PA) or Ubiquitin-Vinylmethylester (Ub-VME). So called suicide substrates, Ub-PA and Ub-VME both react covalently with catalytic cysteine residues of active DUBs resulting in a visible shift of ~ 8 kDa of investigated DUB (see 3.10.6).

Western blot experiments proved that the OTUD3 protein level in fibroblasts from patients (787, 788) and controls (ctrl1, ctrl2) was not altered. Furthermore, if the cysteine inhibitor Ub-PA was added to the cell lysates, ubiquitin got equally covalently linked to the active site of OTUD3 (Figure 11B). Preincubation with NEM prevented the ubiquitin conjugation (Figure 11C).

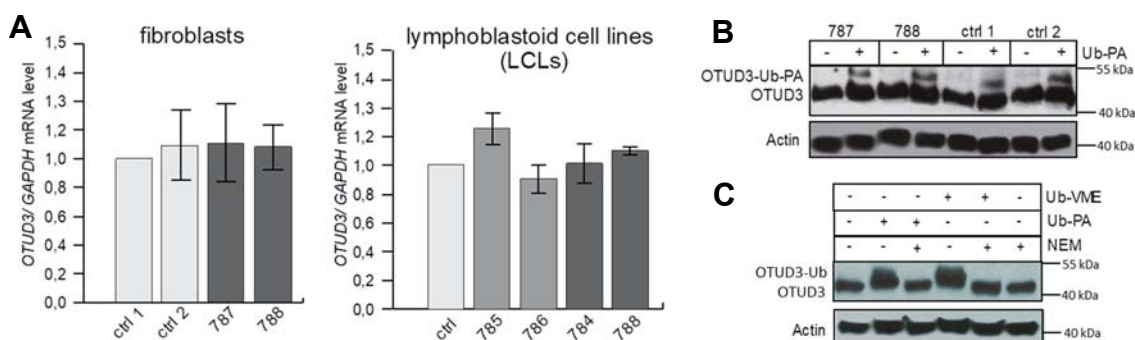


Figure 11) Patients possess unchanged OTUD3 mRNA and protein levels.

A) Inherited *OTUD3* AGA deletion revealed no influence on the relative mRNA level. qPCR analyses of relative *OTUD3* mRNA levels in primary fibroblast and LCL cultures of affected children (dark grey) and controls. qPCR data were obtained from three different culture passages and are presented as mean \pm SEM. Ctrl1, ctrl2 are sex-, age- and passage matched controls and 784, 787, 788 are affected *OTUD3* defect patients, whereas 785 and 786 are heterozygous, healthy siblings. For evaluation ctrl1 was selected as reference (ctrl1 *OTUD3* mRNA level = 1; light grey) and GAPDH was used as endogenous control. B) *OTUD3* p.Lys356del protein as well as amounts of conjugated ubiquitin substrate Ub-PA to *OTUD3* was comparable to controls. 20 μg of each cell lysate was loaded for SDS-PAGE and Western blot analyses. C) As indicated 1 μg of Ub-PA, Ub-VME or preincubation with 10 mM NEM was conducted in control fibroblasts. Blot membranes were decorated with primary polyclonal anti-*OTUD3* antibody (Novus Biologicals, 1:2000) followed by secondary HRP-coupled anti-rabbit IgG antibody (Invitrogen, 1:2000). As loading control actin blots are presented developed by applying anti-actin antibody (BD Biosciences, 1:5000).

Next, potentially misrouted cellular localization of *OTUD3* due to p.Lys356del mutation was investigated by immunofluorescence microscopy (see 3.11.8). Endogenous *OTUD3* was stained in patients (787, 788) and control fibroblasts. Fibroblasts of both showed that endogenous *OTUD3* mainly localizes in the cytosol, especially in

perinuclear regions. In addition, the staining pattern looked structured reminding of filaments like tubulin networks (Figure 12A).

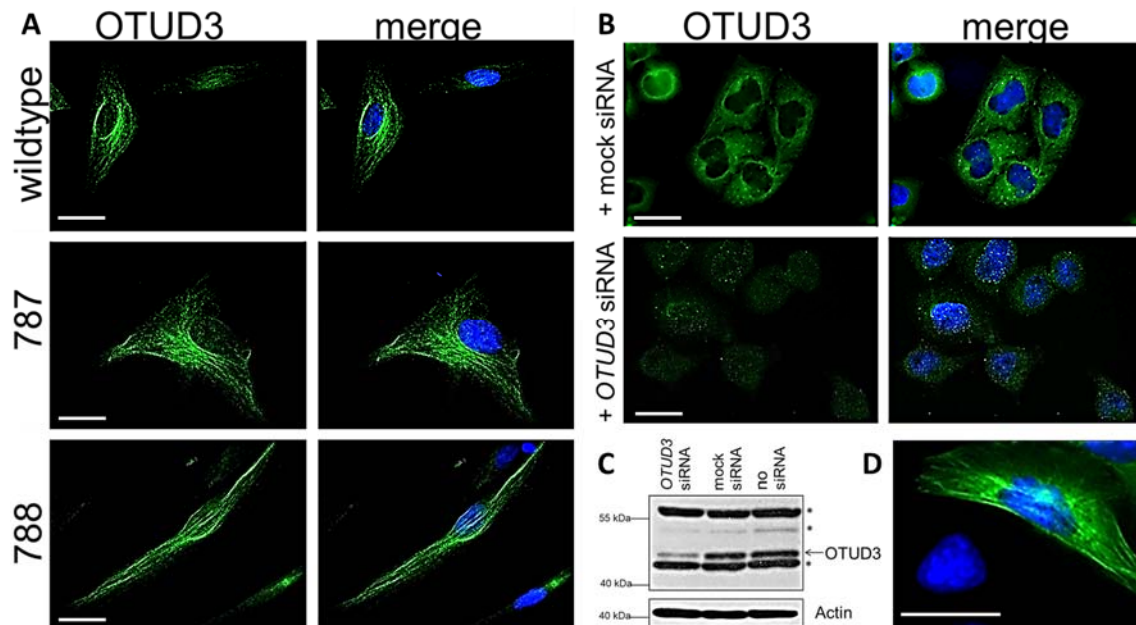


Figure 12) OTUD3 p.Lys356del does not alter localization of the protein. A) Comparison of the localization of OTUD3 in primary human fibroblasts showed no obvious difference between control (OTUD3 wildtype) or patients (787, 788). OTUD3 localizes predominantly in the cytosol. Cytosolic localization looks filamentous. Fibroblasts were stained with anti-OTUD3 (1:100, Novus Biologicals) and Alexa-488 coupled secondary antibody (1:200, Invitrogen) (green) after PFA fixation of the cells. DNA was stained with DAPI (blue). Merge- overlay of OTUD3 und DAPI staining. B) Transfection of siRNAs targeting endogenous *OTUD3* mRNA reduced the OTUD3 staining in contrast to mock siRNA transfected HeLa cells. Four *OTUD3* specific siRNAs (each 20 nmol) were simultaneously transfected using HiPerfect transfection reagent. After 24 hours cells were fixed with 4% PFA and stained as in A. C) Western blot analyses of endogenous OTUD3 was reduced in HEK293T cells transfected with *OTUD3* siRNAs, whereas in mock siRNA and untransfected cells the OTUD3 amount was equal. 20 µg cell lysate were loaded and as loading control an actin blot is presented. * indicate unspecific detected protein bands. A polyclonal anti-OTUD3 antibody (Novus Biologicals, 1:2000) followed by secondary HRP-coupled anti-rabbit IgG antibody (Invitrogen, 1:2000) was used. As loading control actin blots are presented developed by applying anti-actin antibody (BD Biosciences, 1:5000). D) Transfection and expression of *N*-terminal GFP-tagged OTUD3 (green) in HEK293T further confirmed the detected localization of endogenous OTUD3 shown in A. DNA is stained with DAPI (blue). White bars in A,B and D indicate a size of 10 µM.

To assess the specificity of the applied anti-OTUD3 antibody siRNA experiments were performed. HeLa cells were transfected with four siRNAs (each 20 nM) directed against *OTUD3* mRNA. As control, mock siRNA was transfected (see 3.11.4). *OTUD3* siRNA transfected cells showed reduced and less filamentous staining via microscopy analyses and lowered OTUD3 protein level via Western blot investigation in comparison to mock transfected cells (Figure 12B/C). Moreover, *N*-terminal GFP-tagged *OTUD3* was transfected in HEK293T cells approving the observed tubulin-like

localization pattern of endogenous OTUD3 too (Figure 12D).

Conclusively, neither *OTUD3* transcription, translation, cysteine protease active site nor localization was apparently affected by the recently identified *OTUD3* mutation. However, finding of potential colocalization of endogenous OTUD3 with tubulin-like structures was further investigated (see 4.5).

4.3.2 Patient LCLs show altered pSMAD1/5 levels

Regulation of signaling pathways like Wnt (TRABID), TGF β (OTUB1, A20) or nF-KB (A20, Cezanne) is described for several members of the OTU subfamily of DUBs [162,162–165]. Here, BMP signaling pathway was investigated.

Therefore, pSMAD1/5 levels were analyzed in LCLs of patients (784 and 788) and sex- and age-matched controls via FACS based read out (see 3.10.4).

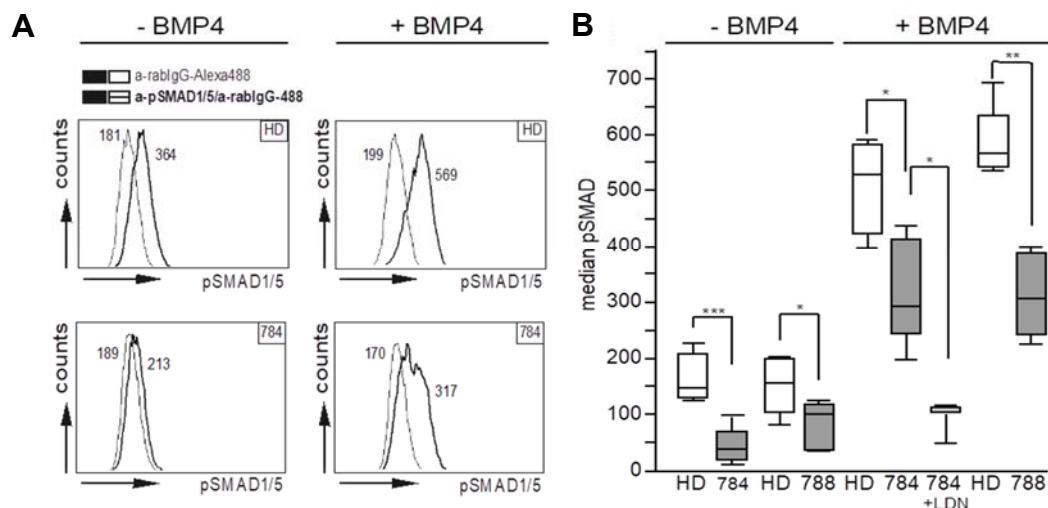


Figure 13) BMP signaling is attenuated in LCLs of patients with AS-like features.

A/B) Basal as well as BMP4-induced intracellular pSMAD1/5 levels are significantly reduced in patient-derived LCL cultures. LCLs derived from patients (784, 788) and sex- and age-matched healthy donor s (HD) were cultured and treated with or without 100ng/ml BMP4 for 20 h. Cells were fixed with 4% PFA and permeabilized with methanol. Intracellular pSMAD1/5 levels were stained using anti-phospho-SMAD1/5 (Ser463/465) and secondary anti-rabbit IgG-Alexa488 antibody. As control, BMPR1A inhibitor LDN-193189 was added 15 min prior to BMP4 administration. A) Representative histograms are presented for basal and BMP4 induced pSMAD1/5 levels of patient 784 and a sex- and age- matched healthy donor (HD) control. Values indicate measured median fluorescence intensity (MFI). Light grey peaks represent cells stained with secondary antibody (as background signal) and black peaks show cells stained with pSMAD1/5 and secondary antibody. B) Statistical evaluation of basal and BMP4 induced pSMAD1/5 level in HD (white bars) and patients (gray bars). Note, pSMAD1/5 signaling in LCLs of patients is desensitized and LDN193189 abolishes BMP4 induced pSMAD1/5 signaling. Data are obtained from 3-7 independent experiments and median fluorescence intensities for pSMAD1/5 were obtained by subtraction of control staining with secondary antibody (*p <0.05; **p<0.01; ***p<0.001; unpaired t-test).

Cells were cultured in absence or presence of 100ng/ml BMP4. BMPR1A inhibitor LDN-193189 was added 15 min prior BMP4 administration to abolish BMP4 induced pSMAD1/5 signaling as control.

Basal pSMAD1/5 levels were significantly lowered in patient derived cells in comparison to matched controls. BMP4 administration led in patient and control cells to a strong activation of BMP4 signaling detected by strongly increasing pSMAD1/5 levels. Notably, patient cells showed less activation of BMP4 induced pSMAD1/5 pathway. As expected, preincubation with synthetic BMPR1A inhibitor LDN-193189 abolished phosphorylation of SMAD1/5 proteins (Figure 13 A/B). Interestingly, basal and BMP4 induced and BMPR1A inhibitor preincubated pSMAD1/5 level of patient 784 were not significantly altered.

4.3.3 Patient LCLs possess higher proliferation activity

Recent findings of altered pSMAD1/5 signaling properties in patient LCLs and co-localization of endogenous OTUD3 with tubulin-like structures in primary fibroblasts led to the investigation of altered cell growth or metabolic activity in patients.

First, mitochondrial activity as read out for metabolic cell activity was measured via well-established 3-(4,5-dimethylthiazol-2-yl)-2,5-diphenyltetrazolium bromide (MTT) dye assay. MTT dye gets reduced by cellular NAD(P)H- dependent oxidoreductases forming an insoluble and violet formazan product. Absorption of the formazan product can be measured at a wavelength of 590 nm. The MTT assay was performed in two different modes (see 3.11.7). First, a constant cell number of patient (784 and 788) and matched control LCLs was applied for MTT experiment. The investigation revealed significant elevated mitochondrial activity in patient derived LCLs (Figure 14A1/2).

Secondly, MTT experiment was recorded as time dependency read out and thus reflecting the number of viable cells. Within 72 h the number of viable cells of patient LCLs increased ~3.5 fold, whereas control cell viability ascended only ~2.5 fold (Figure 14B1/2). To verify the results obtained by MTT assay cell counting assay was performed (see 3.11.2). Therefore, 5×10^4 viable LCLs of patients and controls were seeded at day 1. Discrimination between living and dead cells was realized by trypan blue staining. After 72 h at 37°C cells were counted again. Patient viable cells number was ~ 3.0 fold, in contrast to control cells which divided 1.6~fold (Figure 14 C1/2).

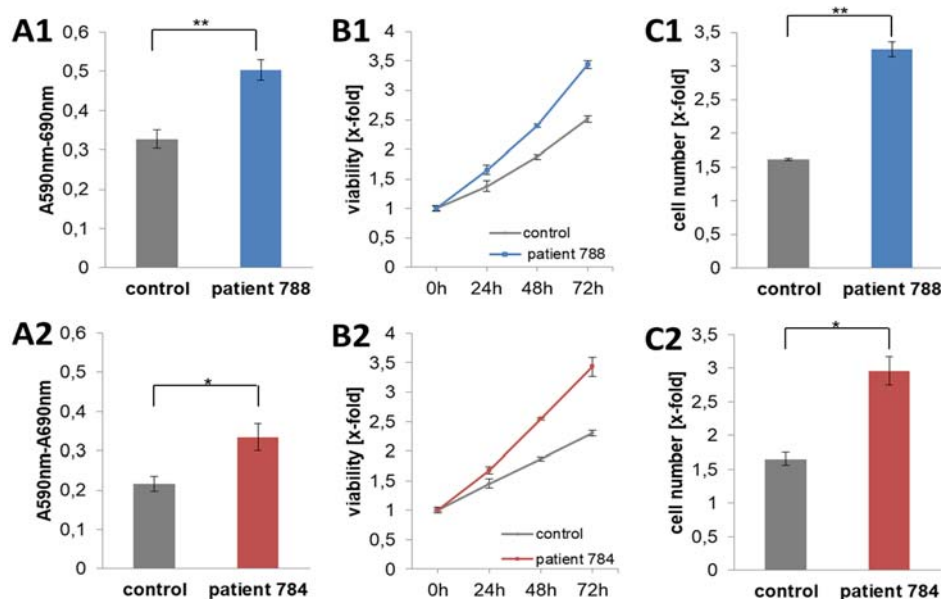


Figure 14) In patient LCLs viability is enhanced. A1/A2) Comparing constant LCL cell numbers of patients (784, 788) and matched controls higher metabolic activity of patient derived cells was detected. 5×10^5 cells were analyzed 2 h after MTT dye was added to the cells. Assays were performed in triplicates and in five independent experiments. Results are presented as mean \pm SEM. B1/B2) MTT assay was performed in a time dependency set up. Higher viability of patient cells (784 and 788) was measured. 1×10^5 cells were seeded at day 1 ($t=0$) and at indicated time points MTT assay was performed. MTT signal at $t=0$ h was set to 1 and results are given as x-fold viability reflecting the number of viable cells. Experiment was performed once and data are shown as mean \pm SD. C1/C2) LCLs of patients show elevated proliferation rates. Living cells were counted using a Neubauer chamber and trypan blue staining. At day 1 and after 72 h at 37°C cells were counted. Shown is the cell number expressed as x-fold value after 72 h of cultivation compared to day 1. All samples were seeded and evaluated as duplicates. Three independent experiments were performed and data are given as mean \pm SEM. Statistical significance was calculated in A and C by applying unpaired t-test (* $p < 0.05$; ** $p < 0.01$; *** $p < 0.001$).

4.4 OTUD3 is differentially expressed in human tissues

Recently discovered patients bearing *OTUD3* defect showed neurological features like secondary microcephaly, intellectual disability, alalia, ataxia and seizures. Hence, the expression pattern of *OTUD3* mRNA was evaluated in a set of 18 human organs followed by a detailed investigation of 13 brain areals (see 3.9.8 and 3.9.9).

Notably, *OTUD3* mRNA was present in all examined tissues. The analyzed *OTUD3* mRNA levels revealed organ dependent differences (Figure 15A). Tissues like heart and skeletal muscle showed low *OTUD3* expression, whereas tissues like pancreas, spleen, lymph and partoid possessed similar *OTUD3* mRNA levels like the selected reference tissue liver. In many tissues (ovary, lung, thymus, colon, adrenal gland, kidney, stomach) the *OTUD3* expression was 2-3 fold elevated. The highest *OTUD3* expression was detected in skin and testis. As assumed, high *OTUD3* mRNA levels (~4-fold elevated in comparison to liver expression) were measured in fetal brain and adult brain tissue (Figure 15A).

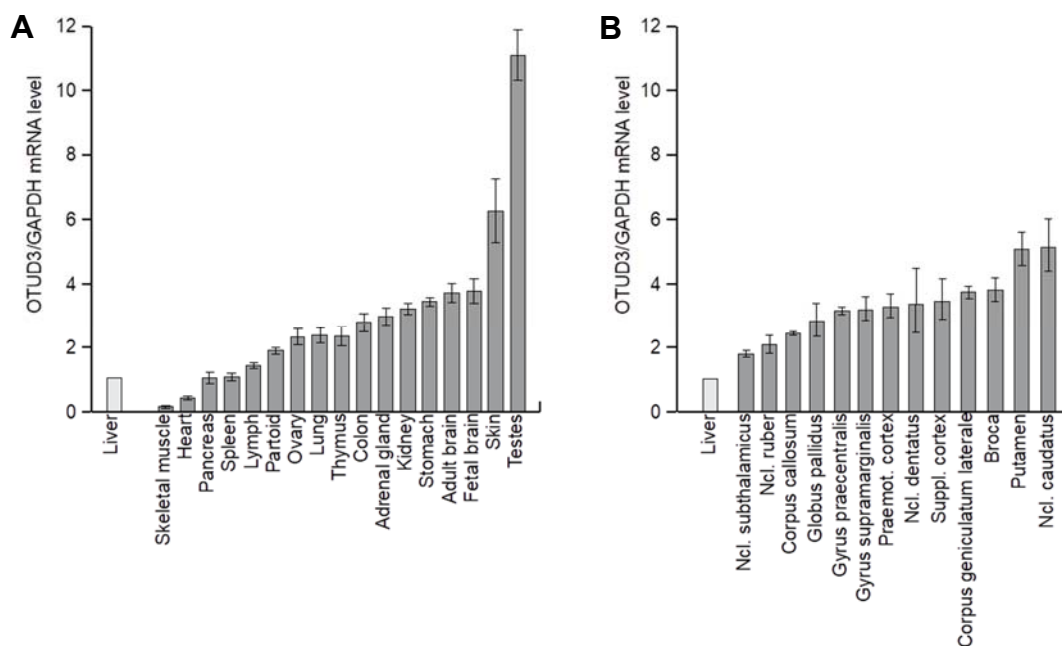


Figure 15) *OTUD3* is differentially expressed in human tissues and particularly high in human brain areas. Shown are relative mRNA levels of *OTUD3* in indicated human tissues (A) or specific anatomic brain areas (B) studied in qPCR experiments. For evaluation liver was selected as reference tissue (*OTUD3* mRNA level Liver =1) and *GAPDH* mRNA levels served as endogenous control. Ncl.-nucleus.

Further qPCR studies focused on the *OTUD3* expression in human brain areas derived from post-mortem material. Brain areas were chosen with major functions in the control of movements, the development of speech and visualisation, according to the observed disabilities in the affected children. All investigated brain areas showed a high *OTUD3* expression that was 2-5 fold higher than detected in liver. Highest expression was obtained in caudate nucleus and putamen, which form together the dorsal striatum, and is responsible for voluntary movements. Furthermore, high *OTUD3* mRNA levels were measured in supramarginal gyrus and broca tissue, both important regions for language perception, processing and speech development and lateral geniculate nucleus, a center located within the thalamus that receives sensory input from the retina (Figure 15B).

Concluding, *OTUD3* mRNA was present in all examined tissues, but the notably high expression of *OTUD3* in human brain might highlight its potential importance and role in neurodevelopmental processes.

4.5 Localization studies of OTUD3

4.5.1 Endogenous OTUD3 localization is conserved across species and tissues

In primary fibroblasts of index patients with AS-like phenotype and matched controls we detected unaltered localization of OTUD3 mutant protein (see 4.3.1).

However, filamentous structures of OTUD3 localization within the cytosol were noticed. This finding led to the investigation and comparison of endogenous OTUD3 staining in cell lines of different human tissues and species and co-staining experiments with tubulins. Endogenous OTUD3 localization was studied via immunofluorescence microscopy (see 3.11.8) in human primary fibroblasts, HEK293T, HaCAT and HeLa cells, as well as in mouse hippocampal neuronal cell line HT22 and embryonic mouse fibroblasts NIH3T3.

Similar filamentous OTUD3 staining patterns overlapping with α -tubulin stained structures were found in all tested cell lines (Figure 16). More dotted OTUD3 staining was detected in mouse cell lines, suggesting less specificity of the applied antibody for mouse OTUD3 protein. Nonetheless, in mouse fibroblasts NIH3T3 OTUD3 co-staining with tubulin was visible in regions with high tubulin presence. In neuronal HT22 cells OTUD3 staining partially overlays with α -tubulin staining in perinuclear regions and regions of high tubulin network density.

Note, that only about 30% of cells showed distinct tubulin-like structures of OTUD3 staining. To further prove OTUD3 and tubulin association cells were treated with 10 μ M nocodazole before fixation. Upon nocodazole addition typical α -tubulin stained filaments disappeared as well as filamentous OTUD3 staining. Nocodazole experiments were performed with all human derived cell lines (HeLa, HEK293T, primary fibroblasts, HaCAT) with similar results (Figure 16, representative data shown for primary fibroblasts).

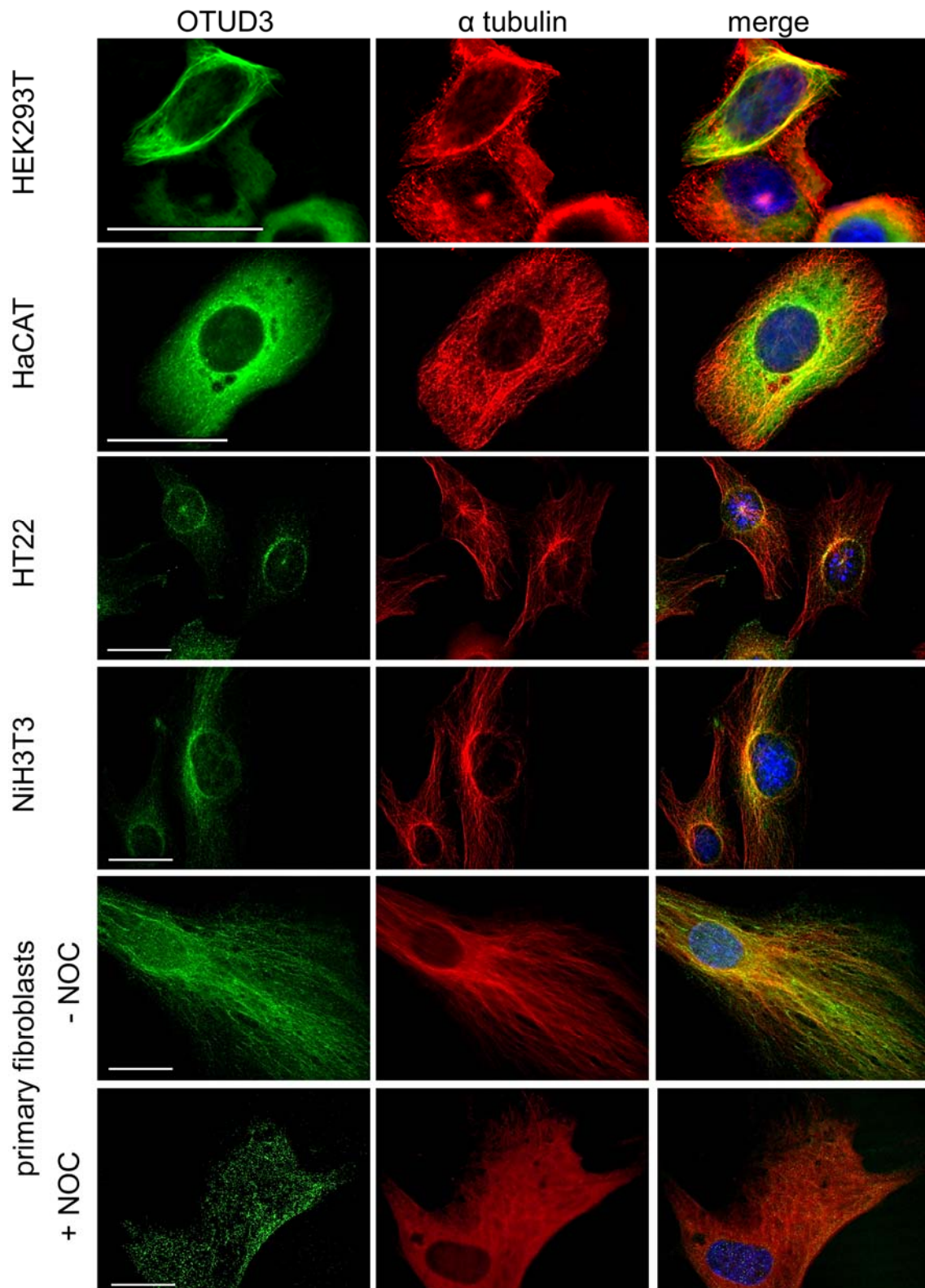


Figure 16) Endogenous OTUD3 co-localizes with microtubule structures across species and tissues. Indicated cell lines were seeded on coverslips and were fixed with 4% PFA and permeabilized with PBS containing 0.2% (v/v) Triton X-100. Polyclonal primary anti-OTUD3 antibody (1:100, Novus Biologicals) was incubated over night at 4°C, whereas Alexa-488 coupled secondary antibody (1:200, Invitrogen) was applied for 1 h at 37°C (green). α -tubulin was stained with anti- alpha tubulin antibody (1:500, Sima-Aldrich) and Alexa-568 coupled secondary antibody (1:1000, Sigma-Aldrich) (red). DNA was stained with DAPI (blue). If indicated, 10 μ M nocodazole was added to the cells before fixation. White scale bars indicate 20 μ m.

4.5.2 OTUD3 decorates mitotic spindles, primary cilia and midbody

To further assess OTUD3's association with typical tubulin network structures HeLa cells were cell cycle synchronized and different stages of mitosis were imaged (see 3.11.5 and 3.11.8). OTUD3 was found on mitotic spindles in metaphase and late telophase/ end stage of cytokinesis (Figure 17A). Notably, OTUD3 decorates the midbody, a structure of bundled tubulin filaments (Figure 17B). In addition, in starved mouse NiH3T3 fibroblasts OTUD3 was present on primary cilia axoneme (Figure 17C).

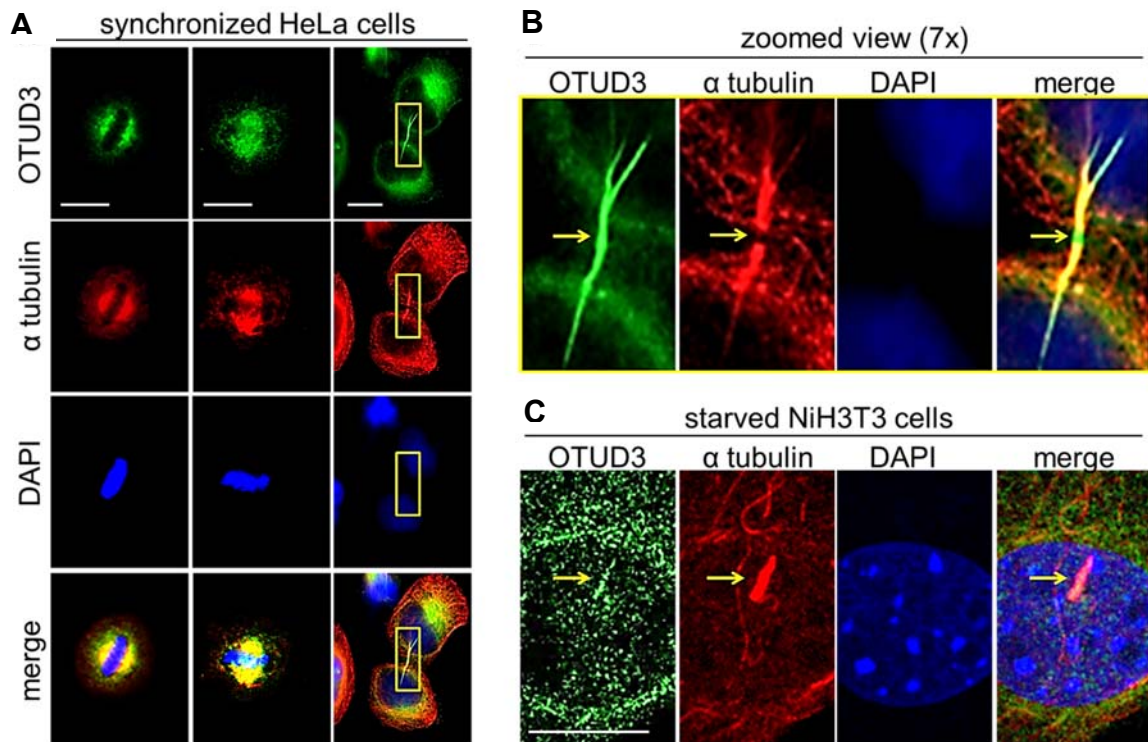


Figure 17) Endogenous OTUD3 decorates typical cellular tubulin structures like mitotic spindles, the mid body and primary cilia. A) Synchronized HeLa cells show OTUD3 colocalization with α -tubulin stained mitotic spindles. B) Zoomed view of the highlighted yellow box in A. The yellow arrow marks OTUD3 staining of the mid body. C) In starved NiH3T3 cells, OTUD3 decorates the axoneme of primary cilia. Cells were stained in accordance to Figure 16 in A/B, whereas for C) anti-acetylated tubulin antibody (Sigma, 1:500) was used. White scale bars indicate 10 μ m.

4.5.3 Terminal domains of OTUD3 mediate microtubule binding and localization

Detected colocalization of OTUD3 with tubulin filaments and structures raised the question of a microtubule-binding site within OTUD3. Therefore plasmids containing *N*-terminal GFP tagged *OTUD3* variants (full-length and *N*- or *C*-terminal truncated constructs) were generated (see 3.9.3 and 3.9.4). HeLa cells were transfected with respective plasmids using lipofectamine2000 reagent kit (see 3.11.4). After 16 h cells were fixed and stained with α -tubulin specific antibody and imaged via immunofluorescence microscopy (Figure 18). Full-length GFP tagged OTUD3 localized

as endogenous protein. *N*-terminal truncated OTUD3 variants lacking the *N*-terminus, the OTU and UBA domain still showed filamentous staining. Furthermore, lack of *N*-terminal domain always led to detection of more pronounced tubulin-like structured OTUD3-GFP signal as for wildtype protein. While about 30% of cells successfully transfected with plasmid coding for GFP-OTUD3 wildtype protein were seen with tubulin-like structured staining, about 90% of cells successfully transfected with plasmid coding GFP-OTUD3 variant lacking the *N*-terminal domain featured filamentous patterns. Strikingly, if only a GFP tagged variant of OTUD3's C-terminus was overexpressed tubulin-like structures were detected too. On the other hand, if C-terminal truncated GFP tagged variants lacking the C-terminus alone or in combination with the UBA domain were transfected no tubulin-like structures were visible. As seen in protein sequence alignments, the OTUD3 C-terminus is conserved across species and is in general highly charged. Interestingly, a highly conserved stretch comprising amino acids 340-363 possesses a calculated pI of 11 using ProtParam tool and is rich of charged amino acids especially K, Q and R (Figure 20A/B/C). Thus, this stretch fulfills typical microtubule interaction criteria.

Secondly, upon overexpression of C-terminal truncated OTUD3 variants a shift of GFP-OTUD3 staining from the cytosol to the nucleus was observed (Figure 18). This finding raised the question, if OTUD3 contains a nuclear export signal (NES), or a nuclear leading sequence (NLS) or both. To investigate NES presence within OTUD3, *N*-terminal GFP tagged OTUD3 variants were transfected in HEK293T in presence or absence of leptomycin B. Leptomycin B is an inhibitor of CRM1 (exportin 1) leading to nuclear accumulation of NES containing proteins. Addition of leptomycin B led to the accumulation of GFP-OTUD3 signal for full-length protein and all *N*-terminal truncated OTUD3 variants, suggesting a putative nuclear export signal (NES) located within the C-terminus of OTUD3 (Figure 19). Whenever *N*-terminal GFP tagged OTUD3 C-terminus was transfected and leptomycin B was added, cells died rapidly and no microscopy pictures could be taken.

Using NES prediction server NetNES 1.1 and blasting a highly conserved and hydrophobic amino acid stretch distal of the OTUD3 C-terminus a putative NES was identified (Figure 20D).

The potential NES likely resembles a **RxxxRxxRxR** motif, at which R represents a hydrophobic amino acid and x any other amino acid. In human the putative NES sequence is probably ³⁸⁹LVKTEAALN³⁹⁸. Note, that across species hydrophobic residues R of this NES are conserved suggesting functional relevance (Figure 20B).

Transfection of GFP tagged C-terminal truncated OTUD3 variants showed no difference between leptomycin B untreated or treated localization patterns (Figure 19).

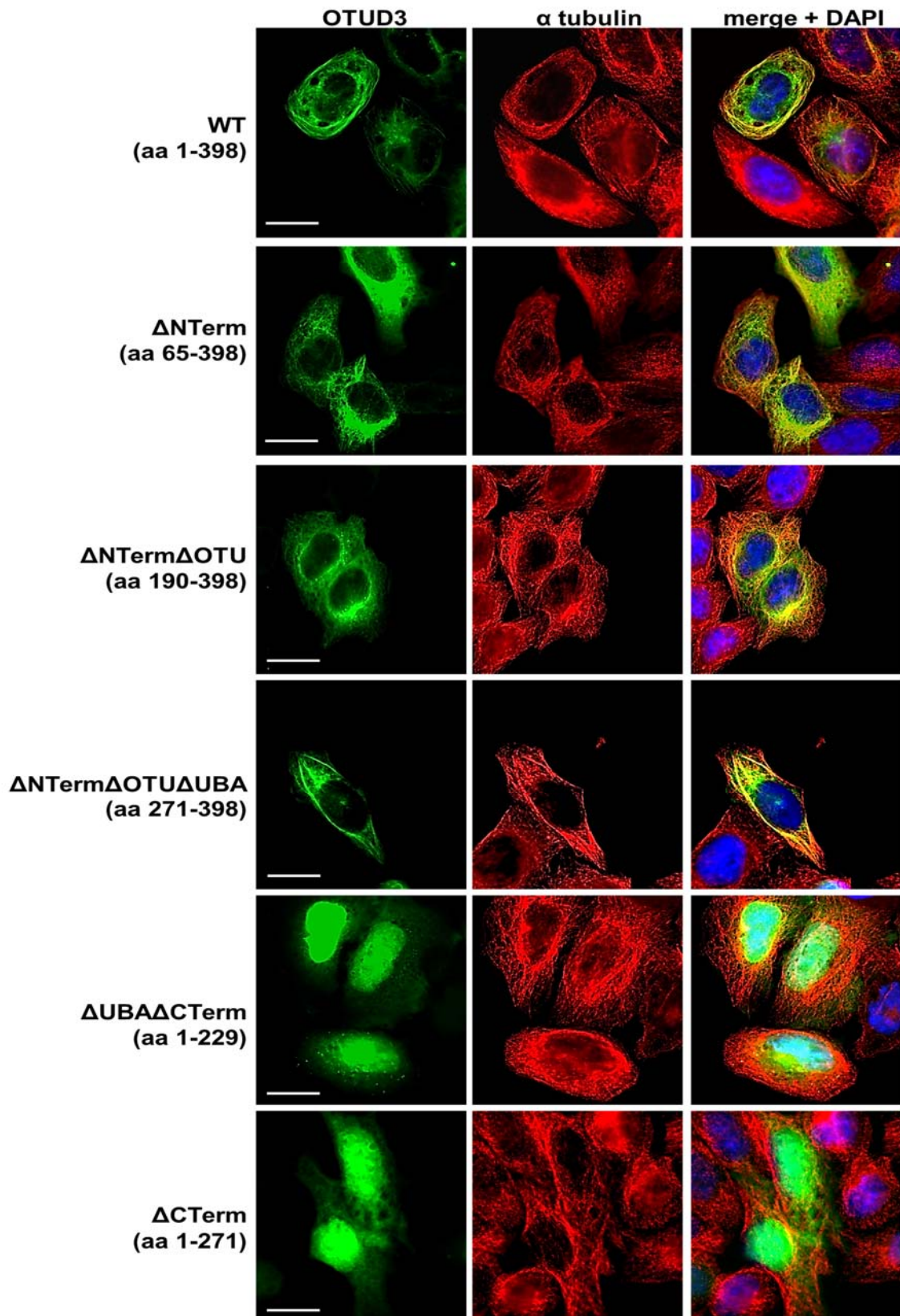


Figure 18) OTUD3 localization is guided by a microtubule-binding site, a NES and NLS. HeLa cells were transfected with plasmids coding indicated *N*-terminal GFP-tagged OTUD3 variants (green). After fixation in methanol α -tubulin was stained with anti α -tubulin antibody (1:500, Sima-Aldrich) and Alexa-568 coupled secondary antibody (1:1000, Sigma-Aldrich) (red). DNA was stained with DAPI (blue). White scale bars represent 10 μ M. C-terminal OTUD3 domain shows colocalization with microtubules. Lack of C-terminal domain leads to nuclear accumulation of OTUD3.

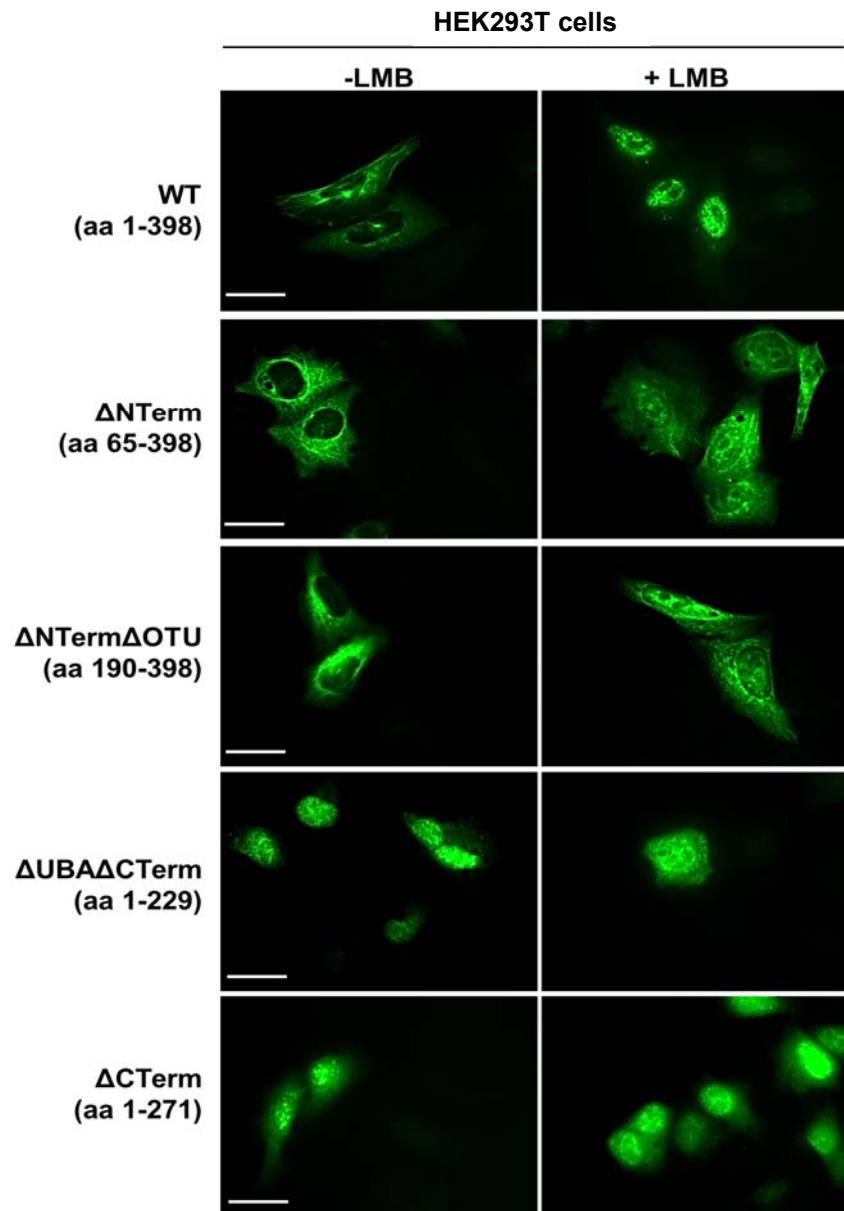


Figure 19) OTUD3 possesses a potential NES and NLS within its C- or N-terminus. HEK293T cells were transiently transfected with indicated *N*-terminal GFP-tagged OTUD3 variants. Cells were incubated with or without leptomycin B before fixation with methanole and subsequent imaging. Note, addition of leptomycin B induces nuclear accumulation of *N*-terminal truncated OTUD3 variants. Lack of C-terminal domain leads to predominantly nuclear localization of OTUD3 regardless of leptomycin B incubation. White scale bar represents a size of 10 μ m.

In both scenarios GFP-OTUD3 signal was present in the nucleus and the cytosol, while signal intensity was higher in the nucleus (Figure 19).

Taken together from immunofluorescence experiments, a potential NLS might be present within the *N*-terminus or the OTU domain of OTUD3. It was hypothesized, that the NLS is located within the *N*-terminus, because the OTU domain is highly conserved for enabling catalytic cysteine protease activity. Blasting full-length OTUD3 amino acid sequence by applying NLStradamus (prediction tool) a putative NLS was predicted within the *N*-terminus of the protein spanning residues 3-41 (Figure 20A).

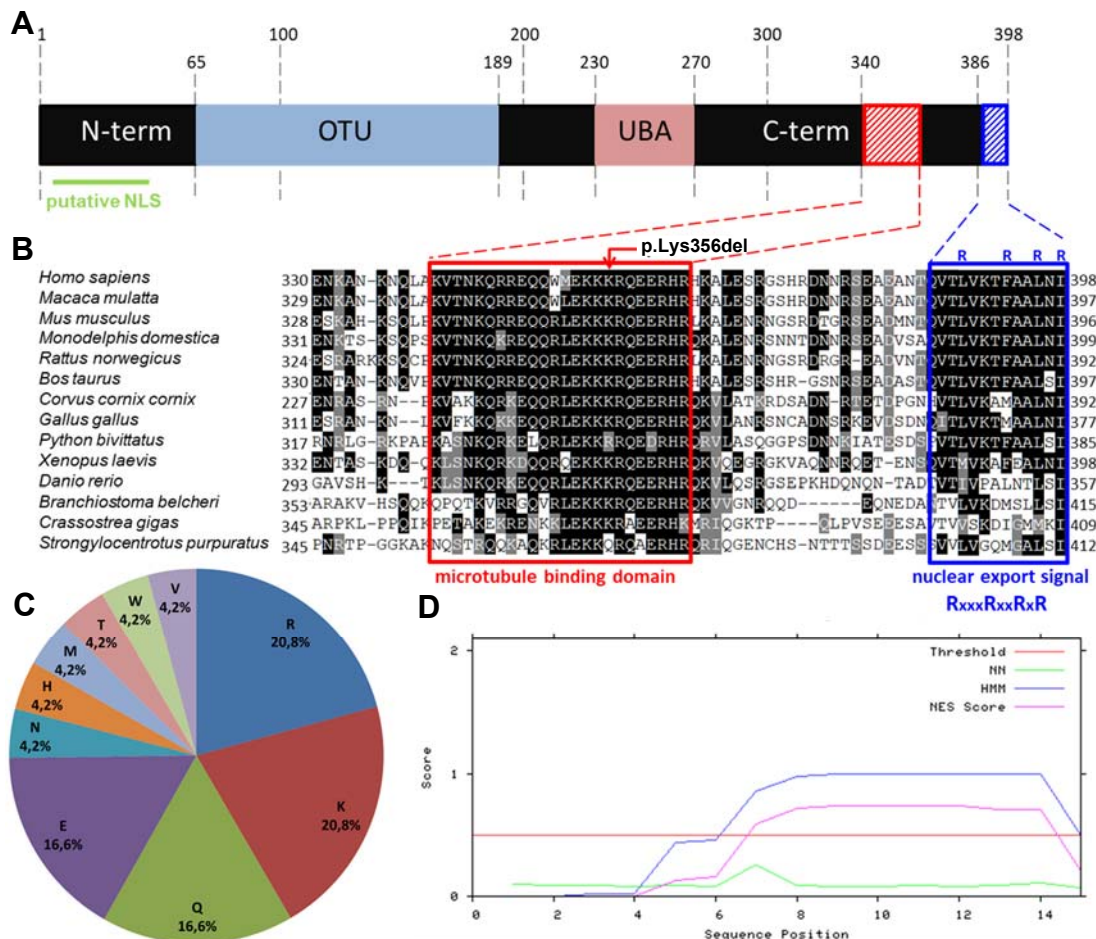


Figure 20) N- and C-terminal regions of OTUD3 enable nuclear-cytoplasmic shuttling. A) Schematic presentation of OTUD3 domains. B) Amino acid alignment of OTUD3 of different species. Putative microtubule binding domain is marked with a red box and a potential NES is marked with a blue box. C) Pie chart of the amino acid distribution of the putative microtubulin binding site demonstrates a highly charged character of this entity. D) NES prediction result applying NES NetServer1.1 tool. The prediction tool identified the distal residues of OTUD3 as NES. The distal 15 residues where analysed. NES is predicted for residues above threshold (red line).

4.5.4 OTUD3 co-sediments with polymerized microtubules

To biochemically establish the interaction between OTUD3 and polymerized microtubules co-sedimentation assay was performed (see 3.10.5). HeLa cells were transiently transfected with pCS2+ plasmid coding for wildtype OTUD3. After 16-20 h of expression at 37°C, cells were lysed and fractionated into polymerized and unpolymerized tubulins by ultracentrifugation experiment. Via anti-OTUD3 western blot analysed samples represented the total cell lysate, a nuclear/ debris fraction and the fraction of unpolymerized/soluble tubulins and the polymerized/ insoluble/ pellet microtubule fraction. As control 10 µg of untransfected and OTUD3 transfected lysate were loaded. Anti α-tubulin blots served as loading control. OTUD3 protein was detected in all separated cellular fractions (Figure 21). Thus, OTUD3 co-pelleted via ultracentrifugation with polymerized microtubules, as expected and seen via immunofluorescence microscopy experiments (see results 4.3.1, 4.5.1 and 4.5.2).

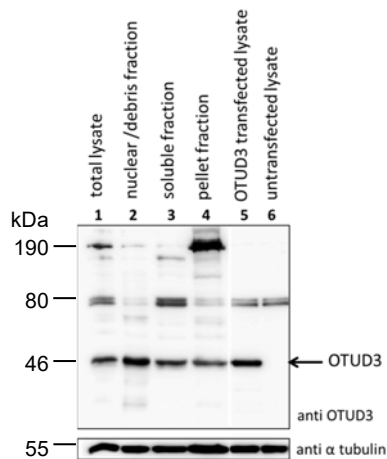


Figure 21: OTUD3 is present in polymerized tubulin fraction. Wildtype *OTUD3* was overexpressed in HeLa cells. Via differential centrifugation steps cell compartments were fractionated in nuclear/ debris fraction, a soluble and insoluble pellet fraction. Samples of each fraction were loaded on SDS PAGE gel. Western Blot was performed applying anti *OTUD3* antibody (Novus Biologicals, 1:200). As loading control anti α -tubulin antibody (Sigma, 1:500) was used.

4.6 *OTUD3* knock-out using CRISPR/ Cas9 technology

4.6.1 Generation and screening of positive *OTUD3* knock-out clones

Here, a protocol was established to generate *OTUD3* k.o. cell lines using a commercially available *OTUD3* CRISPR/Cas9 KO plasmid mixture (Santa Cruz Biotechnology) (see 3.11.9). The plasmid stock comprised three plasmids, whereof each plasmid contains a unique guide RNA, a GFP reporter for selection of transfected cells and a Cas9 coding sequence. One guide RNA target site is located 3' of *OTUD3* exon 3, and two sites within exon 4 (Figure 22A).

HeLa and HEK293T cells were seeded in 6 well plates and at 70% confluency cells were transfected with *OTUD3* CRISPR/Cas9 KO plasmid mixture and Lipofectamine 2000 reagent (see 3.11.4). After 36 h incubation at 37°C cells were detached and resuspended in cultivation medium. 96-well plates were prefilled with 200 μ l of a 1:1 mixture of cultivation and conditioned medium and a final FCS concentration of 20% for single cell sorting. Conditioned medium was collected from the respective cell line and sterile filtered through a 0.45 μ m syringe filter to avoid contamination with untransfected cells. GFP positive cells were single cell sorted in 96-well plates at the core facility cell sorting (Martin-Luther-University Halle-Wittenberg) using BD LSR Fortessa II instrument. Plates were centrifuged 1 min at 300 g. Next, plates were incubated at 37°C. Medium was changed every five days. After 2-3 weeks, wells containing small colonies were transferred into 12-well plates and after further 2-3 weeks into 6-well plates. Medium FCS concentration was reduced from 20% to 10% in steps of 2.5% every third day after cells were seeded in 12-well plates. Conditioned medium was reduced accordingly from 50% to 0% in 10% steps.

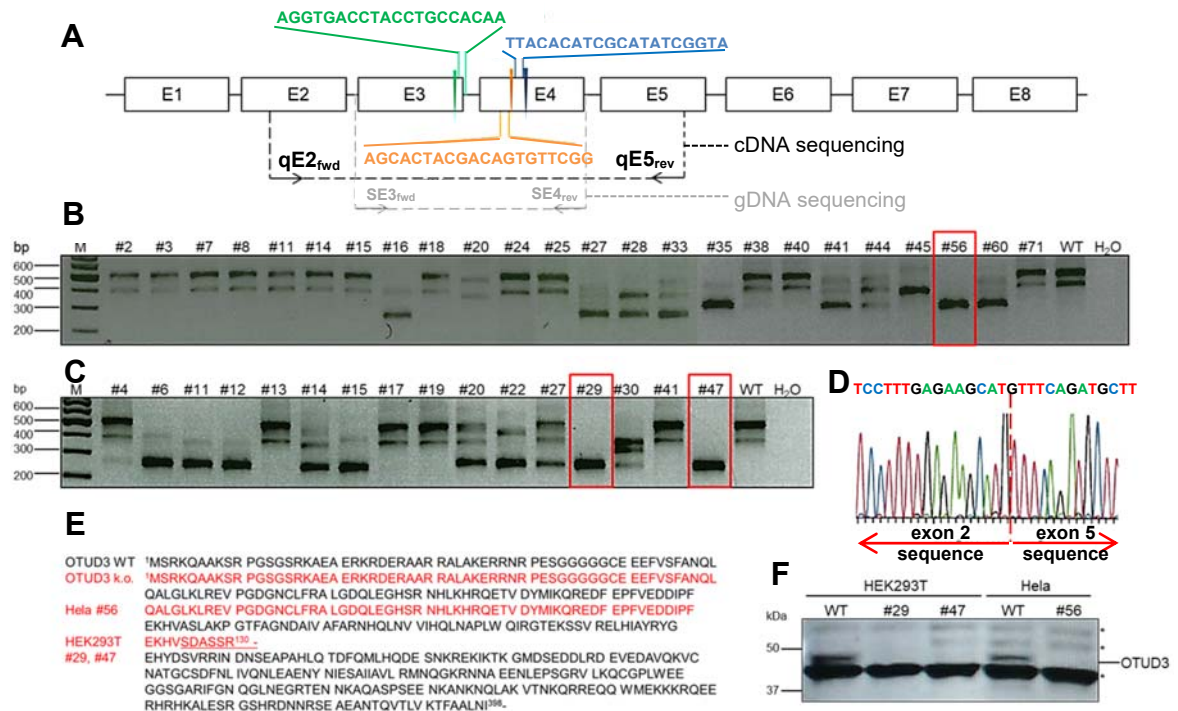


Figure 22: Screening and identification of *OTUD3* k.o. clones. A) Scheme of *OTUD3* exons and introns. Location and sequences of all three sense guide RNAs are shown in green, dark blue and orange. Respective DSB sites induced by Cas9 are shown as wedges. Used primers for gDNA and cDNA sequencing and locations are depicted. Primer sequences see 3.5. B) PCR products of 24 potential HeLa and C) 16 HEK293T *OTUD3* k.o. clones were loaded on 2% agarose gels. PCR products represent region spanning exon 2 to exon 5 of *OTUD3*. In comparison to wildtype cells (WT) HeLa clone #56 and HEK293T clones #29 and #47 showed a single PCR fragment suggesting deletion of exon 3 and 4. D) Representative Sanger sequence of HeLa clone #56 obtained via sequencing of cDNA. On cDNA level exon 2 and exon 5 sequences are adjacent and exon 3 and 4 sequence is missing. Same results were obtained for HEK293T clones #29 and #47. E) Comparison of human *OTUD3* wildtype protein sequence (black) and translated cDNA sequence of k.o. clones (red). Note, a stop codon is introduced at position 131 in k.o. clones. F) Western blot analyses of *OTUD3* k.o. clones. All analysed k.o. clones showed no presence of *OTUD3* protein. * marks unspecific bands. 20 μ g of total cell lysates were loaded on 14% SDS PA gels. Western Blot was performed applying anti *OTUD3* antibody (1:250, Novus Biologicals). Subsequently, the PCR product was Sanger sequenced (see 3.9.5).

OTUD3 k.o. clones were screened by cDNA analyses, DNA sequencing, and Western blot analyses. In case of HeLa cells, 65 single clones from one 96 well plate built colonies and were saved as cryocultures. 24 of these clones were selected for RNA isolation and cDNA synthesis (see 3.9.8, 3.9.9). To screen for positive *OTUD3* k.o. clones a PCR approach on cDNA level was chosen. Given the three *OTUD3*-specific 20 nt guide RNA sequences that direct the Cas9 protein to induce site specific double strand breaks (DSBs) within the genomic DNA a loss of exonic and intronic gDNA encompassing *OTUD3* exon 3 to 4 was expected. Therefore PCR primers were used to generate a PCR product spanning exon 2 to exon 5 on cDNA level (see 3.5, primer

qE2_{fwd} and qE5_{rev}). From 24 analysed clones only one clone (#56) revealed a homozygously induced DSB (Figure 22B, red box).

cDNA sequencing proved, that *OTUD3* exon 2 sequence gets directly fused to exon 5 sequence while splicing and exons 3 and 4 are missing on both alleles (Figure 22D). Translation of this transcript leads to a frameshift and introduces a preliminary stop codon (Figure 22E). On DNA level the sites of induced DSB's were confirmed located 3' within exon 3 and centered within exon 4 of *OTUD3* by sequencing (SE3_{fwd}/SE4_{rev}). For HEK293T cells only 31 clones from 96 well plate formed colonies and were followed up. From 16 investigated clones two clones (#29, #47) showed homozygously altered PCR fragments on agarose gel in comparison to wildtype cDNA product (Figure 22C). cDNA sequencing of both clones confirmed missing exons 3 and 4 of *OTUD3* (representatively shown result for HEK293T in Figure 23D). When DNA of clone #29 was sequenced DSB sites were confirmed. Finally, in all three clones (#29, #47, #56) no *OTUD3* protein was detected confirming successful generation of *OTUD3* k.o. in HEK293T and HeLa cells (Figure 22F).

4.6.2 *OTUD3* k.o. has cell line specific effects on cell morphology

In order to gain first knowledge about consequences of *OTUD3* k.o. HEK293T and HeLa k.o. cells were compared to wildtype cells via light-microscopy. As in this thesis *OTUD3* was identified as MAP wildtype and *OTUD3* k.o. cell lines were fixed after 16 h of incubation at 37°C and stained for α -, β - and γ -tubulins. No obvious quantitative or structural changes of the stained tubulins were seen (data not shown). However, both k.o. cell lines revealed altered cell morphology when living cells were analyzed via microscopy instead (Figure 23). HeLa k.o. cells presented with an enlarged size and a more rounded appearance in comparison to wildtype cells. In case of HEK293T, *OTUD3* k.o. cells were comparable in size with wildtype cells. In contrast, elongated and more frequent filapodia were detected in k.o. cells. In summary, *OTUD3* k.o. resulted in cell line specific alterations of cell morphology.

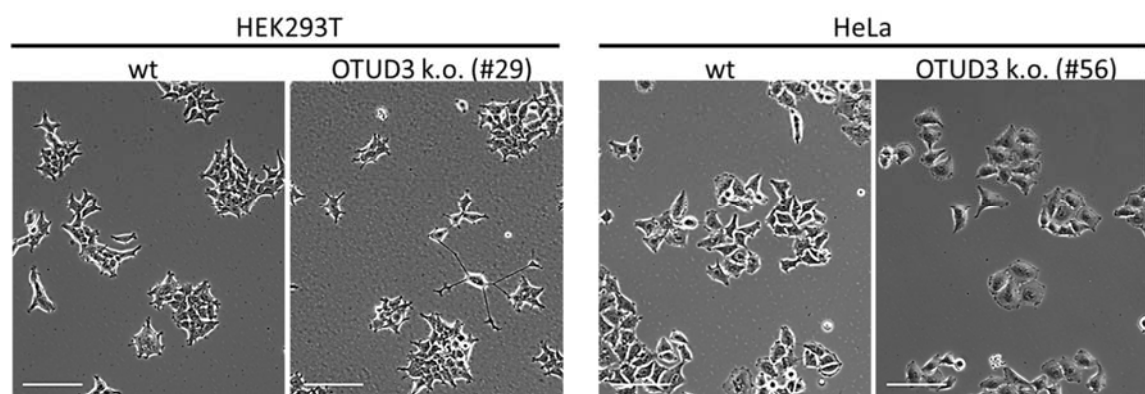


Figure 23) Cell morphology is altered in HEK293T and HeLa k.o. cells. Micrographs were taken 16 h after seeding and incubation at 37°C. White scale bars indicate 100 μ m.

5. Discussion

5.1 Correlation of *OTUD3* genotypes to AS-like phenotypes

5.1.1 *OTUD3* as candidate gene for neurodevelopmental disease

Dysfunctions of DUBs are associated with several diseases like metabolic, cardiovascular, cancer and neurodegeneration. In context of *OTUD3* recent publications focused on its role in cancer, because the tumor suppressor PTEN was discovered in 2015 as *OTUD3* interaction partner and substrate [128]. Interestingly, *in vivo* results proved a tumor-suppressing or tumor-promoting function of *OTUD3* in a cell- and tissue-dependent manner. *OTUD3* k.o. in mice resulted in an increased susceptibility to breast cancer and a decreased susceptibility for non-small lung cancer [134]. A correlation of Mendelian inherited *OTUD3* mutations within patient cohorts of different cancer entities was not described so far. One genotype-phenotype link for patients suffering from ulcerative colitis exists from genome wide association studies. Region spanning genes *RNF186-OTUD3-PLA2G2E* at chromosome arm 1p36.13 is described as risk loci for ulcerative colitis [166].

To elucidate *OTUD3* as potential novel gene for inherited diseases conservation of gene arrangements surrounding *OTUD3* was investigated. In Mammalia, Aves, Actinopterygii and Amphibia high conservation was observed, except for zebrafish. In accordance to published data from Crotalinae snakes upstream of *OTUD3* a linear arrangement of *PLA2* genes was detected [167]. Interestingly, *OTUD3* gene is adjacent to a cluster of *PLA2* genes coding for secretory acting proteins. If *OTUD3* gets secreted from cells is unknown. Alignment of *OTUD3* amino acid sequences of 25 eukaryotes confirmed high evolutionary conservation. Especially, mammals and oviparous form closely related branches. Besides highly conserved OTU and UBA domain, C- and N-terminal domains of *OTUD3* revealed high conservation. Interestingly, a C-terminal located isoleucine residue was found in all analyzed organism and up to sea urchins and oysters. In lipoxygenases C-terminal conserved isoleucine binds iron and is thereby critical for enzyme activity [168,169]. If *OTUD3* or another OTU family DUB is a metal-binding protein is not known.

Furthermore, in fluorescence microscopy analyses of endogenous stained *OTUD3* it was noticed that nuclear and cytosolic distribution patterns in several mice and human cell lines were similar as well as colocalization with tubulin structures. qPCR analyses of *OTUD3* within 18 human organs showed organ dependent *OTUD3* mRNA expression. Here obtained *OTUD3* expression results are comparable to published expression data from the human protein atlas database [170]. For example, organs like skin and testis showed highest expression. In respect to neurodevelopmental disease high expression of *OTUD3* in fetal and adult brain was detected, as well as high

expression in further 13 investigated brain areal tissues managing voluntary movements, speech development and visualization perception. Reconsidering the phenotype of here investigated patients it is noteworthy that highest expression levels of *OTUD3* were found in the caudate nucleus and putamen that build up the dorsal striatum. The striatum is responsible for voluntary movements. Thus, the ataxia-like signs and seizures of patients harbouring putatively disease causing homozygous *OTUD3* c.1061_1063delAGA mutation might be a result of altered *OTUD3* function in the striatum. In addition, detection of high *OTUD3* expression in areals like supramarginal gyrus and broca (both involved in language perception and speech development) and lateral geniculate nucleus (obtains sensory input from retina) may be in line with lack of speech and visual defects of patients.

Taken together, highly conserved *OTUD3* gene locus, protein sequence and cellular localization as well as high expression levels in brain accentuate *OTUD3* as plausible candidate gene in neurodevelopmental disease.

5.1.2 Evaluation of *OTUD3* SNV and CNV results

This thesis is based on a consanguineous index family with four severely affected children presenting a neurodevelopmental phenotype. In 2012, the disease locus was mapped to chromosome 1p36.12 including 58 genes by indirect prenatal diagnostics and genome wide linkage-scan with adjacent fine mapping and haplotype analyses. An affection of an unborn fetus was excluded and a healthy child was born upon [137]. Targeted Sanger sequencing of genes within the linkage-interval revealed that *OTUD3* c.1061_1063delAGA mutation co-segregated with disease. Affected children were homozygous, whereas healthy parents and siblings were heterozygous for *OTUD3* AGA deletion reflecting an autosomal recessive inheritance. *OTUD3* c.1061_1063delAGA is so far not annotated homozygous in ExAc or gnomAD and predicted to be disease causing applying MutationTaster. After finishing this thesis, targeted enrichment of the exome of index patient 784 was performed with SureSelect All Exon Kit V2 (Agilent) and libraries were sequenced on the HiSeq 1500 platform (Illumina). Functional analysis and American College of Medical Genetics and Genomics (ACMG) classification were carried out using Ingenuity (QIAGEN). Variants with an allele frequency above 0.01 in healthy control individuals from large population studies were excluded and further variant filtering was done according to diagnostic quality scores, phenotype (intellectual disability and microcephaly) and an autosomal recessive or dominant model of inheritance [171,172]. Besides *OTUD3* c.1061_1063delAGA mutation, additional 46 homozygous variants were found, but did not uncover any other candidate mutation classified as pathogenic or likely pathogenic according to ACMG criteria [173]. However, several unclassified variants

(UCVs) with unknown clinical relevance (predicted deleterious or gain of function variants within the linkage region) were found and will be further elucidated (work in progress, Institute of Human Genetics, Halle).

Affected children showed overlapping clinical phenotypes of AS patients. The AS is a rare genetic disorder, characterized by developmental delay, mental retardation, absent of speech and motor impairments as consequence of a deficient ubiquitin E3 ligase E6AP, encoded by the *UBE3A* gene [174–177]. Up to 70 % of AS patients show deletions of the *UBE3A* containing 15q11.2-q13 region, whereas in 7% of patients mechanism of paternal uniparental disomy of chromosome 15 is disease causing. In addition, *UBE3A* loss of function mutations in the maternal copy account for 10% of AS patients. Imprinting defects within the imprinting center region 15q11.2-q13 are rare with 2-5%. Interestingly, nearly 10% of AS patients remain without an identified molecular defect [178,179]. This suggests that other factors involved in the ubiquitination process could play a role in AS development.

A cohort of 121 AS-like patients, but without detected *UBE3A* defect was selected for *OTUD3* sequencing by Sanger method. Novel patients with homozygous or heterozygous c.1061_1032delAGA (p.Lys356del) variation were not found. In 24% of patients *OTUD3* SNVs were identified. If SNVs were likely pathogenic or benign was investigated using commonly used prediction tools MutationTaster2, PolyPhen-2 and population datasets like 1000Genomes and gnomAD. Heterozygous or homozygous missense variants resulting in A333T alone or combined with N321S exchange were considered to be benign. Interestingly, in eight patients a heterozygous silent SNV (rs61769077; c.603G>A; p.T201T) was predicted by MutationTaster2 to be disease causing, because of a putatively induced splice site defect. However, MAF of 0.04 was considered too high for disease relevance as well as heterozygosity of this variation. To securely exclude an effect of rs61769077 for neurodevelopmental disease family anamnesis, *OTUD3* mRNA expression analyses as well as *OTUD3* protein level analyses are needed. So far only DNA samples of these eight patients were available for analyses. Another patient possessed a heterozygous R347Q exchange. Prediction tools failed for evaluation of this variant, because of contrary results. MAF of R347Q was 0.01 and rare. If parents are affected, or if R347Q is *de novo* is not known. However, assuming a recessive mode of inheritance, a second mutation would have to be found. In summary, so far no novel *OTUD3* SNVs within AS-like cohort were assumed likely pathogenic.

Of interest, in 12% of the analyzed AS-like cohort sequencing results for *OTUD3* exon 1 are missing. Without success it was extensively tried to obtain PCR products with so far six different primer pairs, nested PCR set-ups, high PCR amplification cycles (up to

40 rounds) as well as with PCR additives like betaine or DMSO. In addition, primers located within exon 1 of *OTUD3* were used without obtaining PCR products too. Exon 1 of *OTUD3* is characterized by a high GC content of 76% implicating an obstacle for PCR approaches. In gnomAD, *OTUD3* exon 1 per-base mean depth of coverage derived from exomes was low with only 10. However, sequences of exon 1 were obtained in 88% of patients without hurdles. Thus, another reason might be the deletion of *OTUD3* exon 1 in 12% of AS-like patients. Reconsidering the phenotype of index patients and of AS-like cohort other neurodevelopmental syndromes has been described where exon 1 deletion is assumed to be disease causing. For example deletion of exon 1 of the *MCT8* gene occurs in patients with Allan-Herndon-Dudley syndrome (AHDS) [180]. Encoded membrane protein functions in the transport of triiodothyronine into neurons. AHDS is a X-linked type of mental retardation with clinical presentation of delay in developmental milestones, muscle hypotonia and hypoplasia, ataxia as well as difficulties or complete absence of speech [181]. In 2015; a case was published where the promoter region and exon 1 of *AUTS2* gene was *de novo* deleted and associated with autism spectrum disorder and developmental delay [182].

To securely attest the lack of *OTUD3* exon 1 in 12% of AS-like cohort further analyses are needed for example via long-range PCR, array CGH, experiments on mRNA level, parental DNA analyses or MLPA to map the size and location of the hypothesized deletion. In line with lacking *OTUD3* exon 1 sequencing data the design of a suitable probe for exon 1 and further CNV analyses of *OTUD3* exons via MLPA assay failed too. Here, two different probes for exon 1 were designed and included within the MLPA P300 reference probe-set derived from MRC Holland. Obtained peaks after capillary electrophoresis had very low intensity or peaks were asymmetric when tested with control DNA (data not shown). Thus, no CNV data are available for *OTUD3* exon 1 reflecting again the bad accessibility of *OTUD3* exon 1 by PCR based approaches. However, 105 DNA samples of AS-like cohort patients and of 96 healthy blood donors were analysed for CNVs of *OTUD3* exons 2-8. In all healthy donor samples no CNVs were detected verifying the robustness of the established MLPA assay and rare occurrence of *OTUD3* CNVs. Within the AS-like cohort four unrelated patients (ID: 04999, 05251, 06116, 06273) possessed several CNVs including intragenic duplications and deletions.

DNA samples of these four patients were further analysed by qPCR of each exon 2-8 and by overlapping long-range PCR spanning exons 1-2, 2-4, 4-7 and 7-8. qPCR data mainly confirmed the obtained CNV results from MLPA experiments in particular for exon 6 duplications within all four AS-like patients. Differences between MLPA and qPCR results were noticed and might be due to the following limitations: qPCR primers

and MLPA probes had different annealing positions within the exons, varying qPCR primer pair efficacy, GC content, repeat sequences, contaminations (e.g. phenol)/ DNA quality and MLPA assay was only designed to quantify up to twofold excess of an exon in comparison to control DNA. The latter is due to a technical limitation in quantifying too high probe peaks in capillary electrophoresis (fluorescence signal cut-off). Methodical differences of MLPA and qPCR for the detection of CNVs are known from human *β -defensin* gene locus analyses that provided inconsistent results for absolute copy numbers [183]. Other inter-method quantifications proved that MLPA is superior to qPCR approach in CNV detection [184].

Next, potential *OTUD3* CNV harbouring patients were analysed via long-range PCR covering all eight *OTUD3* exons in an overlapping PCR product design. While for applied 96 control DNAs all expected PCR fragments could be generated, only in patient 05251 a single fragment for region of exon 7-8 in low amount was detectable. These findings suggest that in all four patients both *OTUD3* alleles might be affected by multiple CNVs. If so, it could be speculated that found CNVs might be causative for AS-like phenotype. Intragenic inversions, or genom-wide rearranged/ transposed positions of single exons can not be excluded by the performed experiments. Strikingly, parental DNA analyses of patient 04999 via sequencing, MLPA, qPCR and long-range PCR displayed no CNV abnormalities. Thus, in patient 04999 CNVs were proved to be *de novo*. CNVs gained much attention in pathogenesis and clinical modulation of phenotypes for other diseases like autism, Fragile X syndrome or schizophrenia. CNVs can change gene dosages, interrupt coding sequences, can influence adjectant gene regulation and sometimes they can cause exon shuffling [185,186]. But CNVs contribute to genetic heterogeneity of the human genome and validation for disease relevance is a current obstacle. Large control cohorts were analysed and it was shown that every person carries a set of CNVs that are mostly benign [187,188]. However, the relevance of CNVs of DUBs was shown for *OTUD7A* that regulates neurodevelopmental phenotypes in the 15q.13.3 microdeletion syndrome. Reduced *OTUD7A* levels were linked to dendritic spine and neurite outgrowth deficiencies [189]. Follow up experiments with all *OTUD3* CNV positive AS-like patients should include parental (DNA/ RNA) analysis, (m)RNA analyses as well as attempts to further map and confirm the deletion or duplication breakpoints and of course size and location of gene aberrations within *OTUD3*.

Most striking, we got aware of a severely diseased boy with symptoms like intellectual disability, congenital blindness, hypotonia, scoliosis, speech limited to a few words and motoric deficits. A potential genotype-phenotype match to our index family with AS-like defect on GeneMatcher platform enabled us to contact the Department of Clinical

Genetics, Erasmus Medical Center in Rotterdam (NL). The affected boy has a healthy twin and healthy consanguineous parents originating from Bulgaria. The affected twin possessed a homozygous *OTUD3* mutation (rs1311291528, c.G739A; p.D247N), whereas mother, father and healthy sibling was heterozygous for the mutation reflecting an autosomal recessive inheritance. c.G739A mutation resides at the 5'-start of exon 6 of *OTUD3* and thus might be relevant for transcript splicing as predicted as consequence by MutationTaster and PolyPhen-2. On protein level, D247N exchange is located within the evolutionary conserved center of the UBA domain of *OTUD3* as important site for protein-protein interactions. Comprehensively, prediction databases MutationTaster, PolyPhen-2 and SIFT classified the novel identified *OTUD3* mutation as disease causing, possibly damaging and deleterious. In gnomAD, ExAC or 1000Genomes homozygous c.G739A mutation was not found. Investigations of the functional relevance of c.G739A *OTUD3* variant in diseased twin are ongoing.

Patients harbouring *OTUD3* p.Lys356del and p.D247N mutation showed clinical overlaps in respect to speech, intellectual disability, motoric deficits as well as visual defects and facial appearance underlining the potential relevance of *OTUD3* in a spectrum of inherited neurodevelopmental diseases.

5.1.3 p.Lys356del *OTUD3* mutation and cellular consequences

Searching for first cellular consequences with potential clinical relevance for *OTUD3* p.Lys356del defect patients *OTUD3* expression levels were measured via qPCR in LCLs and primary fibroblasts of patients and compared to matched controls. No differences were detected between patient and control *OTUD3* mRNA levels. Alternative splicing was not investigated. In accordance to unaltered *OTUD3* mRNA expression, *OTUD3* protein amounts were found to be similar between patient and controls.

Next, cysteine protease activity of *OTUD3* was assessed. Cell lysates were supplemented with cysteine inhibitor Ub-PA or Ub-VME (suicide substrates) that gets irreversibly linked to active sites of functional cysteine proteases. This experiment proved: 1) Endogenous *OTUD3* was verified as a functional cysteine protease, because of its ability to link different cysteine inhibitors (Ub-PA and Ub-VME) to the active site and the prevention of ubiquitin conjugation to *OTUD3* due to preincubation with the cysteine inhibitor NEM. So far, *OTUD3* was classified as cysteine protease due to sequence alignments and identification of the catalytic OTU domain and by *in vitro* ubiquitin conjugation assays applying truncated purified *OTUD3* from *E.coli* [127]. 2) The active cysteine protease site of *OTUD3* seems to be not directly influenced by the lysine deletion p.Lys356del. However, minor changes in the amount of *OTUD3* protein or an altered accessibility to the active site can not be excluded. It remains

further unclear if deleted lysine residue is further modified by e.g. ubiquitin, UBLs, methylation or acetylation. It is known for ubiquitin itself that six of seven lysine residues can become acetylated and thereby minor conformational changes are induced altering signaling outcomes [53,55]. In 2020 it was published that OTUD3 possesses three specific acetylation sites: Lys129, Lys322 and Lys332. Viral infection was associated with OTUD3 Lys129 deacetylation, OTUD3 inactivation and enhancement of the innate antiviral immunity [190].

In immunofluorescence microscopy predominant cytosolic and less nuclear endogenous OTUD3 localization was observed. Notably, colocalization of OTUD3 and tubulin filaments was detected. Nonetheless, primary fibroblasts of patients and controls uncovered no distinct differences. Other DUBs are known that are tubulin associated, expressed in a cell-cycle dependent manner or regulate mitosis namely USP9X, USP21, USP35, USP44, AMSH, CYLD or CEZANNE [191]. Exemplified for CYLD, protein levels decrease when cells exit from mitosis, localizes to microtubules during interphase and migrates to the midbody during telophase. Depleted CYLD cells showed delayed mitosis entry, whereas overexpression was concomitant with fragmented or multinucleated cells, impaired chromosome segregation and cytokinesis [192,193]. To further analyse OTUD3 wildtype and p.Lys356del effects on expression and localization cell-cycle dependent analyses should be focused.

Next, a potential role of OTUD3 in BMP signaling pathway was hypothesized based on recent and unpublished findings from group of Prof. Hollemann (Martin-Luther-University Halle-Wittenberg). In model organism *Xenopus laevis* an *otud3* k.d. via morpholino technology was generated. *otud3* morphants revealed a spectrum of phenotypic alterations that included bent tails, malformed heads and eyes, reduced pigmentation and a movement disorder reminding of the phenotype of OTUD3 p.Lys356del defect children. Interestingly, *otud3* morphants showed overlapping characteristics of *Tsg* k.d. morphants in *Xenopus* [194]. *Tsg* is a BMP modulatory protein that was shown to interact with BMP4 and inhibitor chordin and is involved in early developmental processes like axis determination [195]. In addition, DUBs like USP15 and OTUD4 protect BMPR1A (ALK3) as well as SMAD4 protein from degradation [196,197]. Here, OTUD3 p.Lys356del patient LCLs showed that basal pSMAD1/5 levels as well as BMP4 induced pSMAD1/5 levels were significantly lowered. Preincubation with synthetic BMPR1A inhibitor LDN-193189 abolished phosphorylation of SMAD1/5 proteins. Notably, basal and BMP4 induced and BMPR1A inhibitor preincubated pSMAD1/5 level in OTUD3 defect patient was not significantly altered suggesting a very low rate of BMP signaling in patient.

Lastly, LCLs of patients reflected higher metabolic activity than controls in MTT assay and possessed higher proliferation rates of viable cells. USP family member DUB CYLD was described as tumor suppressor in several malignancies like melanoma, salivary gland, cervical and lung cancer [198–202]. As OTUD3, CYLD localizes to microtubules and the midbody [192,203,204]. Conclusions whether OTUD3 acts directly, indirectly, as activator or inhibitor of BMP4 induced pSMAD1/5 signaling, cell metabolic activity, cell viability or proliferation stays unacknowledged. However, regulation of signaling pathways like Wnt (TRABID), TGF β (OTUB1, A20) or nF-KB (OTUD7B, A20) seems to be a common feature for members of the OTU subfamily of DUBs and within this thesis OTUD3 was linked to BMP pathway [162–165,205].

5.2 Functional relevance of OTUD3's terminal domains

5.2.1 Identification of a microtubule-binding site

A common feature of DUBs is their multi-domain architecture. Thereby, the catalytic core fold defines the classification into six subfamilies of DUBs [62]. In case of OTUD3, sequence alignments identified a highly conserved OTU domain resembling a catalytic triad of a cysteine protease and secondly a UBA interaction site. A truncated *OTUD3* variant was expressed and protein was purified from *E.coli* and crystallized [127]. To date, the available crystal structure spans 160 aa residues and contains the OTU and UBA domain (aa 49-209), whereas the *N*-terminal (aa 1-48) and *C*-terminal regions (aa 210-398) of OTUD3 were missing.

In this thesis a potential microtubule-binding site located within the *C*-terminus of OTUD3 (aa 340-363) was identified. Co-staining of endogenous OTUD3 and α -tubulin within different human and mouse cell lines showed in about 30% of cells an overlap of OTUD3 signal and filamentous tubulin structures. While fluorescence microscopy the endogenous staining of OTUD3 showed fast bleaching of the signal assuming low levels of endogenous OTUD3 protein. In addition, cells were fixed using 4% PFA and not with methanole, because the applied polyclonal anti-OTUD3 antibody was not compatible. Nonetheless, endogenous OTUD3 was found to decorate mitotic spindles in metaphase and late telophase of cell cycle synchronized HeLa cells and notably the midbody. In serum starved mouse fibroblasts NIH3T3 OTUD3 was present on primary cilia axoneme.

A first global assessment of 20 DUBs and their localization patterns was conducted in *Schizosaccharomyces pombe* [206]. An orthologue of human OTUD3 was not assessed. Next, localizations of 66 *N*-terminal GFP-tagged deubiquitinases were published in a systematic survey [207]. Here, only USP21 was reported to be associated with the microtubular cytoskeletal network. USP21 was further characterized and found to bind directly to microtubules via a novel microtubule binding

motif located within its *N*-terminus (aa 59-75). Interestingly, USP 21 was reported to be involved in primary cilia formation in A549 cells and neurite outgrowth in PC12 cells. In this survey, localization of OTUD3 was described being cytosolic and nuclear in accordance to the results of this thesis. In contrast, no microtubule association was found. It is not surprising that here identified similar localization patterns of OTUD3 and USP21 result in overlapping functional descriptions. In 2018 it was published that USP21 and OTUD3 antagonize ZNF598-mediated 40S ribosomal protein ubiquitylation and thereby play an important role in ribosomal quality control [208]. Another already known microtubule associated DUB CYLD localized to the cytosol and plasma membrane, but displayed no expected microtubule colocalization within systemic DUB localization report from Urbe et.al. [192,207]. Thus, this finding underlines that GFP-tags can interfere with correct localization of proteins. However, k.d. of endogenous OTUD3 by applying siRNA technology, overexpression of *N*-terminal GFP-tagged OTUD3 and nocodazole experiments confirmed comprehensively the colocalization of OTUD3 with tubulin filaments.

A set of *N*-terminal GFP-tagged OTUD3 variants were cloned and transfected into HeLa cells to further investigate a potential microtubule binding site within OTUD3. If *N*-terminal GFP-tagged wildtype OTUD3 was transfected, as seen for endogenous stained OTUD3, about 30% of GFP-positive cells showed microtubule association suggesting OTUD3 interacts with both free and polymerized tubulins. If *N*-terminal truncated variants were transfected about 90% of GFP-positive cells showed a strong pronounced association of OTUD3 with polymerized microtubules. Thus, it can be hypothesized that the *N*-terminal domain of OTUD3 contains a negative regulatory tubulin-binding domain (e.g. by recruiting other binding partners or by controlled posttranslational modifications inducing conformational changes) or simply its fold sterically limits the access of microtubulins to an OTUD3 interaction site. Finally, variants lacking the OTUD3 C-terminus showed no tubulin filament colocalization, whereas if variant of OTUD3's C-terminus was analyzed association with tubulin polymers was detected. Here, protein sequence alignments within the eukaryotic kingdom uncovered a highly conserved and charged stretch as putative microtubulin binding site within OTUD3's C-terminus. In human the stretch comprises aa 340-363 and has a pI of 11 using ProtParam tool. Microtubule binding motifs were described as highly charged domains with a high pI around 10 [209]. A protein blast with the putative microtubule binding motif revealed two hits in the human proteome: OTUD3 and Tankyrase-1. Similarity of both sequences was low, but interestingly Tankyrase-1 triggered polymerization of poly(ADP-ribose) is required for spindle structure formation and function [210]. A sequence similar to the tubulin-binding domain of Tau (KKVaVvR)

was found in USP21 (KKLeLgR) [207,211]. In comparison, identified microtubulin binding motif within OTUD3 (human: ³⁴⁰NKANKNQLAKVTNKQRREQQ WMEKKKRQEERHR³⁶³) appears elongated and lysine-rich.

As first biochemical prove of OTUD3 and tubulin interaction free tubulin and polymerized tubulin fractions were separated via ultracentrifugation assay after untagged *OTUD3* was overexpressed in HeLa cells. OTUD3 cosedimented with polymerized tubulins. Further investigations of OTUD3 and tubulin interaction were conducted in the context of a master thesis [212]. Via co-immunoprecipitation assays β -tubulin was identified as OTUD3 interaction partner. If OTUD3 binds directly to β -tubulin or indirectly via other so far unknown tubulin binding proteins is not known. In addition, co-immunoprecipitation assay does not allow a discrimination of monomeric β -tubulin or polymerized filaments. Unpublished mass spectrometry data obtained in collaboration with group of Prof. Kessler (Nuffield Department of Medicine; University of Oxford; experiments performed by Carolin Mai, IPC Martin-Luther-University Halle-Wittenberg) showed an OTUD3-dependent tubulin deubiquitination. In addition, here generated HeLa OTUD3 k.o. cell line (clone #56) exhibited higher levels of co-immunoprecipitated (ubiquitinated) β -tubulin than wildtype cells [212]. Further experiments are needed to characterize which types of ubiquitination and which complexes of β -tubulin subunits are formed and regulated by OTUD3 activity. High reversibility of ubiquitination is a big obstacle while isolation and characterization of ubiquitinated proteins. Therefore, a powerful read out tool called ubiquitin-specific tandem ubiquitin binding entities (TUBEs) was developed for specific detection and isolation of polyubiquitinated proteins [213]. Further OTUD3 β -tubulin studies should consider that in eukaryotes multiple isotypes of tubulins exist. In case of β -tubulin eight isotypes are known in human [214]. Expression of these isotypes can depend on cell types like neurons, platelet and sperm and it was shown that they are interchangeable for proper function [215]. Taking in account the neurodevelopmental phenotype of AS-like patients embryonic and neuronal cell lines are of interest.

This thesis enabled the identification of OTUD3 as microtubulin associated protein (MAP) and characterization of an interaction site within OTUD3's C-terminus. Follow up studies could acknowledge OTUD3 interaction with β -tubulin and an OTUD3 dependent tubulin deubiquitylation.

5.2.2 Description of NES und NLS sequences

In 2012, cellular localization pattern of OTUD3 was described mainly cytosolic and less nuclear in accordance to here presented microscopy findings of endogenous and overexpressed protein [207]. Novel here, overexpression of GFP-tagged C-terminal truncated OTUD3 variants shifted localization from the cytosol to the nucleus in all

analyzed cell lines. Combining both findings the presence of a C-terminal located NES of OTUD3 was hypothesized. *In silico* NES prediction identified a hydrophobic C-terminal NES stretch of OTUD3. The predicted NES resembles common **RxxxRxxRxR** motif. **R** represents a hydrophobic amino acid and x any other amino acid. In human the putative NES sequence is likely ³⁸⁹LVKTFAALNI³⁹⁸. Across species the hydrophobic residues R of this NES are highly conserved suggesting functional relevance.

CRM1 (exportin) is the most common mammalian nuclear export protein that facilitates the transport of large macromolecules including RNA and protein across the nuclear membrane to the cytoplasm via recognition of NES motifs [216]. Leptomycin B is a potent inhibitor of CRM1 leading to nuclear accumulation of NES containing proteins [217]. Addition of Leptomycin B to HEK293T cells and staining of endogenous OTUD3 or visualization of all GFP-tagged N-terminal truncated OTUD3 variants showed accumulation of OTUD3 in the nucleus. Thus, a NES C-terminal of OTUD3 was confirmed. Notably, cells rapidly died if a construct coding OTUD's C-terminus was overexpressed. This suggests that OTUD3 plays important roles in the cytoplasm as well as in the nucleus and that disbalance of protein distribution might be lethal.

Recently, follow up studies were performed with OTUD3 variants lacking the here supposed C-terminal NES (EGFP-OTUD3 Δ NES). In contrast to wildtype cells, cells overexpressing EGFP-OTUD3 Δ NES showed distinct nuclear protein accumulation. If wildtype NES was replaced by an artificial NES distribution of OTUD3 appeared predominantly cytosolic again [212].

Blasting full-length OTUD3 amino acid sequence by applying NLStradamus (NLS prediction tool) a putative NLS was predicted within the N-terminus spanning residues 3-41 in human. Depletion and rescue experiments with an artificial NLS are needed to confirm the putative NLS. Taken together, nuclear and cytosolic distribution and microtubule association of OTUD3 it can be hypothesized that binding to cytosolic tubules is kind of a safety mechanism to anchor OTUD3 cytosolic. Known example is the glucocorticoid receptor- HSP90 complex. In absence of steroid ligand the glucocorticoid receptor is cytosolic, but upon steroid binding translocates to the nucleus via importin β -HSP90 axis [218]. USP15 is predominantly cytoplasmic, but shuttles to the nucleus at prophase [219]. USP15 maintains genome integrity by regulating TOP2A but although plays important roles at mitochondria and polysomes [219–221]. So far it is known that USP15 can get alternatively spliced, ubiquitinated and phosphorylated (S229), whereat the latter selectively abrogates the role USP15 in maintaining genome integrity[221]. Interestingly, OTUD3 shares similarities with USP15: 1) OTUD3 possesses a phosphorylation site (S224) [222]. 2) OTUD3 was reported to associate with and regulate TOP2A [135].

5.3 Consequences of *OTUD3* dysfunction

Here, CRISPR/Cas9 was applied to generate *OTUD3* k.o. in cervical cancer cell line HeLa and embryonic kidney cell line HEK293T.

Comprehensively, in both cell lines the *OTUD3* k.o. was confirmed: A) *OTUD3* protein was absent in Western blot analyses. B) DSB sites were confirmed by DNA sequencing (data available upon request). C) cDNA sequencing and D) amino acid translation proved in both cell lines exon 3 and 4 skipping, frame shift and thereby the introduction of an early stop codon within *OTUD3* transcript. For catalytic cysteine protease activity of *OTUD3* residues D73, C76 and H182 are conserved and needed within the active site of the OTU domain [127]. Premature stop codon was identified at aa position 131. Thus, H182 as part of catalytic triad is missing as well as other highly conserved amino acids that build up the substrate binding pocket of *OTUD3*.

So far, only limited data about *OTUD3* loss of function and cellular consequences exist. In zebrafish k.d of *otud3* resulted in serious dysmorphic development of axis and the notochord [223]. As described in 5.1.2 unpublished results from suppression of *Otud3* function in *Xenopus* led to bent tails, malformed cranial structures and eyes, reduced pigmentation and a movement disorder at early developmental stages. In addition, BMP pathway modulation was shown in animal cap explant experiments (group of Prof. Hollemann, Martin-Luther-University Halle-Wittenberg). High-doses of *Bmp4* were known to repress neural differentiation marker *ncam1* expression [224]. In contrast, co-injection of *Bmp4* and *Otud3* RNA induced a twofold elevated *ncam1* expression indicating *otud3* inhibits *Bmp4* signaling. In our patients a desensitized pSMAD1/5 signaling before and after BMP4 induction was measured in LCLs. Both findings link *OTUD3* to BMP signaling pathway. In cancer cell lines HepG2, HCT116 and HeLa it was recently shown that *OTUD3* k.d. by shRNA technique promoted cell proliferation and migration [134]. In patients a promoted effect on cell proliferation and mitochondrial activity in MTT assay was detected in LCLs. Surprisingly, here generated *OTUD3* k.o. in HeLa and HEK293T cells uncovered no effect on cell proliferation in a recent master thesis [212]. So far, only a cell line specific effect on the morphology of cells was described in this thesis. Since some years contradictory results from k.d. and k.o. experiments and comparability of both is under extensive debate [225]. Techniques for k.o. generation are thought to have lower incidences of off target effects compared with RNA interference or morpholino methods. In 2015 it was published that 80% of zebrafish morphants did not phenocopy carriers of null mutations [226]. Another explanation for contrary results between k.d. and k.o. experiments might be genetic compensation mechanisms like X inactivation [227]. For *Toxoplasma gondii* such a compensatory effect was already hypothesized for TgOTUD3A k.o. [228].

6. Summary

Autosomal recessive transmitted *OTUD3* mutation c.1061_1063delAGA (p.Lys356del) was firstly described in association with AS-like phenotypes. Diseased patients presented with secondary microcephaly, delayed motor development and central muscular hypotonia, intellectual disabilities, seizures, alalia and visual defects.

Synteny and phylogeny analyses proved a high conservation during evolution of the *OTUD3* gene and protein. Patient LCLs possessed a strongly desensitized basal and BMP4 induced pSMAD1/5 signaling and enhanced cell viability and growth.

To further establish *OTUD3* as potential candidate gene in neurodevelopmental disease a cohort of AS-like patients, but negative *UBE3A* diagnostics was selected for *OTUD3* sequencing and CNV analyses. In 24% percent of patients a set of *OTUD3* SNVs was found, but none of these variations were predicted to be likely disease causing. However, four unrelated patients were identified with several CNVs of *OTUD3* exons. In one patient CNVs were *de novo*, because parents were tested CNV negative. Most important, a second family with one diseased boy and neurodevelopmental syndrome bearing homozygous *OTUD3* c.G739A mutation (p.D247N) was explored at the Department of Clinical Genetics, Erasmus Medical Center in Rotterdam (NL).

OTUD3 was comprehensively identified as first MAP within the OTU DUB subfamily. Endogenous staining of *OTUD3* showed colocalization with tubulin filaments as well as GFP-tagged transient *OTUD3* overexpression. *OTUD3* decorated typical structures composed of microtubules like mitotic spindles, the midbody and primary cilia. Nocodazole addition abolished *OTUD3* colocalization with tubulin filaments, as well as an ultracentrifugation assay confirmed the *OTUD3* presence within polymerized tubulin fraction. Finally, truncated *N*-terminal GFP-tagged *OTUD3* variants were transfected in HeLa cells and proved that the *C*-terminus of *OTUD3* bears a potential microtubule-binding site. It was further shown that cytosolic and nuclear *OTUD3* localization is mediated by a *C*-terminal NES and a putative *N*-terminal NLS.

Lastly, *OTUD3* k.o. in HeLa and HEK293T cells was established by CRISPR/Cas9 methodology and cell line dependent morphological consequences in respect to altered cell size in HeLa and altered filapodia appearance in HEK293T cells were detected.

Conclusively, the existence of two unrelated families bearing diseased children with homozygous *OTUD3* defects, as well as patients with potential CNVs of *OTUD3* exons linked *OTUD3* as likely novel gene candidate for human neurodevelopmental syndromes. Secondly, novel functions of so far uncharacterized *N*- and *C*-terminal *OTUD3* domains like microtubule association and nuclear-cytosol shuttling of *OTUD3* were detected. Gained knowledge about *OTUD3* builds a mandatory basis for further basic research e.g. with here generated *OTUD3* k.o. cell lines.

7. References

- [1] E.S. Lander, L.M. Linton, B. Birren, et al., Initial sequencing and analysis of the human genome, *Nature* 409 (2001) 860–921. <https://doi.org/10.1038/35057062>.
- [2] Human Genome Sequencing Consortium, International, Finishing the euchromatic sequence of the human genome, *Nature* 431 (2004) 931–945. <https://doi.org/10.1038/nature03001>.
- [3] I. Ezkurdia, D. Juan, J.M. Rodriguez, et al., Multiple evidence strands suggest that there may be as few as 19 000 human protein-coding genes, *Human Molecular Genetics* 23 (2014) 5866–5878. <https://doi.org/10.1093/hmg/ddu309>.
- [4] O.N. Jensen, Modification-specific proteomics: characterization of post-translational modifications by mass spectrometry, *Curr. Opin. Chem. Biol.* 8 (2004) 33–41. <https://doi.org/10.1016/j.cbpa.2003.12.009>.
- [5] Y. Zhao, O.N. Jensen, Modification-specific proteomics: Strategies for characterization of post-translational modifications using enrichment techniques, *Proteomics* 9 (2009) 4632–4641. <https://doi.org/10.1002/pmic.200900398>.
- [6] G. Goldstein, M. Scheid, U. Hammerling, D.H. Schlesinger, H.D. Niall, E.A. Boyse, Isolation of a polypeptide that has lymphocyte-differentiating properties and is probably represented universally in living cells, *Proceedings of the National Academy of Sciences* 72 (1975) 11–15. <https://doi.org/10.1073/pnas.72.1.11>.
- [7] A. Hershko, A. Ciechanover, The ubiquitin system, *Annu. Rev. Biochem.* 67 (1998) 425–479. <https://doi.org/10.1146/annurev.biochem.67.1.425>.
- [8] R.M. Hofmann, C.M. Pickart, Noncanonical MMS2-encoded ubiquitin-conjugating enzyme functions in assembly of novel polyubiquitin chains for DNA repair, *Cell* 96 (1999) 645–653.
- [9] J. Spence, S. Sadis, A.L. Haas, D. Finley, A ubiquitin mutant with specific defects in DNA repair and multiubiquitination, *Mol. Cell Biol.* 15 (1995) 1265–1273.
- [10] S.C. Shih, K.E. Sloper-Mould, L. Hicke, Monoubiquitin carries a novel internalization signal that is appended to activated receptors, *EMBO J.* 19 (2000) 187–198. <https://doi.org/10.1093/emboj/19.2.187>.
- [11] K. Haglund, S. Sigismund, S. Polo, I. Szymkiewicz, P.P. Di Fiore, I. Dikic, Multiple monoubiquitination of RTKs is sufficient for their endocytosis and degradation, *Nat. Cell Biol.* 5 (2003) 461–466. <https://doi.org/10.1038/ncb983>.
- [12] L. Sun, Z.J. Chen, The novel functions of ubiquitination in signaling, *Curr. Opin. Cell Biol.* 16 (2004) 119–126. <https://doi.org/10.1016/j.ceb.2004.02.005>.
- [13] K.F. Winkhofer, Parkin and mitochondrial quality control: Toward assembling the puzzle, *Trends in Cell Biology* 24 (2014) 332–341. <https://doi.org/10.1016/j.tcb.2014.01.001>.
- [14] A. Ciechanover, Proteolysis: from the lysosome to ubiquitin and the proteasome, *Nat. Rev. Mol. Cell Biol.* 6 (2005) 79–87. <https://doi.org/10.1038/nrm1552>.
- [15] K. Cadwell, L. Coscoy, Ubiquitination on nonlysine residues by a viral E3 ubiquitin ligase, *Science* 309 (2005) 127–130. <https://doi.org/10.1126/science.1110340>.
- [16] J.M.D. Vosper, G.S. McDowell, C.J. Hindley, C.S. Fiore-Herliche, R. Kucerova, I. Horan, A. Philpott, Ubiquitylation on canonical and non-canonical sites targets the transcription factor neurogenin for ubiquitin-mediated proteolysis, *J. Biol. Chem.* 284 (2009) 15458–15468. <https://doi.org/10.1074/jbc.M809366200>.
- [17] A. Ciechanover, N-terminal ubiquitination: More protein substrates join in, *Trends in Cell Biology* 14 (2004) 103–106. <https://doi.org/10.1016/j.tcb.2004.01.004>.
- [18] R.J. Deshaies, C.A.P. Joazeiro, RING domain E3 ubiquitin ligases, *Annu. Rev. Biochem.* 78 (2009) 399–434. <https://doi.org/10.1146/annurev.biochem.78.101807.093809>.
- [19] C.E. Berndsen, C. Wolberger, New insights into ubiquitin E3 ligase mechanism, *Nat. Struct. Mol. Biol.* 21 (2014) 301–307. <https://doi.org/10.1038/nsmb.2780>.
- [20] A.P. Hutchins, S. Liu, D. Diez, D. Miranda-Saavedra, The repertoires of ubiquitinating and deubiquitinating enzymes in eukaryotic genomes, *Mol. Biol. Evol.* 30 (2013) 1172–1187. <https://doi.org/10.1093/molbev/mst022>.
- [21] M. Hochstrasser, Origin and function of ubiquitin-like proteins, *Nature* 458 (2009) 422–429. <https://doi.org/10.1038/nature07958>.

- [22] J. Herrmann, L.O. Lerman, A. Lerman, Ubiquitin and ubiquitin-like proteins in protein regulation, *Circ. Res.* 100 (2007) 1276–1291. <https://doi.org/10.1161/01.RES.0000264500.11888.f0>.
- [23] R.L. Welchman, C. Gordon, R.J. Mayer, Ubiquitin and ubiquitin-like proteins as multifunctional signals, *Nat Rev Mol Cell Biol* 6 (2005) 599–609. <https://doi.org/10.1038/nrm1700>.
- [24] R.T. Hay, SUMO, *Molecular Cell* 18 (2005) 1–12. <https://doi.org/10.1016/j.molcel.2005.03.012>.
- [25] M.J. Matunis, A novel ubiquitin-like modification modulates the partitioning of the Ran-GTPase-activating protein RanGAP1 between the cytosol and the nuclear pore complex, *The Journal of Cell Biology* 135 (1996) 1457–1470. <https://doi.org/10.1083/jcb.135.6.1457>.
- [26] T. Kamitani, K. Kito, H.P. Nguyen, E.T.H. Yeh, Characterization of NEDD8, a Developmentally Down-regulated Ubiquitin-like Protein, *Journal of Biological Chemistry* 272 (1997) 28557–28562. <https://doi.org/10.1074/jbc.272.45.28557>.
- [27] van der Veen, Annemarthe G, H.L. Ploegh, Ubiquitin-like proteins, *Annu. Rev. Biochem.* 81 (2012) 323–357. <https://doi.org/10.1146/annurev-biochem-093010-153308>.
- [28] K.L. Rock, C. Gramm, L. Rothstein, K. Clark, R. Stein, L. Dick, D. Hwang, A.L. Goldberg, Inhibitors of the proteasome block the degradation of most cell proteins and the generation peptides presented on MHC class I molecules, *Cell* 78 (1994) 761–771.
- [29] D. Komander, M. Rape, The Ubiquitin Code, *Annu. Rev. Biochem.* 81 (2012) 203–229. <https://doi.org/10.1146/annurev-biochem-060310-170328>.
- [30] S. Sigismund, S. Polo, P.P. Di Fiore, Signaling through monoubiquitination, *Curr. Top. Microbiol. Immunol.* 286 (2004) 149–185.
- [31] M. Sadowski, R. Suryadinata, A.R. Tan, S.N.A. Roesley, B. Sarcevic, Protein monoubiquitination and polyubiquitination generate structural diversity to control distinct biological processes, *IUBMB Life* 64 (2012) 136–142. <https://doi.org/10.1002/iub.589>.
- [32] H.N. Ramanathan, Y. Ye, Cellular strategies for making monoubiquitin signals, *Crit. Rev. Biochem. Mol. Biol.* 47 (2012) 17–28. <https://doi.org/10.3109/10409238.2011.620943>.
- [33] V. Chau, J.W. Tobias, A. Bachmair, D. Marriott, D.J. Ecker, D.K. Gonda, A. Varshavsky, A multiubiquitin chain is confined to specific lysine in a targeted short-lived protein, *Science* 243 (1989) 1576–1583.
- [34] Z.J. Chen, L.J. Sun, Nonproteolytic functions of ubiquitin in cell signaling, *Molecular Cell* 33 (2009) 275–286. <https://doi.org/10.1016/j.molcel.2009.01.014>.
- [35] C. Alfano, S. Faggiano, A. Pastore, The Ball and Chain of Polyubiquitin Structures, *Trends Biochem. Sci.* (2016). <https://doi.org/10.1016/j.tibs.2016.01.006>.
- [36] C.-W. Park, K.-Y. Ryu, Cellular ubiquitin pool dynamics and homeostasis, *BMB Reports* 47 (2014) 475–482. <https://doi.org/10.5483/BMBRep.2014.47.9.128>.
- [37] K. Iwai, H. Fujita, Y. Sasaki, Linear ubiquitin chains: NF- κ B signalling, cell death and beyond, *Nat. Rev. Mol. Cell Biol.* 15 (2014) 503–508. <https://doi.org/10.1038/nrm3836>.
- [38] S. Rahighi, F. Ikeda, M. Kawasaki, et al., Specific recognition of linear ubiquitin chains by NEMO is important for NF- κ B activation, *Cell* 136 (2009) 1098–1109. <https://doi.org/10.1016/j.cell.2009.03.007>.
- [39] W. Kim, E.J. Bennett, E.L. Huttlin, et al., Systematic and quantitative assessment of the ubiquitin-modified proteome, *Molecular Cell* 44 (2011) 325–340. <https://doi.org/10.1016/j.molcel.2011.08.025>.
- [40] L. Jin, A. Williamson, S. Banerjee, I. Philipp, M. Rape, Mechanism of ubiquitin-chain formation by the human anaphase-promoting complex, *Cell* 133 (2008) 653–665. <https://doi.org/10.1016/j.cell.2008.04.012>.
- [41] K.E. Wickliffe, S. Lorenz, D.E. Wemmer, J. Kuriyan, M. Rape, The mechanism of linkage-specific ubiquitin chain elongation by a single-subunit E2, *Cell* 144 (2011) 769–781. <https://doi.org/10.1016/j.cell.2011.01.035>.
- [42] M. Gatti, S. Pinato, A. Maiolica, F. Rocchio, M.G. Prato, R. Aebersold, L. Penengo, RNF168 promotes noncanonical K27 ubiquitination to signal DNA damage, *Cell Rep.* 10 (2015) 226–238. <https://doi.org/10.1016/j.celrep.2014.12.021>.

- [43] P. Chastagner, A. Israël, C. Brou, Itch/AIP4 mediates Deltex degradation through the formation of K29-linked polyubiquitin chains, *EMBO Rep.* 7 (2006) 1147–1153. <https://doi.org/10.1038/sj.embor.7400822>.
- [44] W.-C. Yuan, Y.-R. Lee, S.-Y. Lin, et al., K33-Linked Polyubiquitination of Coronin 7 by Cul3-KLHL20 Ubiquitin E3 Ligase Regulates Protein Trafficking, *Molecular Cell* 54 (2014) 586–600. <https://doi.org/10.1016/j.molcel.2014.03.035>.
- [45] W.P. Bozza, Q. Liang, P. Gong, Z. Zhuang, Transient kinetic analysis of USP2-catalyzed deubiquitination reveals a conformational rearrangement in the K48-linked diubiquitin substrate, *Biochemistry* 51 (2012) 10075–10086. <https://doi.org/10.1021/bi3009104>.
- [46] R. Varadan, O. Walker, C. Pickart, D. Fushman, Structural properties of polyubiquitin chains in solution, *J. Mol. Biol.* 324 (2002) 637–647.
- [47] C.H. Emmerich, A. Ordureau, S. Strickson, J.S.C. Arthur, P.G.A. Pedrioli, D. Komander, P. Cohen, Activation of the canonical IKK complex by K63/M1-linked hybrid ubiquitin chains, *Proc. Natl. Acad. Sci. U. S. A.* 110 (2013) 15247–15252. <https://doi.org/10.1073/pnas.1314715110>.
- [48] F. Galisson, L. Mahrouche, M. Courcelles, E. Bonneil, S. Meloche, M.K. Chelbi-Alix, P. Thibault, A novel proteomics approach to identify SUMOylated proteins and their modification sites in human cells, *Mol. Cell. Proteomics* 10 (2011) 4796. <https://doi.org/10.1074/mcp.M110.004796>.
- [49] I.A. Hendriks, R.C.J. D'Souza, B. Yang, M. Verlaan-de Vries, M. Mann, A.C.O. Vertegaal, Uncovering global SUMOylation signaling networks in a site-specific manner, *Nat. Struct. Mol. Biol.* 21 (2014) 927–936. <https://doi.org/10.1038/nsmb.2890>.
- [50] R.K. Singh, S. Zerath, O. Kleifeld, M. Scheffner, M.H. Glickman, D. Fushman, Recognition and cleavage of related to ubiquitin 1 (Rub1) and Rub1-ubiquitin chains by components of the ubiquitin-proteasome system, *Mol. Cell. Proteomics* 11 (2012) 1595–1611. <https://doi.org/10.1074/mcp.M112.022467>.
- [51] C. Choudhary, C. Kumar, F. Gnad, M.L. Nielsen, M. Rehman, T.C. Walther, J.V. Olsen, M. Mann, Lysine acetylation targets protein complexes and co-regulates major cellular functions, *Science* 325 (2009) 834–840. <https://doi.org/10.1126/science.1175371>.
- [52] A. Lundby, K. Lage, B.T. Weinert, et al., Proteomic analysis of lysine acetylation sites in rat tissues reveals organ specificity and subcellular patterns, *Cell Rep.* 2 (2012) 419–431. <https://doi.org/10.1016/j.celrep.2012.07.006>.
- [53] K.N. Swatek, D. Komander, Ubiquitin modifications, *Cell Res.* 26 (2016) 399–422. <https://doi.org/10.1038/cr.2016.39>.
- [54] F.C. Fiesel, M. Ando, R. Hudec, et al., (Patho-)physiological relevance of PINK1-dependent ubiquitin phosphorylation, *EMBO Rep.* 16 (2015) 1114–1130. <https://doi.org/10.15252/embr.201540514>.
- [55] T. Wauer, K.N. Swatek, J.L. Wagstaff, et al., Ubiquitin Ser65 phosphorylation affects ubiquitin structure, chain assembly and hydrolysis, *EMBO J.* 34 (2015) 307–325. <https://doi.org/10.15252/emboj.201489847>.
- [56] O. Wiborg, M.S. Pedersen, A. Wind, L.E. Berglund, K.A. Marcker, J. Vuust, The human ubiquitin multigene family: some genes contain multiple directly repeated ubiquitin coding sequences, *EMBO J.* 4 (1985) 755–759.
- [57] R.T. Baker, P.G. Board, The human ubiquitin-52 amino acid fusion protein gene shares several structural features with mammalian ribosomal protein genes, *Nucl Acids Res* 19 (1991) 1035–1040. <https://doi.org/10.1093/nar/19.5.1035>.
- [58] K.L. Redman, M. Rechsteiner, Identification of the long ubiquitin extension as ribosomal protein S27a, *Nature* 338 (1989) 438–440. <https://doi.org/10.1038/338438a0>.
- [59] A. Hershko, A. Ciechanover, H. Heller, A.L. Haas, I.A. Rose, Proposed role of ATP in protein breakdown: conjugation of protein with multiple chains of the polypeptide of ATP-dependent proteolysis, *Proc. Natl. Acad. Sci. U. S. A.* 77 (1980) 1783–1786.
- [60] D. Komander, M.J. Clague, S. Urbe, Breaking the chains: structure and function of the deubiquitinases, *Nat. Rev. Mol. Cell Biol.* 10 (2009) 550–563. <https://doi.org/10.1038/nrm2731>.

- [61] S. Bhattacharya, M.K. Ghosh, Cell death and deubiquitinases: perspectives in cancer, *Biomed Res. Int.* 2014 (2014) 435197. <https://doi.org/10.1155/2014/435197>.
- [62] M.J. Clague, I. Barsukov, J.M. Coulson, H. Liu, D.J. Rigden, S. Urbe, Deubiquitylases from genes to organism, *Physiol. Rev.* 93 (2013) 1289–1315. <https://doi.org/10.1152/physrev.00002.2013>.
- [63] A.C. Storer, R. Menard, Catalytic mechanism in papain family of cysteine peptidases, *Methods Enzymol.* 244 (1994) 486–500.
- [64] L.H. Weaver, W.R. Kester, L.F. ten Eyck, B.W. Matthews, The structure and stability of thermolysin, *Experientia Suppl.* 26 (1976) 31–39.
- [65] Y. Sato, A. Yoshikawa, A. Yamagata, et al., Structural basis for specific cleavage of Lys 63-linked polyubiquitin chains, *Nature* 455 (2008) 358–362. <https://doi.org/10.1038/nature07254>.
- [66] M.A. Liz, M.M. Sousa, Deciphering cryptic proteases, *Cell. Mol. Life Sci.* 62 (2005) 989–1002. <https://doi.org/10.1007/s00018-005-4544-2>.
- [67] M. Renatus, S.G. Parrado, A. D'Arcy, et al., Structural basis of ubiquitin recognition by the deubiquitinating protease USP2, *Structure* 14 (2006) 1293–1302. <https://doi.org/10.1016/j.str.2006.06.012>.
- [68] D. Komander, D. Barford, Structure of the A20 OTU domain and mechanistic insights into deubiquitination, *Biochem. J.* 409 (2008) 77–85. <https://doi.org/10.1042/BJ20071399>.
- [69] E. Meulmeester, M. Kunze, H.H. Hsiao, H. Urlaub, F. Melchior, Mechanism and consequences for paralog-specific sumoylation of ubiquitin-specific protease 25, *Molecular Cell* 30 (2008) 610–619. <https://doi.org/10.1016/j.molcel.2008.03.021>.
- [70] S.V. Todi, B.J. Winborn, K.M. Scaglione, J.R. Blount, S.M. Travis, H.L. Paulson, Ubiquitination directly enhances activity of the deubiquitinating enzyme ataxin-3, *EMBO J.* 28 (2009) 372–382. <https://doi.org/10.1038/emboj.2008.289>.
- [71] M.J. Edelmann, H.B. Kramer, M. Altun, B.M. Kessler, Post-translational modification of the deubiquitinating enzyme otubain 1 modulates active RhoA levels and susceptibility to *Yersinia* invasion, *FEBS J.* 277 (2010) 2515–2530. <https://doi.org/10.1111/j.1742-4658.2010.07665.x>.
- [72] E.S. Coyne, S.S. Wing, The business of deubiquitination - location, location, location, *F1000Res.* 5 (2016). <https://doi.org/10.12688/f1000research.7220.1>.
- [73] M.J. Clague, C. Heride, S. Urbe, The demographics of the ubiquitin system, *Trends in Cell Biology* 25 (2015) 417–426. <https://doi.org/10.1016/j.tcb.2015.03.002>.
- [74] Y.M. Ma, E. Boucrot, J. Villen, E.B. Affar, S.P. Gygi, H.G. Gottlinger, T. Kirchhausen, Targeting of AMSH to endosomes is required for epidermal growth factor receptor degradation, *J. Biol. Chem.* 282 (2007) 9805–9812. <https://doi.org/10.1074/jbc.M611635200>.
- [75] M.I. Sierra, M.H. Wright, P.D. Nash, AMSH interacts with ESCRT-0 to regulate the stability and trafficking of CXCR4, *J. Biol. Chem.* 285 (2010) 13990–14004. <https://doi.org/10.1074/jbc.M109.061309>.
- [76] S. Niendorf, A. Oksche, A. Kisser, et al., Essential role of ubiquitin-specific protease 8 for receptor tyrosine kinase stability and endocytic trafficking in vivo, *Mol. Cell. Biol.* 27 (2007) 5029–5039. <https://doi.org/10.1128/MCB.01566-06>.
- [77] I. Berlin, H. Schwartz, P.D. Nash, Regulation of epidermal growth factor receptor ubiquitination and trafficking by the USP8.STAM complex, *J. Biol. Chem.* 285 (2010) 34909–34921. <https://doi.org/10.1074/jbc.M109.016287>.
- [78] G.C. Hassink, B. Zhao, R. Sompallae, M. Altun, S. Gastaldello, N.V. Zinin, M.G. Masucci, K. Lindsten, The ER-resident ubiquitin-specific protease 19 participates in the UPR and rescues ERAD substrates, *EMBO Rep.* 10 (2009) 755–761. <https://doi.org/10.1038/embo.2009.69>.
- [79] B. Wiles, M. Miao, E. Coyne, L. Larose, A.V. Cybulsky, S.S. Wing, USP19 deubiquitinating enzyme inhibits muscle cell differentiation by suppressing unfolded-protein response signaling, *Mol. Biol. Cell* 26 (2015) 913–923. <https://doi.org/10.1091/mbc.E14-06-1129>.
- [80] P. Zhu, W. Zhou, J. Wang, et al., A histone H2A deubiquitinase complex coordinating histone acetylation and H1 dissociation in transcriptional regulation, *Molecular Cell* 27 (2007) 609–621. <https://doi.org/10.1016/j.molcel.2007.07.024>.

- [81] L. Feng, J. Wang, J. Chen, The Lys63-specific deubiquitinating enzyme BRCC36 is regulated by two scaffold proteins localizing in different subcellular compartments, *J. Biol. Chem.* 285 (2010) 30982–30988. <https://doi.org/10.1074/jbc.M110.135392>.
- [82] D. Komander, F. Reyes-Turcu, J.D.F. Licchesi, P. Odenwaelder, K.D. Wilkinson, D. Barford, Molecular discrimination of structurally equivalent Lys 63-linked and linear polyubiquitin chains, *EMBO Rep.* 10 (2009) 466–473. <https://doi.org/10.1038/embo.2009.55>.
- [83] M. Hu, P. Li, L. Song, P.D. Jeffrey, T.A. Chenova, K.D. Wilkinson, R.E. Cohen, Y. Shi, Structure and mechanisms of the proteasome-associated deubiquitinating enzyme USP14, *EMBO J.* 24 (2005) 3747–3756. <https://doi.org/10.1038/sj.emboj.7600832>.
- [84] D. Komander, C.J. Lord, H. Scheel, S. Swift, K. Hofmann, A. Ashworth, D. Barford, The structure of the CYLD USP domain explains its specificity for Lys63-linked polyubiquitin and reveals a B box module, *Molecular Cell* 29 (2008) 451–464. <https://doi.org/10.1016/j.molcel.2007.12.018>.
- [85] M.J. Edelmann, A. Iphofer, M. Akutsu, et al., Structural basis and specificity of human otubain 1-mediated deubiquitination, *Biochem. J.* 418 (2009) 379–390. <https://doi.org/10.1042/BJ20081318>.
- [86] A. Bremm, S.M.V. Freund, D. Komander, Lys11-linked ubiquitin chains adopt compact conformations and are preferentially hydrolyzed by the deubiquitinase Cezanne, *Nat. Struct. Mol. Biol.* 17 (2010) 939–947. <https://doi.org/10.1038/nsmb.1873>.
- [87] D. Flierman, van der Heden van Noort, Gerbrand J, R. Ekkebus, P.P. Geurink, T.E.T. Mevissen, M.K. Hospenthal, D. Komander, H. Ovaa, Non-hydrolyzable Diubiquitin Probes Reveal Linkage-Specific Reactivity of Deubiquitylating Enzymes Mediated by S2 Pockets, *Cell Chem. Biol.* 23 (2016) 472–482. <https://doi.org/10.1016/j.chembiol.2016.03.009>.
- [88] E.M. Cooper, C. Cutcliffe, T.Z. Kristiansen, A. Pandey, C.M. Pickart, R.E. Cohen, K63-specific deubiquitination by two JAMM/MPN+ complexes: BRISC-associated Brcc36 and proteasomal Poh1, *EMBO J.* 28 (2009) 621–631. <https://doi.org/10.1038/emboj.2009.27>.
- [89] J. McCullough, M.J. Clague, S. Urbe, AMSH is an endosome-associated ubiquitin isopeptidase, *The Journal of Cell Biology* 166 (2004) 487–492. <https://doi.org/10.1083/jcb.200401141>.
- [90] B.J. Winborn, S.M. Travis, S.V. Todi, et al., The deubiquitinating enzyme ataxin-3, a polyglutamine disease protein, edits Lys63 linkages in mixed linkage ubiquitin chains, *J. Biol. Chem.* 283 (2008) 26436–26443. <https://doi.org/10.1074/jbc.M803692200>.
- [91] H. Angelman, 'Puppet' Children A Report on Three Cases, *Developmental Medicine & Child Neurology* 7 (1965) 681–688. <https://doi.org/10.1111/j.1469-8749.1965.tb07844.x>.
- [92] W. Reik, J. Walter, Genomic imprinting: parental influence on the genome, *Nat. Rev. Genet.* 2 (2001) 21–32. <https://doi.org/10.1038/35047554>.
- [93] S.J. Chamberlain, RNAs of the human chromosome 15q11-q13 imprinted region, *Wiley Interdiscip. Rev. RNA* 4 (2013) 155–166. <https://doi.org/10.1002/wrna.1150>.
- [94] C. Rougeulle, H. Glatt, M. Lalonde, The Angelman syndrome candidate gene, UBE3A/E6-AP, is imprinted in brain, *Nat. Genet.* 17 (1997) 14–15. <https://doi.org/10.1038/ng0997-14>.
- [95] E.G. Puffenberger, R.N. Jinks, H. Wang, et al., A homozygous missense mutation in HERC2 associated with global developmental delay and autism spectrum disorder, *Hum. Mutat.* 33 (2012) 1639–1646. <https://doi.org/10.1002/humu.22237>.
- [96] G.V. Harlalka, E.L. Baple, H. Cross, et al., Mutation of HERC2 causes developmental delay with Angelman-like features, *J. Med. Genet.* 50 (2013) 65–73. <https://doi.org/10.1136/jmedgenet-2012-101367>.
- [97] S. Kuhnle, U. Kogel, S. Glockzin, A. Marquardt, A. Ciechanover, K. Matentzoglou, M. Scheffner, Physical and functional interaction of the HECT ubiquitin-protein ligases E6AP and HERC2, *J. Biol. Chem.* 286 (2011) 19410–19416. <https://doi.org/10.1074/jbc.M110.205211>.
- [98] C.A. Williams, D.J. Driscoll, A.I. Dagli, Clinical and genetic aspects of Angelman syndrome, *Genet. Med.* 12 (2010) 385–395. <https://doi.org/10.1097/GIM.0b013e3181def138>.

- [99] M.D. Stanley Fahn, The 2013 Aspen Course on Parkinson's Disease and Other Movement Disorders, 2013. <http://www.medscape.org/viewarticle/815515> (access: 15.12.2016).
- [100] D. Jia, B. Tang, Y. Shi, et al., A deletion mutation of the VHL gene associated with a patient with sporadic von Hippel-Lindau disease, *J. Clin. Neurosci.* 20 (2013) 842–847. <https://doi.org/10.1016/j.jocn.2012.06.013>.
- [101] J. Lowe, A. Blanchard, K. Morrell, G. Lennox, L. Reynolds, M. Billett, M. Landon, R.J. Mayer, Ubiquitin is a common factor in intermediate filament inclusion bodies of diverse type in man, including those of Parkinson's disease, Pick's disease, and Alzheimer's disease, as well as Rosenthal fibres in cerebellar astrocytomas, cytoplasmic bodies in muscle, and mallory bodies in alcoholic liver disease, *J. Pathol.* 155 (1988) 9–15. <https://doi.org/10.1002/path.1711550105>.
- [102] A.E. Lang, A.M. Lozano, Parkinson's disease. First of two parts, *N. Engl. J. Med.* 339 (1998) 1044–1053. <https://doi.org/10.1056/NEJM199810083391506>.
- [103] K. Nuytemans, J. Theuns, M. Cruts, C. van Broeckhoven, Genetic etiology of Parkinson disease associated with mutations in the SNCA, PARK2, PINK1, PARK7, and LRRK2 genes: a mutation update, *Hum. Mutat.* 31 (2010) 763–780. <https://doi.org/10.1002/humu.21277>.
- [104] M. Cruts, J. Theuns, C. van Broeckhoven, Locus-specific mutation databases for neurodegenerative brain diseases, *Hum. Mutat.* 33 (2012) 1340–1344. <https://doi.org/10.1002/humu.22117>.
- [105] T. Kitada, S. Asakawa, N. Hattori, et al., Mutations in the parkin gene cause autosomal recessive juvenile parkinsonism, *Nature* 392 (1998) 605–608. <https://doi.org/10.1038/33416>.
- [106] C.B. Lucking, A. Durr, V. Bonifati, et al., Association between early-onset Parkinson's disease and mutations in the parkin gene, *N. Engl. J. Med.* 342 (2000) 1560–1567. <https://doi.org/10.1056/NEJM200005253422103>.
- [107] K.K. Dev, H. van der Putten, B. Sommer, G. Rovelli, Part I: parkin-associated proteins and Parkinson's disease, *Neuropharmacology* 45 (2003) 1–13.
- [108] I. Garcia-Higuera, T. Taniguchi, S. Ganesan, M.S. Meyn, C. Timmers, J. Hejna, M. Grompe, A.D. D'Andrea, Interaction of the Fanconi anemia proteins and BRCA1 in a common pathway, *Molecular Cell* 7 (2001) 249–262.
- [109] J. Lisztwan, G. Imbert, C. Wirbelauer, M. Gstaiger, W. Krek, The von Hippel-Lindau tumor suppressor protein is a component of an E3 ubiquitin-protein ligase activity, *Genes Dev.* 13 (1999) 1822–1833.
- [110] V.R. Gordeuk, A.I. Sergueeva, G.Y. Miasnikova, et al., Congenital disorder of oxygen sensing: association of the homozygous Chuvash polycythemia VHL mutation with thrombosis and vascular abnormalities but not tumors, *Blood* 103 (2004) 3924–3932. <https://doi.org/10.1182/blood-2003-07-2535>.
- [111] M.D. Kaytor, S.T. Warren, Aberrant protein deposition and neurological disease, *J. Biol. Chem.* 274 (1999) 37507–37510.
- [112] H. Scheel, S. Tomiuk, K. Hofmann, Elucidation of ataxin-3 and ataxin-7 function by integrative bioinformatics, *Human Molecular Genetics* 12 (2003) 2845–2852. <https://doi.org/10.1093/hmg/ddg297>.
- [113] Y. Kawaguchi, T. Okamoto, M. Taniwaki, et al., CAG expansions in a novel gene for Machado-Joseph disease at chromosome 14q32.1, *Nat. Genet.* 8 (1994) 221–228. <https://doi.org/10.1038/ng1194-221>.
- [114] S.-R. Gan, W. Ni, Y. Dong, N. Wang, Z.-Y. Wu, Population genetics and new insight into range of CAG repeats of spinocerebellar ataxia type 3 in the Han Chinese population, *PLoS One* 10 (2015) e0134405. <https://doi.org/10.1371/journal.pone.0134405>.
- [115] K.D. Wilkinson, K.M. Lee, S. Deshpande, P. Duerksen-Hughes, J.M. Boss, J. Pohl, The neuron-specific protein PGP 9.5 is a ubiquitin carboxyl-terminal hydrolase, *Science* 246 (1989) 670–673.
- [116] J.F. Doran, P. Jackson, P.A. Kynoch, R.J. Thompson, Isolation of PGP 9.5, a new human neurone-specific protein detected by high-resolution two-dimensional electrophoresis, *J. Neurochem.* 40 (1983) 1542–1547.

- [117] J. Lowe, H. McDermott, M. Landon, R.J. Mayer, K.D. Wilkinson, Ubiquitin carboxyl-terminal hydrolase (PGP 9.5) is selectively present in ubiquitinated inclusion bodies characteristic of human neurodegenerative diseases, *J. Pathol.* 161 (1990) 153–160. <https://doi.org/10.1002/path.1711610210>.
- [118] R. Setsuie, K. Wada, The functions of UCH-L1 and its relation to neurodegenerative diseases, *Neurochem. Int.* 51 (2007) 105–111. <https://doi.org/10.1016/j.neuint.2007.05.007>.
- [119] C. Das, Q.Q. Hoang, C.A. Kreinbring, et al., Structural basis for conformational plasticity of the Parkinson's disease-associated ubiquitin hydrolase UCH-L1, *Proc. Natl. Acad. Sci. U. S. A.* 103 (2006) 4675–4680. <https://doi.org/10.1073/pnas.0510403103>.
- [120] E. Leroy, R. Boyer, G. Auburger, et al., The ubiquitin pathway in Parkinson's disease, *Nature* 395 (1998) 451–452. <https://doi.org/10.1038/26652>.
- [121] K. Bilguvar, N.K. Tyagi, C. Ozkara, et al., Recessive loss of function of the neuronal ubiquitin hydrolase UCHL1 leads to early-onset progressive neurodegeneration, *Proc. Natl. Acad. Sci. U. S. A.* 110 (2013) 3489–3494. <https://doi.org/10.1073/pnas.1222732110>.
- [122] M.T. Carter, M.T. Geraghty, L. de La Cruz, R.R. Reichard, L. Boccutto, C.E. Schwartz, C.L. Clericuzio, A new syndrome with multiple capillary malformations, intractable seizures, and brain and limb anomalies, *Am. J. Med. Genet. A* 155A (2011) 301–306. <https://doi.org/10.1002/ajmg.a.33841>.
- [123] G.M. Mirzaa, A.R. Paciorkowski, C.D. Smyser, M.C. Willing, A.C. Lind, W.B. Dobyns, The microcephaly-capillary malformation syndrome, *Am. J. Med. Genet. A* 155A (2011) 2080–2087. <https://doi.org/10.1002/ajmg.a.34118>.
- [124] B. Isidor, S. Barbarot, C. Beneteau, C. Le Caignec, A. David, Multiple capillary skin malformations, epilepsy, microcephaly, mental retardation, hypoplasia of the distal phalanges: report of a new case and further delineation of a new syndrome, *Am. J. Med. Genet. A* 155A (2011) 1458–1460. <https://doi.org/10.1002/ajmg.a.34048>.
- [125] L.M. McDonnell, G.M. Mirzaa, D. Alcantara, et al., Mutations in STAMBP, encoding a deubiquitinating enzyme, cause microcephaly-capillary malformation syndrome, *Nat. Genet.* 45 (2013) 556–562. <https://doi.org/10.1038/ng.2602>.
- [126] D.H. Margolin, M. Kousi, Y.-M. Chan, et al., Ataxia, dementia, and hypogonadotropism caused by disordered ubiquitination, *N. Engl. J. Med.* 368 (2013) 1992–2003. <https://doi.org/10.1056/NEJMoa1215993>.
- [127] T.E.T. Mevissen, M.K. Hospenthal, P.P. Geurink, et al., OTU deubiquitinases reveal mechanisms of linkage specificity and enable ubiquitin chain restriction analysis, *Cell* 154 (2013) 169–184. <https://doi.org/10.1016/j.cell.2013.05.046>.
- [128] L. Yuan, Y. Lv, H. Li, et al., Deubiquitylase OTUD3 regulates PTEN stability and suppresses tumorigenesis, *Nat. Cell Biol.* 17 (2015) 1169–1181. <https://doi.org/10.1038/ncb3218>.
- [129] J. Li, C. Yen, D. Liaw, et al., PTEN, a putative protein tyrosine phosphatase gene mutated in human brain, breast, and prostate cancer, *Science* 275 (1997) 1943–1947.
- [130] P.A. Steck, M.A. Pershouse, S.A. Jasser, et al., Identification of a candidate tumour suppressor gene, MMAC1, at chromosome 10q23.3 mutated in multiple advanced cancers, *Nat. Genet.* 15 (1997) 356–362. <https://doi.org/10.1038/ng0497-356>.
- [131] T. Maehama, J.E. Dixon, The tumor suppressor, PTEN/MMAC1, dephosphorylates the lipid second messenger, phosphatidylinositol 3,4,5-trisphosphate, *J. Biol. Chem.* 273 (1998) 13375–13378.
- [132] M.S. Song, L. Salmena, P.P. Pandolfi, The functions and regulation of the PTEN tumour suppressor, *Nat. Rev. Mol. Cell Biol.* 13 (2012) 283–296. <https://doi.org/10.1038/nrm3330>.
- [133] Q. Pu, Y.-R. Lv, K. Dong, W.-W. Geng, H.-D. Gao, Tumor suppressor OTUD3 induces growth inhibition and apoptosis by directly deubiquitinating and stabilizing p53 in invasive breast carcinoma cells, *BMC Cancer* 20 (2020) 583. <https://doi.org/10.1186/s12885-020-07069-9>.
- [134] T. Du, H. Li, Y. Fan, et al., The deubiquitylase OTUD3 stabilizes GRP78 and promotes lung tumorigenesis, *Nat. Commun.* 10 (2019) 2914. <https://doi.org/10.1038/s41467-019-10824-7>.

- [135] X. Kang, C. Song, X. Du, et al., PTEN stabilizes TOP2A and regulates the DNA decatenation, *Sci. Rep.* 5 (2015) 17873. <https://doi.org/10.1038/srep17873>.
- [136] C.S. Downes, D.J. Clarke, A.M. Mullinger, J.F. Gimenez-Abian, A.M. Creighton, R.T. Johnson, A topoisomerase II-dependent G2 cycle checkpoint in mammalian cells, *Nature* 372 (1994) 467–470. <https://doi.org/10.1038/372467a0>.
- [137] M. Arelin, B. Schulze, B. Muller-Myhsok, et al., Genome-wide linkage analysis is a powerful prenatal diagnostic tool in families with unknown genetic defects, *Eur. J. Hum. Genet.* 21 (2013) 367–372. <https://doi.org/10.1038/ejhg.2012.198>.
- [138] Designing synthetic MLPA probes. https://www.mlpa.com/WebForms/WebFormDBData.aspx%3FTag%3D_zjCZBtdOUyAt3KF3EwRZhpApz9QEm7akikAm7AOEGw1vtZvffaZPOiTL2Q5u1wfg4HMFjIW2l7gg.+&cd=2&hl=de&ct=clnk&gl=de&client=firefox-b (access: 22 December 2016).
- [139] T. Pfirrmann, A. Lokapally, C. Andreasson, P. Ljungdahl, T. Hollemann, SOMA: a single oligonucleotide mutagenesis and cloning approach, *PLoS One* 8 (2013) e64870. <https://doi.org/10.1371/journal.pone.0064870>.
- [140] de la Campa, A G, S.S. Springhorn, P. Kale, S.A. Lacks, Proteins encoded by the DpnI restriction gene cassette. Hyperproduction and characterization of the DpnI endonuclease, *J. Biol. Chem.* 263 (1988) 14696–14702.
- [141] F. Sanger, S. Nicklen, A.R. Coulson, DNA sequencing with chain-terminating inhibitors, *Proc. Natl. Acad. Sci. U. S. A.* 74 (1977) 5463–5467.
- [142] K.J. Livak, T.D. Schmittgen, Analysis of relative gene expression data using real-time quantitative PCR and the 2(-Delta Delta C(T)) Method, *Methods* 25 (2001) 402–408. <https://doi.org/10.1006/meth.2001.1262>.
- [143] MLPA one tube protocol via <https://support.mrcholland.com/downloads/files/mlpa-general-protocol-one-tube> (access: 15.12.2015).
- [144] BLAST: Basic Local Alignment Search Tool. <https://blast.ncbi.nlm.nih.gov/Blast.cgi> (access: 22.12.2019).
- [145] T-COFFEE Multiple Sequence Alignment Server. <http://tcoffee.vital-it.ch/apps/tcoffee/index.html> (access: 22.12.2019).
- [146] Phylogeny.fr: Home. <http://www.phylogeny.fr/> (access: 22.12.2019).
- [147] DYOGEN, 2013. <http://www.genomicus.biologie.ens.fr/> (access: 22.12.2019).
- [148] Home - Gene - NCBI. <https://www.ncbi.nlm.nih.gov/gene> (access: 22.12.2019).
- [149] Xenbase Home. <http://www.xenbase.org/entry/> (access: 22.12.2019).
- [150] U.K. Laemmli, Cleavage of structural proteins during the assembly of the head of bacteriophage T4, *Nature* 227 (1970) 680–685.
- [151] <http://www.cbsscientific.com/pdf/EBXInstructionManual.2010.pdf> (access: 26.12.2016)
- [152] U. Arnold, R. Ulbrich-Hofmann, Quantitative protein precipitation from guanidine hydrochloride-containing solutions by sodium deoxycholate/trichloroacetic acid, *Anal. Biochem.* 271 (1999) 197–199. <https://doi.org/10.1006/abio.1999.4149>.
- [153] T. Pfirrmann, D. Emmerich, P. Ruokonen, et al., Molecular mechanism of CHRDL1-mediated X-linked megalocornea in humans and in *Xenopus* model, *Human Molecular Genetics* 24 (2015) 3119–3132. <https://doi.org/10.1093/hmg/ddv063>.
- [154] Santa Cruz Biotechnology, OTUD3 CRISPR Knockout and Activation Products (h). https://www.scbt.com/scbt/product/otud3-crispr-knockout-and-activation-productsh/?jsessionid=yKb7YI5XxFWbtDSqZ5Q8y6HkZz8oQmefpnh7A3Ziz_eCHza01nDOI-354688853 (access: 02.08.2018).
- [155] K. Hofmann, P. Bucher, The UBA domain: a sequence motif present in multiple enzyme classes of the ubiquitination pathway, *Trends Biochem. Sci.* 21 (1996) 172–173. [https://doi.org/10.1016/S0968-0004\(96\)30015-7](https://doi.org/10.1016/S0968-0004(96)30015-7).
- [156] J. Clayton-Smith, Angelman syndrome: A review of the clinical and genetic aspects, *J. Med. Genet.* 40 (2003) 87–95. <https://doi.org/10.1136/jmg.40.2.87>.
- [157] N. Sobreira, F. Schiettecatte, D. Valle, A. Hamosh, GeneMatcher: a matching tool for connecting investigators with an interest in the same gene, *Hum. Mutat.* 36 (2015) 928–930. <https://doi.org/10.1002/humu.22844>.
- [158] I. Adzhubei, D.M. Jordan, S.R. Sunyaev, Predicting Functional Effect of Human Missense Mutations Using PolyPhen-2, *Current Protocols in Human Genetics* 76 (2013) 7. <https://doi.org/10.1002/0471142905.hg0720s76>.

- [159] B.L. Aken, P. Achuthan, W. Akanni, et al., Ensembl 2017, *Nucleic Acids Res* 45 (2017) D635–D642. <https://doi.org/10.1093/nar/gkw1104>.
- [160] J.M. Schwarz, D.N. Cooper, M. Schuelke, D. Seelow, MutationTaster2: mutation prediction for the deep-sequencing age, *Nat. Methods* 11 (2014) 361–362. <https://doi.org/10.1038/nmeth.2890>.
- [161] K.J. Karczewski, L.C. Francioli, G. Tiao, et al., The mutational constraint spectrum quantified from variation in 141,456 humans, *Nature* 581 (2020) 434–443. <https://doi.org/10.1038/s41586-020-2308-7>.
- [162] A. De, T. Dainichi, C.V. Rathinam, S. Ghosh, The deubiquitinase activity of A20 is dispensable for NF-kappaB signaling, *EMBO Rep.* 15 (2014) 775–783. <https://doi.org/10.15252/embr.201338305>.
- [163] L. Herhaus, M. Al-Salihi, T. Macartney, S. Weidlich, G.P. Sapkota, OTUB1 enhances TGFbeta signalling by inhibiting the ubiquitylation and degradation of active SMAD2/3, *Nat. Commun.* 4 (2013) 2519. <https://doi.org/10.1038/ncomms3519>.
- [164] S.M. Jung, J.-H. Lee, J. Park, et al., Smad6 inhibits non-canonical TGF-beta1 signalling by recruiting the deubiquitinase A20 to TRAF6, *Nat. Commun.* 4 (2013) 2562. <https://doi.org/10.1038/ncomms3562>.
- [165] H. Tran, F. Hamada, T. Schwarz-Romond, M. Bienz, Trabid, a new positive regulator of Wnt-induced transcription with preference for binding and cleaving K63-linked ubiquitin chains, *Genes Dev.* 22 (2008) 528–542. <https://doi.org/10.1101/gad.463208>.
- [166] M.S. Silverberg, J.H. Cho, J.D. Rioux, et al., Ulcerative colitis-risk loci on chromosomes 1p36 and 12q15 found by genome-wide association study, *Nat. Genet.* 41 (2009) 216–220. <https://doi.org/10.1038/ng.275>.
- [167] K. Yamaguchi, T. Chijiwa, N. Ikeda, H. Shibata, Y. Fukumaki, N. Oda-Ueda, S. Hattori, M. Ohno, The finding of a group IIE phospholipase A2 gene in a specified segment of *Protobothrops flavoviridis* genome and its possible evolutionary relationship to group IIA phospholipase A2 genes, *Toxins (Basel)* 6 (2014) 3471–3487. <https://doi.org/10.3390/toxins6123471>.
- [168] X.S. Chen, C.D. Funk, The N-terminal "beta-barrel" domain of 5-lipoxygenase is essential for nuclear membrane translocation, *Journal of Biological Chemistry* 276 (2001) 811–818. <https://doi.org/10.1074/jbc.M008203200>.
- [169] T. Hammarberg, Y.Y. Zhang, B. Lind, O. Radmark, B. Samuelsson, Mutations at the C-terminal isoleucine and other potential iron ligands of 5-lipoxygenase, *Eur. J. Biochem.* 230 (1995) 401–407. <https://doi.org/10.1111/j.1432-1033.1995.0401h.x>.
- [170] <https://www.proteinatlas.org/ENSG00000169914-OTUD3/summary/rna> (access: 11.06.2020).
- [171] G.R. Abecasis, A. Auton, L.D. Brooks, et al., An integrated map of genetic variation from 1,092 human genomes, *Nature* 491 (2012) 56–65. <https://doi.org/10.1038/nature11632>.
- [172] M. Lek, K.J. Karczewski, E.V. Minikel, et al., Analysis of protein-coding genetic variation in 60,706 humans, *Nature* 536 (2016) 285–291. <https://doi.org/10.1038/nature19057>.
- [173] S. Richards, N. Aziz, S. Bale, et al., Standards and guidelines for the interpretation of sequence variants: a joint consensus recommendation of the American College of Medical Genetics and Genomics and the Association for Molecular Pathology, *Genet. Med.* 17 (2015) 405–424. <https://doi.org/10.1038/gim.2015.30>.
- [174] R.D. Nicholls, J.L. Knepper, Genome organization, function, and imprinting in Prader-Willi and Angelman syndromes, *Annu. Rev. Genomics Hum. Genet.* 2 (2001) 153–175. <https://doi.org/10.1146/annurev.genom.2.1.153>.
- [175] A. Dagli, K. Buiting, C.A. Williams, Molecular and Clinical Aspects of Angelman Syndrome, *Mol. Syndromol.* 2 (2012) 100–112.
- [176] T. Kishino, M. Lalonde, J. Wagstaff, UBE3A/E6-AP mutations cause Angelman syndrome, *Nat. Genet.* 15 (1997) 70–73. <https://doi.org/10.1038/ng0197-70>.
- [177] T. Matsuura, J.S. Sutcliffe, P. Fang, R.J. Galjaard, Y.H. Jiang, C.S. Benton, J.M. Rommens, A.L. Beaudet, De novo truncating mutations in E6-AP ubiquitin-protein ligase gene (UBE3A) in Angelman syndrome, *Nat. Genet.* 15 (1997) 74–77. <https://doi.org/10.1038/ng0197-74>.

- [178] B. Sadikovic, P. Fernandes, V.W. Zhang, et al., Mutation Update for UBE3A variants in Angelman syndrome, *Hum. Mutat.* 35 (2014) 1407–1417. <https://doi.org/10.1002/humu.22687>.
- [179] K. Buiting, C. Williams, B. Horsthemke, Angelman syndrome - insights into a rare neurogenetic disorder, *Nat. Rev. Neurol.* 12 (2016) 584–593. <https://doi.org/10.1038/nrneurol.2016.133>.
- [180] B. García-de Teresa, A. González-Del Angel, M.E. Reyna-Fabián, M.d.L. La Ruiz-Reyes, R. Calzada-León, B. Pérez-Enríquez, M.A. Alcántara-Ortigoza, Deletion of exon 1 of the SLC16A2 gene: a common occurrence in patients with Allan-Herndon-Dudley syndrome, *Thyroid* 25 (2015) 361–367. <https://doi.org/10.1089/thy.2014.0284>.
- [181] C.E. Schwartz, M.M. May, N.J. Carpenter, et al., Allan-Herndon-Dudley syndrome and the monocarboxylate transporter 8 (MCT8) gene, *Am. J. Hum. Genet.* 77 (2005) 41–53. <https://doi.org/10.1086/431313>.
- [182] Y. Liu, D. Zhao, R. Dong, et al., De novo exon 1 deletion of AUTS2 gene in a patient with autism spectrum disorder and developmental delay: a case report and a brief literature review, *Am. J. Med. Genet. A* 167 (2015) 1381–1385. <https://doi.org/10.1002/ajmg.a.37050>.
- [183] J.A.L. Armour, R. Palla, P.L.J.M. Zeeuwen, M. den Heijer, J. Schalkwijk, E.J. Hollox, Accurate, high-throughput typing of copy number variation using paralogue ratios from dispersed repeats, *Nucleic Acids Res* 35 (2007) e19. <https://doi.org/10.1093/nar/gkl1089>.
- [184] A. Perne, X. Zhang, L. Lehmann, M. Groth, F. Stuber, M. Book, Comparison of multiplex ligation-dependent probe amplification and real-time PCR accuracy for gene copy number quantification using the beta-defensin locus, *BioTechniques* 47 (2009) 1023–1028. <https://doi.org/10.2144/000113300>.
- [185] B.E. Stranger, M.S. Forrest, M. Dunning, et al., Relative impact of nucleotide and copy number variation on gene expression phenotypes, *Science* 315 (2007) 848–853. <https://doi.org/10.1126/science.1136678>.
- [186] E. Shishido, B. Aleksic, N. Ozaki, Copy-number variation in the pathogenesis of autism spectrum disorder, *Psychiatry Clin. Neurosci.* 68 (2014) 85–95. <https://doi.org/10.1111/pcn.12128>.
- [187] A.J. Iafrate, L. Feuk, M.N. Rivera, M.L. Listewnik, P.K. Donahoe, Y. Qi, S.W. Scherer, C. Lee, Detection of large-scale variation in the human genome, *Nat. Genet.* 36 (2004) 949–951. <https://doi.org/10.1038/ng1416>.
- [188] F. Zhang, W. Gu, M.E. Hurles, J.R. Lupski, Copy number variation in human health, disease, and evolution, *Annu. Rev. Genomics Hum. Genet.* 10 (2009) 451–481. <https://doi.org/10.1146/annurev.genom.9.081307.164217>.
- [189] M. Uddin, B.K. Unda, V. Kwan, et al., OTUD7A Regulates Neurodevelopmental Phenotypes in the 15q13.3 Microdeletion Syndrome, *Am. J. Hum. Genet.* 102 (2018) 278–295. <https://doi.org/10.1016/j.ajhg.2018.01.006>.
- [190] Z. Zhang, X. Fang, X. Wu, et al., Acetylation-Dependent Deubiquitinase OTUD3 Controls MAVS Activation in Innate Antiviral Immunity, *Molecular Cell* 79 (2020) 304–319.e7. <https://doi.org/10.1016/j.molcel.2020.06.020>.
- [191] J. Park, J. Cho, E.E. Kim, E.J. Song, Deubiquitinating Enzymes: A Critical Regulator of Mitosis, *Int. J. Mol. Sci.* 20 (2019). <https://doi.org/10.3390/ijms20235997>.
- [192] F. Stegmeier, M.E. Sowa, G. Nalepa, S.P. Gygi, J.W. Harper, S.J. Elledge, The tumor suppressor CYLD regulates entry into mitosis, *Proc. Natl. Acad. Sci. U. S. A.* 104 (2007) 8869–8874. <https://doi.org/10.1073/pnas.0703268104>.
- [193] Y. Yang, M. Liu, D. Li, J. Ran, J. Gao, S. Suo, S.-C. Sun, J. Zhou, CYLD regulates spindle orientation by stabilizing astral microtubules and promoting dishevelled-NuMA-dynein/dynactin complex formation, *Proc. Natl. Acad. Sci. U. S. A.* 111 (2014) 2158–2163. <https://doi.org/10.1073/pnas.1319341111>.
- [194] I.L. Blitz, K.W.Y. Cho, C. Chang, Twisted gastrulation loss-of-function analyses support its role as a BMP inhibitor during early *Xenopus* embryogenesis, *Development* 130 (2003) 4975–4988. <https://doi.org/10.1242/dev.00709>.
- [195] C. Chang, D.A. Holtzman, S. Chau, et al., Twisted gastrulation can function as a BMP antagonist, *Nature* 410 (2001) 483–487. <https://doi.org/10.1038/35068583>.

- [196] L. Herhaus, M.A. Al-Salihi, K.S. Dingwell, et al., USP15 targets ALK3/BMPRI1A for deubiquitylation to enhance bone morphogenetic protein signalling, *Open Biol.* 4 (2014) 140065. <https://doi.org/10.1098/rsob.140065>.
- [197] M. Inui, A. Manfrin, A. Mamidi, et al., USP15 is a deubiquitylating enzyme for receptor-activated SMADs, *Nat. Cell Biol.* 13 (2011) 1368–1375. <https://doi.org/10.1038/ncb2346>.
- [198] S.-C. Sun, CYLD: a tumor suppressor deubiquitinase regulating NF-kappaB activation and diverse biological processes, *Cell Death Differ.* 17 (2010) 25–34. <https://doi.org/10.1038/cdd.2009.43>.
- [199] C.M. Annunziata, R.E. Davis, Y. Demchenko, et al., Frequent engagement of the classical and alternative NF-kappaB pathways by diverse genetic abnormalities in multiple myeloma, *Cancer Cell* 12 (2007) 115–130. <https://doi.org/10.1016/j.ccr.2007.07.004>.
- [200] P. Ströbel, A. Zettl, Z. Ren, P. Starostik, H. Riedmiller, S. Störkel, H.K. Müller-Hermelink, A. Marx, Spiradenocylindroma of the kidney: clinical and genetic findings suggesting a role of somatic mutation of the CYLD1 gene in the oncogenesis of an unusual renal neoplasm, *Am. J. Surg. Pathol.* 26 (2002) 119–124. <https://doi.org/10.1097/00000478-200201000-00016>.
- [201] Y. Hirai, Y. Kawamata, N. Takeshima, et al., Conventional and array-based comparative genomic hybridization analyses of novel cell lines harboring HPV18 from glassy cell carcinoma of the uterine cervix, *Int. J. Oncol.* 24 (2004) 977–986.
- [202] M. Fukuda, F. Fukuda, Y. Horiuchi, Y. Oku, S. Suzuki, K. Kusama, H. Sakashita, Expression of CYLD, NF-kappaB and NF-kappaB-related factors in salivary gland tumors, *In Vivo* 20 (2006) 467–472.
- [203] J. Gao, L. Huo, X. Sun, M. Liu, D. Li, J.-T. Dong, J. Zhou, The tumor suppressor CYLD regulates microtubule dynamics and plays a role in cell migration, *Journal of Biological Chemistry* 283 (2008) 8802–8809. <https://doi.org/10.1074/jbc.M708470200>.
- [204] S.A. Wickström, K.C. Masoumi, S. Khochbin, R. Fässler, R. Massoumi, CYLD negatively regulates cell-cycle progression by inactivating HDAC6 and increasing the levels of acetylated tubulin, *EMBO J.* 29 (2009) 131–144. <https://doi.org/10.1038/emboj.2009.317>.
- [205] H. Hu, G.C. Brittain, J.-H. Chang, et al., OTUD7B controls non-canonical NF-kappaB activation through deubiquitination of TRAF3, *Nature* 494 (2013) 371–374. <https://doi.org/10.1038/nature11831>.
- [206] I. Kouranti, J.R. McLean, A. Feoktistova, P. Liang, A.E. Johnson, R.H. Roberts-Galbraith, K.L. Gould, A global census of fission yeast deubiquitinating enzyme localization and interaction networks reveals distinct compartmentalization profiles and overlapping functions in endocytosis and polarity, *PLoS Biol.* 8 (2010). <https://doi.org/10.1371/journal.pbio.1000471>.
- [207] S. Urbé, H. Liu, S.D. Hayes, C. Heride, D.J. Rigden, M.J. Clague, Systematic survey of deubiquitinase localization identifies USP21 as a regulator of centrosome- and microtubule-associated functions, *Mol. Biol. Cell* 23 (2012) 1095–1103. <https://doi.org/10.1091/mbc.E11-08-0668>.
- [208] D.M. Garshott, E. Sundaramoorthy, M. Leonard, E.J. Bennett, USP21 and OTUD3 Antagonize Regulatory Ribosomal Ubiquitylation and Ribosome-Associated Quality Control, 2018.
- [209] I. Irminger-Finger, R.A. Laymon, L.S. Goldstein, Analysis of the primary sequence and microtubule-binding region of the Drosophila 205K MAP, *The Journal of Cell Biology* 111 (1990) 2563–2572. <https://doi.org/10.1083/jcb.111.6.2563>.
- [210] P. Chang, M. Coughlin, T.J. Mitchison, Tankyrase-1 polymerization of poly(ADP-ribose) is required for spindle structure and function, *Nat. Cell Biol.* 7 (2005) 1133–1139. <https://doi.org/10.1038/ncb1322>.
- [211] B.L. Goode, P.E. Denis, D. Panda, M.J. Radeke, H.P. Miller, L. Wilson, S.C. Feinstein, Functional interactions between the proline-rich and repeat regions of tau enhance microtubule binding and assembly, *Mol. Biol. Cell* 8 (1997) 353–365. <https://doi.org/10.1091/mbc.8.2.353>.
- [212] Fechtner L. 2019. In-vivo und in-vitro activity profiling of the OTU domain containing deubiquitinating enzyme OTUD3 [Master thesis]. Halle: Universität.

- [213] R. Hjerpe, F. Aillet, F. Lopitz-Otsoa, V. Lang, P. England, M.S. Rodriguez, Efficient protection and isolation of ubiquitylated proteins using tandem ubiquitin-binding entities, *EMBO Rep.* 10 (2009) 1250–1258. <https://doi.org/10.1038/embor.2009.192>.
- [214] L.J. Leandro-García, S. Leskelä, I. Landa, et al., Tumoral and tissue-specific expression of the major human beta-tubulin isoforms, *Cytoskeleton (Hoboken)* 67 (2010) 214–223. <https://doi.org/10.1002/cm.20436>.
- [215] Y. Saillour, L. Broix, E. Bruel-Jungerman, et al., Beta tubulin isoforms are not interchangeable for rescuing impaired radial migration due to Tubb3 knockdown, *Human Molecular Genetics* 23 (2014) 1516–1526. <https://doi.org/10.1093/hmg/ddt538>.
- [216] K.T. Nguyen, M.P. Holloway, R.A. Altura, The CRM1 nuclear export protein in normal development and disease, *Int. J. Biochem. Mol. Biol.* 3 (2012) 137–151.
- [217] N. Kudo, B. Wolff, T. Sekimoto, E.P. Schreiner, Y. Yoneda, M. Yanagida, S. Horinouchi, M. Yoshida, Leptomycin B inhibition of signal-mediated nuclear export by direct binding to CRM1, *Exp. Cell Res.* 242 (1998) 540–547. <https://doi.org/10.1006/excr.1998.4136>.
- [218] P.C. Echeverría, G. Mazaira, A. Erlejman, C. Gomez-Sanchez, G. Piwien Pilipuk, M.D. Galigniana, Nuclear import of the glucocorticoid receptor-hsp90 complex through the nuclear pore complex is mediated by its interaction with Nup62 and importin beta, *Mol. Cell. Biol.* 29 (2009) 4788–4797. <https://doi.org/10.1128/MCB.00649-09>.
- [219] A.B. Fielding, M. Concannon, S. Darling, et al., The deubiquitylase USP15 regulates topoisomerase II alpha to maintain genome integrity, *Oncogene* 37 (2018) 2326–2342. <https://doi.org/10.1038/s41388-017-0092-0>.
- [220] T. Cornelissen, D. Haddad, F. Wauters, et al., The deubiquitinase USP15 antagonizes Parkin-mediated mitochondrial ubiquitination and mitophagy, *Human Molecular Genetics* 23 (2014) 5227–5242. <https://doi.org/10.1093/hmg/ddu244>.
- [221] M. Faronato, V. Patel, S. Darling, L. Dearden, M.J. Clague, S. Urbé, J.M. Coulson, The deubiquitylase USP15 stabilizes newly synthesized REST and rescues its expression at mitotic exit, *Cell Cycle* 12 (2013) 1964–1977. <https://doi.org/10.4161/cc.25035>.
- [222] H. Zhou, S. Di Palma, C. Preisinger, M. Peng, A.N. Polat, A.J.R. Heck, S. Mohammed, Toward a comprehensive characterization of a human cancer cell phosphoproteome, *J. Proteome Res.* 12 (2013) 260–271. <https://doi.org/10.1021/pr300630k>.
- [223] W.K.F. Tse, B. Eisenhaber, S.H.K. Ho, Q. Ng, F. Eisenhaber, Y.-J. Jiang, Genome-wide loss-of-function analysis of deubiquitylating enzymes for zebrafish development, *BMC Genomics* 10 (2009) 637. <https://doi.org/10.1186/1471-2164-10-637>.
- [224] D.C. Weinstein, A. Hemmati-Brivanlou, Neural induction in *Xenopus laevis*: evidence for the default model, *Curr. Opin. Neurobiol.* 7 (1997) 7–12. [https://doi.org/10.1016/s0959-4388\(97\)80114-6](https://doi.org/10.1016/s0959-4388(97)80114-6).
- [225] A.M. Zimmer, Y.K. Pan, T. Chandrapalan, R.W.M. Kwong, S.F. Perry, Loss-of-function approaches in comparative physiology: is there a future for knockdown experiments in the era of genome editing?, *J. Exp. Biol.* 222 (2019). <https://doi.org/10.1242/jeb.175737>.
- [226] F.O. Kok, M. Shin, C.-W. Ni, et al., Reverse genetic screening reveals poor correlation between morpholino-induced and mutant phenotypes in zebrafish, *Dev. Cell* 32 (2015) 97–108. <https://doi.org/10.1016/j.devcel.2014.11.018>.
- [227] M.A. El-Brolosy, D.Y.R. Stainier, Genetic compensation: A phenomenon in search of mechanisms, *PLoS Genet.* 13 (2017) e1006780. <https://doi.org/10.1371/journal.pgen.1006780>
- [228] A. Dhara, R. de Paula Baptista, J.C. Kissinger, E.C. Snow, A.P. Sinai, Ablation of an Ovarian Tumor Family Deubiquitinase Exposes the Underlying Regulation Governing the Plasticity of Cell Cycle Progression in *Toxoplasma gondii*, *mBio* 8 (2017). <https://doi.org/10.1128/mBio.01846-17>.

8. Theses

- 1) OTUD3 is highly evolutionary conserved on genomic and protein level.
- 2) Endogenous full-length OTUD3 possesses cysteine protease activity.
- 3) Inherited and *de novo* OTUD3 defective genotypes might be associated with human neurodevelopmental disease phenotypes.
- 4) Endogenous OTUD3 colocalizes with polymerized tubulin structures.
- 5) OTUD3 is a microtubule associated protein (MAP) and interaction is mediated by a C-terminal microtubule-binding site.
- 6) Cellular localization of OTUD3 is regulated by a potential NLS in the N-terminus and a NES located within the C-terminal region of the protein.
- 7) OTUD3 knock-out changes the morphology of HEK293T and HeLa cells.

III Selbstständigkeitserklärung

Hiermit erkläre ich, dass ich die vorliegende Dissertation mit dem Titel „*Deciphering OTUD3 functions and its potential role in human neurodevelopmental disease*“ selbstständig und nur mit Hilfe der im Anhang befindlichen Quellen angefertigt habe. Textstellen, welche wörtlich oder sinngemäß aus veröffentlichten Schriften entnommen wurden, sind als solche gekennzeichnet. Bei der Durchführung der Untersuchungen zur Generierung der Dissertationsergebnisse, habe ich die Satzung der Martin-Luther-Universität zur „Sicherung guter wissenschaftlicher Praxis“ eingehalten. Die Arbeit habe ich weder im In- noch im Ausland in gleicher oder ähnlicher Form einer anderen Prüfungsbehörde vorgelegt. Die eingereichte schriftliche Version der Arbeit entspricht der Version der Dissertation auf dem elektronischen Speichermedium.

Halle (Saale), den 16.08.2021



Florian Job

IV Erklärung über frühere Promotionsversuche

Ich erkläre, dass ich mich an keiner anderen Hochschule einem Promotionsverfahren unterzogen bzw. eine Promotion begonnen habe.

Halle (Saale), den 16.08.2021



Florian Job

V Danksagung

An dieser Stelle möchte ich mich bei allen bedanken, die mich seit Juni 2014 bis zum Abschluss dieser Promotionsarbeit inspiriert, unterstützt und motiviert haben.

Mein besonderer Dank gilt Frau Prof. Hoffmann, Herrn Prof. Hollemann, Dr. Lorini und Prof. Pfirrmann für die Aufnahme in das wirklich spannende OTUD3-Roux-Projekt. Als Team, zusammen mit Carolin Mai als zweite Doktorandin auf dem OTUD3-Projekt, konnte ich aus den gemeinsamen Treffen in großer Runde stets sowohl fachlichen Input als auch praktische Tipps und Tricks für die Durchführung von Experimenten mitnehmen.

Auch möchte ich dem gesamtem Routine-Labor-Team aus der Humangenetik meinen Dank aussprechen. Dabei möchte ich Frau Schulze, Frau Enders, Frau Bauer, Frau Heinze und Frau Körber-Ferl für die Integration meiner Forschungsproben in die Auftrags-Diagnostik danken. Frau Dr. Foja gilt mein Dank für die Unterstützung beim Umgang mit der qPCR und den gängigen Mutations-Prognose-Tools. Frau Dr. Hagemeister danke ich für die Hilfe bei der Auswertung der MLPA Daten. Im Institut für Physiologische Chemie möchte ich Juliane Herfurth danken, für die Gesellschaft in den frühen Morgenstunden mit Musik und den aktuellen Themen außerhalb eines Laboralltags. Für die tollen Stunden in der Zellkultur und ihre Unterstützung mit Rat und Tat möchte ich Annett Thate danken.

Prof. Rujescu möchte ich für die Bereitstellung der post-mortem Hirnproben danken. Prof. Sperling und dem Charité-Team für die Bereitstellung der zahlreichen DNA Proben. Frau PD Dr. Quandt und PD Dr. Riemann danke ich für die Unterstützung am FACS Gerät.

Gerne möchte ich die Liste noch erweitern, um Dr. Anja Fait, welche mich immer wieder daran erinnert hat, dass es noch eine Doktorarbeit zu schreiben gibt und mir neben einem anspruchsvollen Job in Ihrem Team zeitliche Vakanzen eingeräumt hat.

Und dann gibt es noch die Menschen in meinem Leben, ohne die ich jetzt sicherlich nicht an diesem Punkt stehen würde. Meinen Freunden Dorit Bennmann, Anja Greschuchna und Carolin Mai danke ich für die manchmal dringend nötige Abwechslung und die vielen tollen Tage und Abende in den letzten (bis zu) 14 Jahren. Meiner Mama und Schwester danke ich für Ihre Geduld, das „Ertragen“ meiner Launen und die seelische und moralische Unterstützung in allen Lebenslagen.

Lieber Steffen, liebe Lisa, ihr zwei seid mein größter Halt und meine größte Freude. Zusammen haben wir diesen Meilenstein in meinem Leben erreicht und ich freue mich auf viele weitere in eurer und meiner Zukunft. Zusammen unschlagbar!